MODERN APPLIED SCIENCE

CCSE

CANADIAN CENTER OF SCIENCE AND EDUCATION

Editorial Board

Contents

An Optimized Highly Efficient RF Power Amplifier for WLAN System Application

Mohammed H. Ali, C. K. Chakrabarty, & Mithaq H. Raheema

Department of Electronics and Communication Engineering

University Tenaga Nasional, Selangor 43009, Malaysia

Abstract

The class-AB/ F power amplifier (PA), Class F is commonly understood to be a switching PA, but in fact, it can also be a transconductance PA, depending on how hard the active device is driven. This paper presents the design a multistage class AB/Inverse F power Amplifier with high power added efficiency (PAE) and acceptable linearity for the WLAN applications. The effectiveness of the proposed controller has been verified by comparing proposed method with another methods using simulation study under a variety of conditions. The proposed circuit operation for a WLAN signal delivers a power-added efficiency (PAE) of 43.9% is measured at 32.1-dBm output power and linearity of inverse class F displays the simulation result of 1-dB compression output power of 17.5 dBm at -22.4 dBm input power. Finally, the proposed PA is show a good and acceptable result for the WLAN system.

Keywords: Power amplifier, WLAN system, Harmonic terminations, Biasing voltage

1. Introduction

The integration of wireless communication systems requires stringent capabilities in terms of linearity and efficiency. It is well known that the power amplifier (PA) need to amplify signals efficiently to increase the battery life that typically deliver their highest efficiency at maximum output power in linearity becomes significant (Zhen L., et al., 2002).

Recently, power amplification techniques with inherently more power efficient have been researched to satisfy the requirements (Bing B., & Jayant N., 2002; Bakkaloglu B., & Fontaine P. A., 2005). Such techniques are included load modulation technique, switching mode amplifiers (Nam J., 2005), envelope elimination and restoration (Raab, F. H., et al., 1998), the multi-modes and multiband of operation and envelope tracking (Tsai Pi. H., et al., 2005). The Doherty Power Amplifier is a promising candidate with advantages of high PAE, low cost and simple construction (Kimball D. F., et al., 2006; McMorrow R. J., et al., 1994). Another many advanced techniques have been reported (Kenington P. B., 1999; Matsuge K., et al., 2004) for improve performance of PA however there are many drawbacks such as envelop tracking technique and weighted polynomial digital pre-distortion technique but still these techniques including complex circuit configuration, modest enhancement and high cost.

This paper focus on control the shape and overlap of the drain voltage and/or current waveforms for class-AB/IF power amplifier using appropriate gate biasing and harmonic terminations. First, exploit the harmonic contents so the loss in the active device is minimized. Second, bias the amplifier toward class AB/A (AB or A) to improve the linearity. Finally, the simulation result show that proposed PA are significantly improvement the linearity, efficiency and output power can be achieved with proper harmonic terminations and proper biasing voltage.

2. Proposed Circuit Design

A schematic of the designed PA is shown in Figure 1. The output stage of the power amplifier is a class-AB/F topology with the harmonic control circuits, and the driver multistage is a pre-amplifier that is composed of a class-F amplifier. The specifications of the proposed Power Amplifier are calculated based on (Point R., 2003). Some of the key specifications in the design of this PA are its frequency of operation, gain, output power level, and bias voltages are adaptively modified of the input/output impedances. Traditionally, all the impedances of any RF block are terminated with 50 Ω, especially to aid in the testing of these blocks. In addition, it is easy to see that with the load modulation can be carried out in multistage with different control voltage profiles.

3. Simulation Results

To enable to test the proposed class AB/ Inverse F amplifier, closer examination of the voltages and currents of WLAN amplifier is required. Figure 2 shows the voltage and current waveforms at the drain terminal for the class AB output stage of 3-stages WLAN PA. Recall that this PA provides output power of 17.8 dBm, power gain of 30.7 dB, and PAE of 29.4%.

Figure 3 shows the simulation response of the proposed class AB/Inverse F amplifier at input power of -13 dBm. Higher output power of 19.2 dBm is provided with a power gain of 32.1dB and PAE of 38.7%.

Figure 4 shows the 1-dB compression output power for 3-stages WLAN PA, with output stage of different biasing gate voltages for comparison. The linearity of power amplifier in the proposed mode can be expected to be higher than the traditional class F.

Figure 5 shows this principle, when class AB/F 1-dB compression output power is 16.7 dBm which represents good linearity, compared with that of 10.3 dBm for the traditional class F amplifier. In this proposed switch mode and with the assistance of harmonic impedance components at the output, to improve the efficiency, the 1-dB compression can be increased as a criterion of linearity improvement.

Figure 6, the linearity of inverse class F displays the simulation result of 1-dB compression output power of 17.5 dBm at -22.4 dBm input power. This value represents a very important indicator to combine linearity improvement with all others output requirements such as output power, power gain, and PAE.

Finally, Figure 7 shows testing the simulation response of drive a proper input signal to the output stage with different biasing gate voltages, in which, 3-stages WLAN PA is designed with class AB biasing for each stage in addition to the second and third harmonic impedance components at the output terminal of the output stage. The power-added efficiency was measured to be 43.8%, a very good value, indicating the advantage of these proposed design steps.

4. Conclusion

In this paper, Class AB/F is studied the ideal theoretical solution for the efficiency-linearity tradeoff and have proposed a new concept of a class AB/IF PA 2.4 GHz using multistage technique. However, the performance of this amplifier relies heavily on the realization of the harmonic traps and the input biasing voltage. As for the class-F amplifier, harmonic terminations at the drain are important to improve both efficiency and output power. For the third-harmonic resonator to generate a third-harmonic component of voltage, it requires third-harmonic current which does not exist. The simulation result showed that the proposed significantly improved the efficiency over a broad average output power compared to the conventional balanced amplifier.

References

Bing, B., & Jayant, N. (2002). A cellphone for all standards. *IEEE Spectr.,* 39(5), 34–39. http://dx.doi.org/10.1109/6.999792

Bakkaloglu, B., & Fontaine, P. A. (2005). Multi-mode, multi-band RF transceiver circuits for mobile terminals in deep-submicron CMOS processes. In Proc. *IEEE Radio Freq. integrated Circuits Symp.,* 483–486. http://dx.doi.org/10.1109/RFIC.2005.1489851

Kenington, P. B. (1999). High-linearity RF Amplifier Design, Artech House, Norwood, MA.

Kimball, D. F., Jeong, J., Hsia, C., Draxler, P., Lanfranco, S., Nagy, W., Linthicum, K., et al. (2006). High-efficiency envelope tracking W-CDMA base-station amplifier usingGaN HFETs. *IEEE Trans. Microw. Theory Tech.,* 54(11), 3848-3856. http://dx.doi.org/10.1109/TMTT.2006.884685

Matsuge, K., Hiura, S., Ishida, M., Kitahara, T., & Yamamoto, T. (2004). Full RF module with embedded filters for 2.4 GHz and 5 GHz dual band WLAN applications. *IEEE MTT-s,* 2, 629-632. http://dx.doi.org/10.1109/MWSYM.2004.1336064

McMorrow, R. J., Upton, D. M., & Maloney, P. R. (1994). The microwave Doherty amplifier. *IEEE MTT-S Int. Microwave Symp. Dig.,* 1653-1656. http://dx.doi.org/10.1109/MWSYM.1994.335123

Nam, J., Shin, J. H., & Kim, B. (2005). A handset power amplifier with high efficiency at lowlevel using load modulation technique. *IEEE Trans. Microw. Theory Tech.,* 53(8), 2639-2644. http://dx.doi.org/10.1109/TMTT.2005.852745

Point, R. (2003). An RF CMOS Transmitter Integrating a Power Amplifier and a Transmit/Receive Switch for 802.11b Wireless Local Area Network Applications. *IEEE Radio Frequency Integrated Circuits Symposium,* 431-434. http://dx.doi.org/10.1109/RFIC.2003.1213978

Raab, F. H., Sigmon, B. E., Myers, R. G., & Jackson, R. M. (1998). L-band transmitter using KahnEER technique. *IEEE Trans. Microw. Theory Tech.,* 46(12), 2220-2225. http://dx.doi.org/10.1109/22.739200

Tsai, Pi. H., Metzger, A. G., Zampardi, P. J., Iwamoto, M., & Asbeck, P. M. (2005). Design of highefficiency current-mode class D amplifier for wireless handsets. *IEEE Trans. Microw. TheoryTech.,* 53(1), 144-151. http://dx.doi.org/10.1109/TMTT.2004.839327

Zhen, L., Wenan, Z., Junde, S., & Chunping, H. (2002). Consideration and research issues for the future generation of mobile communication. In Proc. *IEEE Can. Elect. Comput. Eng. Conf.,* 6(1), 44-55. http://dx.doi.org/10.1109/CCECE.2002.1012933
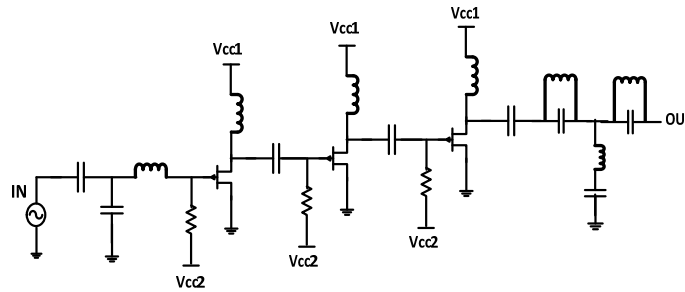
Figure 1. Optimized PA schematic
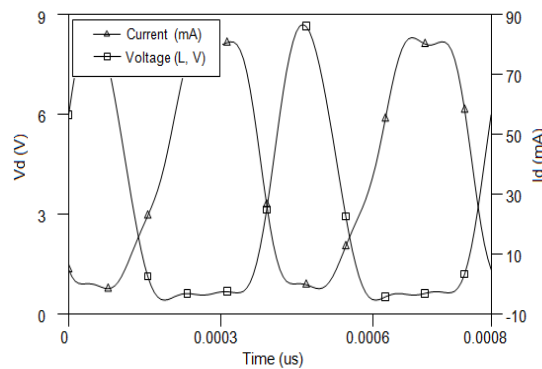
Figure 2. The voltage and current waveforms at the drain terminal
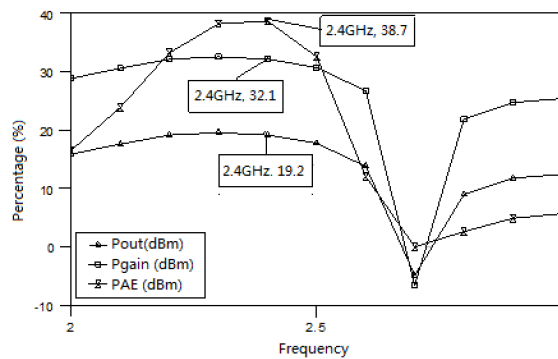
Figure 3. Percentage output power, power gain, and power added efficiency
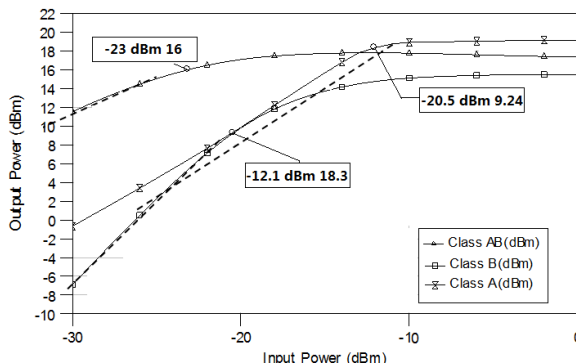
Figure 4. Compression 1-dB linearity output power of 3-stages WLAN PA
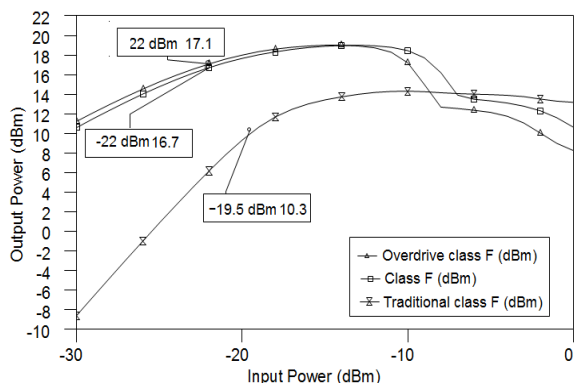
Figure 5. Compression 1-dB output power of 3-stages WLAN switch PA
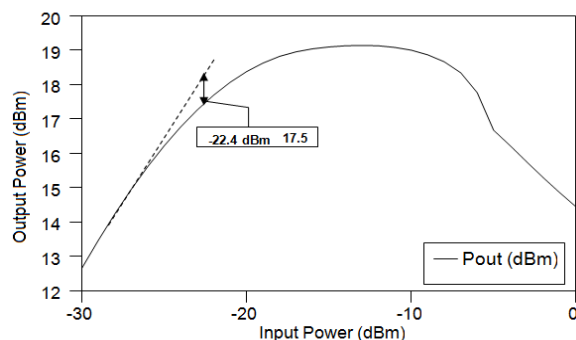
Figure 6. Compression 1-dB output power of proposed class AB/Inverse F 3-stages WLAN PA
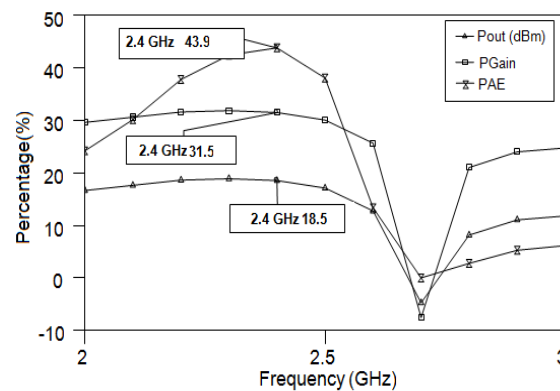
Figure 7. Added efficiency versus the input signal frequency

Effect of Antecedent Conditions on Prediction of Pore-Water Pressure Using Artificial Neural Networks

Muhammad Raza Ul Mustafa

Civil Engineering Department, Universiti Teknologi Petronas, Tronoh 31750, Perak, Malaysia

Tel: 60-19-595-7132   E-mail: raza_geo@hotmail.com

Rezaur Rahman Bhuiyan

Water Resources Engineer, Golder Associates Ltd. Calgary T2A 7W5, Alberta, Canada

Tel: 1-403-299-5600   E-mail: cerezaur@gmail.com

Mohamed Hasnain Isa

Civil Engineering Department, Universiti Teknologi Petronas, Tronoh 31750, Perak, Malaysia

Tel: 60-5-368-7346   E-mail: hasnain_isa@petronas.com.my

Saied Saiedi

Civil Engineering Department, Universiti Teknologi Petronas, Tronoh 31750, Perak, Malaysia

Tel: 60-5-368-7347   E-mail: saied.saiedi@yahoo.com

Harianto Rahardjo

School of Civil & Environmental Engineering, Nanyang Technological University

Nanyang Avenue 639798, Singapore

Tel: 65-6790-5246   E-mail: chrahardjo@ntu.edu.sg

Abstract

The effect of antecedent conditions on the prediction of soil pore-water pressure (PWP) using Artificial Neural Network (ANN) was evaluated using a multilayer feed forward (MLFF) type ANN model. The Scaled Conjugate Gradient (SCG) training algorithm was used for training the ANN. Time series data of rainfall and PWP was used for training and testing the ANN model. In the training stage, time series of rainfall was used as input data in one model whereas, rainfall and pore water pressure with some antecedent conditions was used in second model and corresponding time series of PWP was used as the target output. In the testing stage, data from a different time period was used as input and the corresponding time series of pore-water pressure was predicted. The performance of the model was evaluated using statistical measures of root mean square error (RMSE) and coefficient of determination (R^2). The results of the model prediction revealed that when antecedent conditions (past rainfall and past pore-water pressures) are included in the model input data, the prediction accuracy improves significantly.

Keywords: Antecedent, Artificial Neural Network, Pore-water Pressure, Prediction, Rainfall

1. Introduction

Variations in soil pore-water pressure (PWP) due to rainfall are known to exhibit highly non-linear and complex relationship. This is due to the spatial and temporal variability of precipitation, evaporation pattern and soil properties. The knowledge of PWP is very important in the determination of strength and effective stress of a soil. Excessive PWP increase is known to cause slope failures in areas susceptible to landslide. To arrive at effective remedial and design strategies against slope failure it is necessary to know the PWP changes due to rainfall.

Tensiometers are usually used to measure PWP at different depths of soil. In general, PWP of soils depends on several soil and climate-related factors such as rainfall, soil properties (grain size, porosity, density, etc.), temperature, evaporation, solar radiation, soil depth, and antecedent conditions. Therefore, reliable prediction of pore-water pressure is significantly data-demanding.

Use of Artificial Neural Network (ANN) techniques to solve problems in civil engineering began in the late 1980's (Flood, & Kartam, 1994). Applications of ANN techniques for simulation and forecasting in water resources engineering are few and relatively recent. ANN has been applied with success in estimation and forecasting of discharge capacity of channels (Unal, Mamak, Seckin, & Cobaner, 2010), suspended sediment (Mustafa, Isa, & Rezaur 2011), discharge (Tawfik, Ibharim, & Fahmy, 1997) and hourly and daily stream flows (Kang, Kim, Park, & Ham, 1993). A comprehensive review carried out by the American Society of Civil Engineering (ASCE) Task Committee on Application of ANN in hydrology concluded that ANN can perform well as existing models (ASCE, 2000a, 2000b). The ANN approach to nonlinear behavior modeling is more effective and more efficient whenever an explicit knowledge of the hydrological process is not required (Hsu, Gupta, & Sorooshian, 1995). It appears that for predicting PWP variations application of ANN could be an ideal alternative to regression based approaches.

The objectives of this study are (i) to develop an ANN model using Scaled Conjugate Gradient (SCG) learning algorithm for predicting time series of pore-water pressure responses to variations in rainfall pattern, and (ii) to evaluate the influence of antecedent conditions (past rainfall and past pore-water pressures) on the prediction accuracy of the ANN model.

2. ANN Model Theory

The architecture of ANN is a data processing system that consists of a large number of simple units called neurons or nodes having a local memory and interconnected with weights and biases. ANN differ from the traditional physically based models in a way that, ANN has the ability of self adaptation, can capture functional relationships and extract patterns between input and output variables by learning from examples even if the primary relationship is complex and difficult to describe by a physically based relationship. Thus application of ANN seems appropriate for problems whose solutions necessitate information that are hard to describe and lack of sufficient data or observations. Due to its self-learning, self-adaptable processing, non-linear pattern classification, and identification capabilities, application of ANN to different aspects of hydrologic modeling has attracted interest in recent years (Cigizoglu, 2004; Cigizoglu, & Alp, 2004; Hu, Lam, & Ng, 2001).

Application of an ANN consists of three steps; (i) training, (ii) validation and (iii) testing. Available data are divided for all these steps. Usually, as a rule of thumb, 60% of the available data are used for training, 20% for validation and the remaining 20% for testing. However, this rule is not fixed and could be changed depending on the availability of data. Training and validation could be viewed as the same process because in both steps input and target data are introduced to the network and the network is trained. Therefore, in some instances when a large dataset is not available, training and validation could be combined together in a single training session (i.e. 80% data could be used for training instead of 60% for training and 20% for validation). During testing, a new set of data which has not been used in training is provided to the network to produce the output (prediction). To assess the performance of the ANN model the outputs generated during testing are compared with the corresponding observations.

An ANN is designed by weights between the neurons, transfer function and learning laws (Caudill, 1987). Multilayer Feed Forward (MLFF) networks consists of more than one layer (i.e. input, hidden and output layers) and in Feed Forward (FF) networks all the information are transferred in the forward direction only, i.e. from input neurons to output neurons through the hidden layer. There is no cycle or loop in the feed forward network. The architecture of an MLFF network is shown in Figure 1. Subscripts $i, j,$ and k denote the ith ($1 \leq i \leq L$), j^{th} ($1 \leq j \leq M$), and k^{th} ($1 \leq k \leq N$), neuron in the input, hidden and output layers, respectively. The letters L, M, N denote the number of neurons in the input, hidden and output layers respectively. The symbols y_k and z_k denote the output and target values respectively of the kth neuron in the output layer.

The objective of training is to minimize the error between target and output values by adjusting the weights and biases through an algorithm called the learning law. During training a neuron obtains inputs from the previous layer which is multiplied by its weight and the bias value is added. Thus, the combination of the net weighted inputs and bias net_j to the jth neuron in the hidden layer is represented as

$$net_j = \sum_{i=1}^{L} x_i w_{ji} + b_j \tag{1}$$

where, x_i is the input to the ith neuron in the input layer; w_{ji} is the weight of jth neuron of the hidden layer connected to the ith neuron of the input layer and b_j is the bias of the jth neuron in the hidden layer. The net input to the jth neuron of the hidden layer is then passed through a transfer function f to produce the output of the jth neuron in the hidden layer. If the activation level of neurons is strong enough then it produces an output. The output of the jth neuron in the hidden layer can be expressed as

$$y_j = f(net_j) = f\left(\sum_{i=1}^{L}(x_i w_{ji} + b_j)\right) \tag{2}$$

The output of the hidden layer is an input to the neuron in the output layer and the same operation as in the hidden layer is repeated in the output layer to obtain the output of neurons in the output layer. The net weighted input and bias to the kth neuron in the output layer is represented as

$$net_k = \sum_{j=1}^{M} f(y_j)w_{kj} + b_k = \sum_{j=1}^{M} w_{kj} f\left(\sum_{i=1}^{L}(x_i w_{ji} + b_j)\right) + b_k \tag{3}$$

where, w_{kj} is the weight of kth neuron of the output layer connected to the jth neuron of the hidden layer and b_k is the bias of the kth neuron in the output layer. The output from the kth neuron in the output layer is given by

$$y_k = f(net_k) = f\left(\sum_{j=1}^{M} w_{kj} f\left(\sum_{i=1}^{L}(x_i w_{ji} + b_j)\right) + b_k\right) \tag{4}$$

The error e_k of the kth neuron in the output layer which is the squared difference between the target and output values can be written as

$$e_k = (z_k - y_k)^2 \tag{5}$$

If there are P numbers of input data pairs such that $(1 \leq p \leq P)$, the global error of the network in terms of mean squared error is written as

$$E = \frac{1}{2}\sum_{p=1}^{P}\sum_{k=1}^{N}(z_{pk} - y_{pk})^2 \tag{6}$$

Equation (6) is called the error function of the network and is a function of network connection weights. During training the global error function is minimized by the learning rule. The learning rule enables updating (adjusting) the connection weights through successive iterations such that the difference between target and output values for all dataset is within a predefined tolerance limit.

There are several learning algorithms available, the commonly used ones are the (i) Back propagation (BP), (ii) Back propagation with momentum, (iii) Conjugate Gradient (CG), (iv) Scaled Conjugate Gradient (SCG), (v) Quasi Newton's and (vi) Levenberg-Marquardt (LM) algorithm. Each of these algorithms has its own distinct advantages and weaknesses. However, the SCG algorithm is based on the second order gradient supervised learning rule and is claimed to have learning speed (convergence rate) about 2 times faster than the CG algorithm and about 20 times faster than the regular BP algorithm (Moller, 1993; Schraudolph, & Graepel, 2002). Other major advantages of the SCG algorithm are that it does not depend on any critical user selected parameter (e.g. learning rate, momentum) as in BP algorithm and it does not involve computationally expensive line-search to scale the step size as in CG algorithm, instead it uses a trust-region method to scale the step size(Cestisli & Barkana, 2010; Falas, & Stafylopatis, 2005).

3. Methodology

3.1 Data Source and Study Area

The data used in this study are the time series of pore-water pressure and rainfall records from 3 m soil depth, for a period of three and a half months and at 4 hour interval during dry periods (no rainfall) and 10 min interval during wet periods. The data was collected through a field instrumentation program of a residual soil slope in Yishun, Singapore (Rahardjo, Leong, & Rezaur, 2008; Rezaur, Rahardjo, Leong, & Lee, 2003). The three and a half month time series data consists of 1450 pore-water pressure measurements varying between both positive and negative values with a maximum negative PWP of magnitude −15 kPa. The entire monitoring period spanned over three years and included time series of pore-water pressure and rainfall measurements at 4 different

slopes in 2 major geological formations (Bukit Timah Granitic Formation and Sedimentary Jurong Formation) and at soil depths 0.5, 1, 2, and 3 m. The data was primarily collected with a view to understand rainfall-induced slope failure mechanism (Rahardjo, et al., 2008) and hydrological responses of slopes under tropical climate (Rezaur, et al., 2003). Climate at the study area is hot and humid (equatorial) with no marked dry season. The temperature varies little throughout the year with an annual average of 26.6 °C and a relative humidity of 84% (Meteorological-Service-Singapore, 1997). The soil at the Yishun site is residual soil from the Bukit Timah granite which varies from silty or clayey sand to silty or sandy clay, depending on the degree of weathering, but is commonly sandy clayey silt (Rahardjo, et al., 2008).

3.2 ANN Architecture

Two different ANN model architectures were used in this study; hereafter called the ANN1 and ANN2. ANN1 consisted of one neuron in the input layer for rainfall, 4 neurons in the hidden layer and one neuron in the output layer, denoted by ANN architecture 1–4–1. ANN2 denoted by 8–4–1 architecture, consisted of 8 neurons in the input layer out of which 3 were used for rainfall values (1 current and 2 antecedent) and the remaining 5 were used for PWP (antecedent values). ANN1 architecture was adopted to examine the suitability of modeling the variation of pore-water pressure at the current time u_t as a direct function of variation of rainfall at current time r_t, (i.e $u_t = f(r_t)$), i.e. without accounting for any effect from antecedent conditions. Whereas ANN2 architecture was adopted to examine the suitability of modeling the variation of pore-water pressure as a function of variation of rainfall and pore-water pressure at the present time t and past (antecedent) times ($t–1$, $t–2…… t–5$) such that;

$$u_t = f(r_t, \ r_{t-1}, r_{t-2}, u_{t-1}, u_{t-2}, u_{t-3}, u_{t-4}, u_{t-5}) \tag{7}$$

There is no hard and fast rule for selecting the number of neurons in the hidden layer. In this study, the number of neurons in the hidden layer was arrived at by trial and error method (Maier, & Dandy, 2000). A program code using ANN toolbox in MATLAB was written for the application of the ANN algorithm described in the ANN model and theory section.

3.3 Input Data Selection

Success in the identification of a non-liner system by ANN training depends on the selection of appropriate training data which should be representative of the non-liner system to be mapped during the ANN training (Rojas, 1996). In this study the available three and half month synchronized time series data of pore-water pressure and rainfall was divided into two sets. Data from Oct 12–1998 to Dec 17–1998 (about 70% of the available data) was used for training-validation while data for the period Dec 18–1998 to Jan 24–1999 (remaining 30% of the data) was used for testing (prediction).

3.4 Activation Function Selection

In this study, the hyperbolic tangent sigmoid transfer function, also known as hyperbolic tangent or tansig (Eq. 8) was used for neurons in the hidden layer. Linear transfer function, also known as purelin (Eq. 9) was used for neurons in the output layer.

$$f(x) = \frac{e^x - e^{-x}}{e^x + e^{-x}} \tag{8}$$

$$f(x) = x \tag{9}$$

3.5 Data Normalization

The input and target data (raw data) need to be normalized before use in the ANN training and testing to commensurate with the upper and lower bound limits of the activation functions used in the hidden neurons. This ensures fast processing and convergence during training and minimizes prediction error (Rojas, 1996). Since hyperbolic tangent sigmoid activation function whose upper and lower bounds are in the range of –1 to 1 was used in the hidden layer neurons, the pore-water pressure and rainfall data was normalized by transforming the data to the range of –1 to 1 using the equation;

$$z_p = 2 \times \frac{(x_p - x_{\min})}{(x_{\max} - x_{\min})} - 1 \tag{10}$$

where, z_p is the normalized or transformed data series, x_p is the original data series, $x_{\min}$, $x_{\max}$ are the minimum and the maximum value of the original data series respectively, $1 \le p \le P$ and P is the number of data.

3.6 Performance Evaluation Criteria

In hydrological studies root mean square error (RMSE) is commonly used to evaluate model performance. The ideal value of RMSE for best performance is zero. In this study, the performance of the model was evaluated using RMSE between the observed and predicted values, as

$$\text{RMSE} = \left[\frac{1}{P} \sum_{p=1}^{P} (z_p - y_p)^2 \right]^{1/2} \tag{11}$$

where, z_p and y_p are the observed and predicted values of pore-water pressure, respectively, P is the number of observations for which the error has been computed.

3.7 Stopping Criterion

The rule for stopping the training was based on either the relative error of the sum of square error $E \leq$ goal or the maximum number of given epochs, whichever is satisfied first. In the program code, values of 0.001 and 500 were used for goal and number of epochs, respectively.

4. Results and Discussion

The summary of ANN model performance statistics are shown in Table 1. The performance of both the ANN models in terms of minimizing the mean square error (MSE) to a desired goal and the time and number of epochs to reach the desired goal during training of the networks are shown in Figure 2. ANN1 model started training with an initial global MSE of 5.29 and minimized the MSE to 0.3 within only 3 epochs. Thereafter, the network appears to be trapped with local minima and the MSE remained constant at 0.28 until the maximum number of epochs (500) was reached, the goal however was not achieved (Figure 2a). For ANN2 model the MSE decreased very fast (0.8 to 0.003) for the first 7 epochs and then continued to decrease at a slower rate until the goal (0.001) was reached at 82 epochs (Figure 2a). Similarly, Figure 2b shows that for ANN1 the MSE decreased from 5.29 to 0.3 in 0.02s but remained constant at 0.28 till the training finished at 4s when the maximum number of epochs (500) was reached. The ANN2 model minimized the error very fast and achieved the goal with only 0.83s (Figure 2b).

A comparison between observed and trained time series of pore-water pressures are shown in Figure 3. Figure 3a shows that ANN1 model failed to learn the non-linear behavior of pore-water pressure throughout the training duration and the trained values did not follow the target values. While the ANN2 model learned the complex behavior of the data well, adopted the non-linearity and then followed the same trend as the target values (Figure 3b).

Prediction results of time series of pore–water pressures during testing stage of the ANN models are shown in Figure 4. It is clear that ANN1 (with architecture 1–4–1) which gave poor results during training (Figure 3a) also showed bad performance during testing (Figure 4a). ANN2 (with architecture 8–4–1) performed well during both training (Figure 3b) and prediction (Figure 4b). Figure 3b and Figure 4b show that in both cases i.e. during training and prediction, the trends in the trained and predicted time series followed closely the trends of the observed pore-water pressures.

Comparison between observed pore-water pressures and pore-water pressures predicted by the ANN models are shown in Figure 5. The coefficient of correlation (R^2) and the line of perfect agreement between observed and predicted values are also shown in Figure 5. The correlation between the observed and predicted pore-water pressures for ANN1 is very poor ($R^2=0.065$, Figure 5a) whereas the correlation between the observed and predicted pore-water pressures for ANN2 is good ($R^2=0.973$); confirming the superior performance of ANN2 model (Figure 5b).

A comparison of performance statistics in terms of RMSE, epochs, and time to reach goal in Table 1 show the high superiority of ANN2 over ANN1, both in training and testing stages. Both networks ANN1 and ANN2 were trained with the same learning law (SCG), had the same number of neurons in the hidden (4 neurons) and output (1 neuron) layers; while the only difference between ANN1 and ANN2 was the number of neurons in the input layer (ANN1: 1 input neuron, ANN2: 8 input neurons) and the choice of input parameters. The superior performance of ANN2 over ANN1 both in training and prediction could be attributed to the additional number of neurons in the input layer and the inclusion of antecedent conditions. The 8 input neurons in ANN2 were used to account for antecedent rainfall and pore-water pressure conditions (see Eq.12) and this resulted in superior performance in training and prediction by ANN2. This shows that during pore-water pressure prediction it is necessary to account for antecedent pore-water pressure and rainfall conditions.

The prediction results (Figure 4b, Figure 5b and Table1) also suggest that SCG training algorithm is suitable for pore-water pressure prediction. ANN model with appropriate network architecture can be used for predicting time series of pore-water pressure responses to variations in rainfall pattern. It also appears that time series of pore-water pressure responses to rainfall which is known to be a function of many factors such as rainfall, evaporation, soil properties, antecedent conditions (Rahardjo, et al., 2008; Rezaur, et al., 2003) could be predicted using ANN from the knowledge of a relatively few factors only.

5. Conclusions

Multilayer Feed Forward neural network model with Scaled Conjugate Gradient (SCG) learning algorithm was developed to predict time series of pore-water pressure responses to rainfall. An appropriate network configuration that could map the nonlinear behavior of pore-water pressure responses (at 3 m soil depth) to climatic condition was identified to be 8–4–1. The study indicated that the SCG learning algorithm is suitable for application to problems associated with predictions of non-linear and complex behavior such as pore-water pressure variation during rainfall.

Predictions with a network architecture of 1-4-1 configuration led to unacceptable errors. The superiority of prediction accuracy with 8-4-1 configuration indicates the necessity of incorporating the antecedent values for the parameters. In other words, it is necessary to account for antecedent pore-water pressure and rainfall for prediction of pore-water pressure with reasonable accuracy.

Highly dynamic, non-linear and complex behavior of pore-water pressure, which is a function of many independent variables (i.e. rainfall, evaporation, soil properties, soil depth and antecedent conditions), could be predicted with ANN models with a modest number of input variables.

Acknowledgment

References

ASCE, T. C. (2000a). Artificial Neural Networks in Hydrology. I: Preliminary Concepts pages. *Journal of Hydrologic Engineering,* 5(2), 115-124.

ASCE, T. C. (2000b). Artificial Neural Networks In Hydrology. II: Hydrologic Applications. *Journal of Hydrologic Engineering,* 124-137.

Caudill, M. (1987). Neural Networks Primer, Part I. *AI Expert,* 2(12), 46-52.

Cestisli, B., & Barkana, A. (2010). Speeding up the scaled conjugate gradient algorithm and its application in neuro-fuzzy classifier training. *Soft Computing,* 14, 365-378.

Cigizoglu, H. K. (2004). Estimation and forecasting of daily suspended sediment data by multi-layer perceptrons. *Advances in Water Resources,* 27(2), 185-195. http://dx.doi.org/10.1016/j.advwatres.2003.10.003

Cigizoglu, H. K., & Alp, M. (2004). Rainfall-Runoff Modelling Using Three Neural Network Methods. In L. Falas, T., & Stafylopatis, A. (2005). Symbolic rule extraction with scaled conjugate gradient version of CLARION. *Proceedings of the International Joint Conference on Neural Networks, Montreal, Canada. July 31-August,* 4, 845–848.

Flood, I., & Kartam, N. (1994). Neural network in civil engineering-I: Principles and understanding. *Journal of Computing in Civil Engineering, ASCE,* 8(2), 131-148.

Hsu, K. L., Gupta, H. V., & Sorooshian, S. (1995). Artificial Neural Network Modeling of the Rainfall-Runoff Process. *Water Resour. Res.,* 31(10), 2517-2530. http://dx.doi.org/10.1029/95wr01955

Hu, T. S., Lam, K. C., & Ng, S. T. (2001). River flow time series prediction with a range-dependent neural network. *Hydrological Sciences Journal,* 46(5), 729-745. http://dx.doi.org/10.1080/02626660109492867

Kang, K. W., Kim, J. H., Park, J. C., & Ham, K. J. (1993). Evaluation of hydrological forecasting system based on neural network model. *Proceedings of the 25th Congress of IAHR IAHR Delft, The Netherlands,* 257–264.

Maier, H. R., & Dandy, G. C. (2000). Neural networks for the prediction and forecasting of water resources variables: a review of modelling issues and applications. *Environmental Modelling and Software,* 15(1), 101-124. http://dx.doi.org/10.1016/S1364-8152(99)00007-9

Meteorological-Service-Singapore. (1997). Summary of Observations (Annual Publication), Singapore.

Moller, M. F. (1993). A scaled conjugate gradient algorithm for fast supervised learning. *Neural Networks,* 6(4),

525–533.

Mustafa, M. R., Isa, M. H., & Rezaur, R. B. (2011). A Comparison of Artificial Neural Networks for Prediction of Suspended Sediment Discharge in River- A Case Study in Malaysia. International Conference on Environmental Sciences and Engineering ICESE-211, River View Hotel, Singapore, 372-376.

Rahardjo, H., Leong, E. C., & Rezaur, R. B. (2008). Effect of antecedent rainfall on pore-water pressure distribution characteristics in residual soil slopes under tropical rainfall. *Hydrological Processes,* 22(4), 506-523. http://dx.doi.org/10.1002/hyp.6880

Rezaur, R. B., Rahardjo, H., Leong, E. C., & Lee. (2003). Hydrological behavior of residual soil slopes in Singapore. J*ournal of Hydrologic Engineering, ASCE,* 8(3), 133-144.

Rojas, R. (1996). Neural Networks: A Systematic Introduction. *Springer Verlag,* Berlin, 151–184.

Rutkowski, J., Siekmann, R., Tadeusiewicz, & Zadeh, L. A. (2004). *Artificial Intelligence and Soft Computing – ICAISC* (Eds.)*,* 3070, 166-171, Springer Berlin / Heidelberg.

Schraudolph, N. N., & Graepel, T. (2002). Towards stochastic conjugate gradient methods. Proceedings of the 9th International Conference on Neural Information Processing, ICONIP-2002. *Piscataway,* NJ, USA, 853–856.

Tawfik, M., Ibharim, A., & Fahmy, H. (1997). Hysteresis sensitive Neural Network for modeling rating curves. *Journal of Computing in Civil Engineering, ASCE,* 11(3), 206-211.

Unal, B., Mamak, M., Seckin, G., & Cobaner, M. (2010). Comparison of an ANN approach with 1-D and 2-D methods for estimating discharge capacity of straight compound channels. *Adv. Eng. Softw.,* 41(2), 120-129. http://dx.doi.org/10.1016/j.advengsoft.2009.10.002

Table 1. Performance statistics of ANN models during training and testing

Model	Architecture[**]	Goal	Time (sec)	Epochs	RMSE Training	RMSE Testing
ANN1	1-4-1	0.001	3.28	500[*]	7.87	6.61
ANN2	8-4-1	0.001	0.83	82	0.48	0.98

[*]   Maximum numbers of epochs was reached but did not reach goal

[**]   Number of input neurons-Hidden neurons-Output neurons
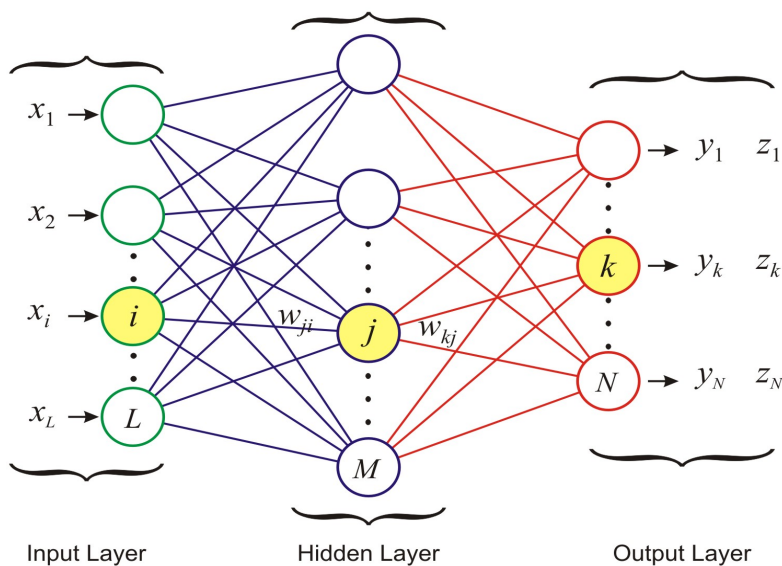
Figure 1. Schematic representation of an MLFF network
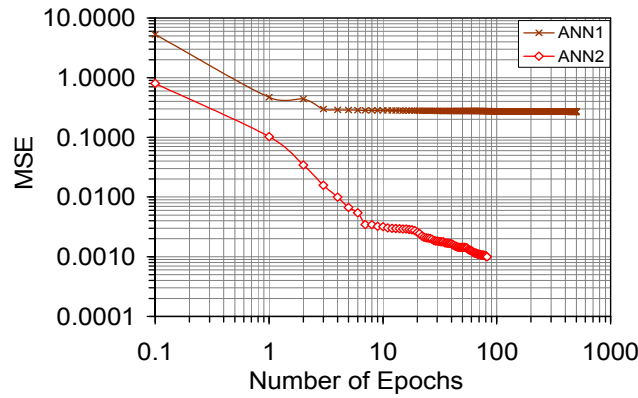
Figure 2a. Comparison of performance in terms of number of epochs to reach goal
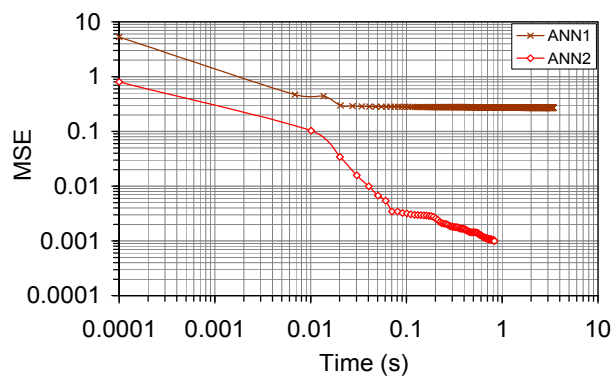
Figure 2b. Comparison of performance in terms of time to reach goal
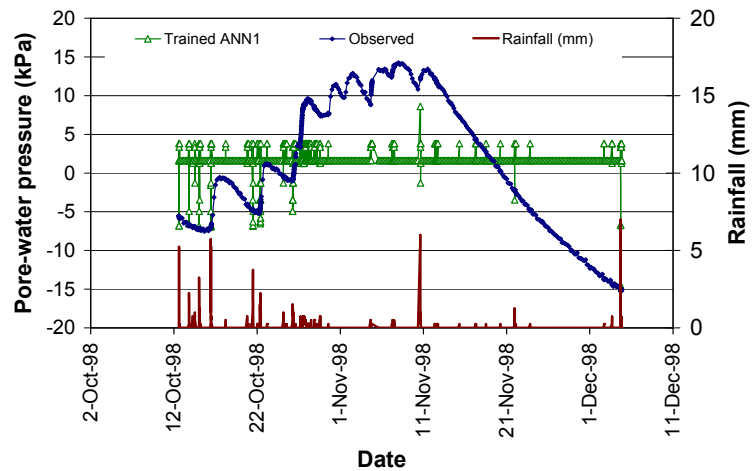
Figure 3a. Comparison between observed and trained time series of pore-water pressures after training using ANN1 model
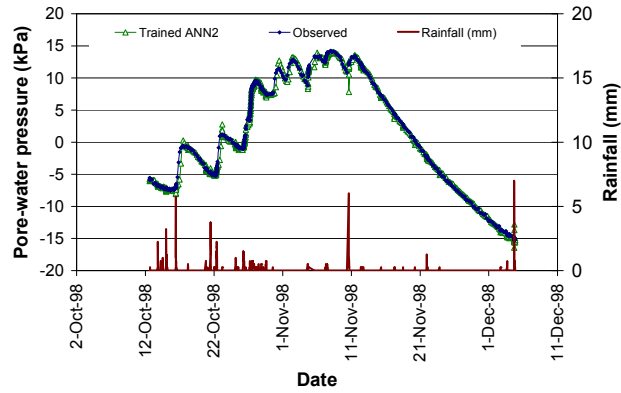
Figure 3b. Comparison between observed and trained time series of pore-water pressures after training using ANN2 model
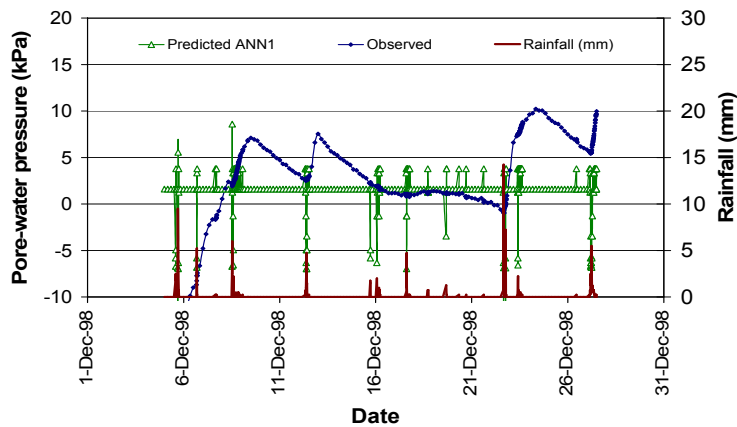
Figure 4a. Comparison between observed and predicted time series of pore-water pressures obtained during testing of ANN1 model
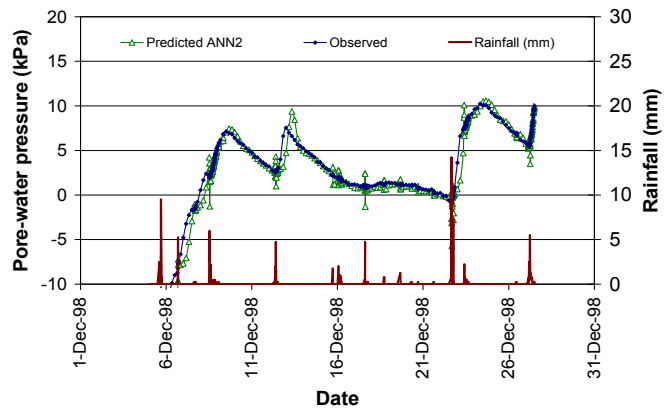
Figure 4b. Comparison between observed and predicted time series of pore-water pressures obtained during testing of ANN2 model
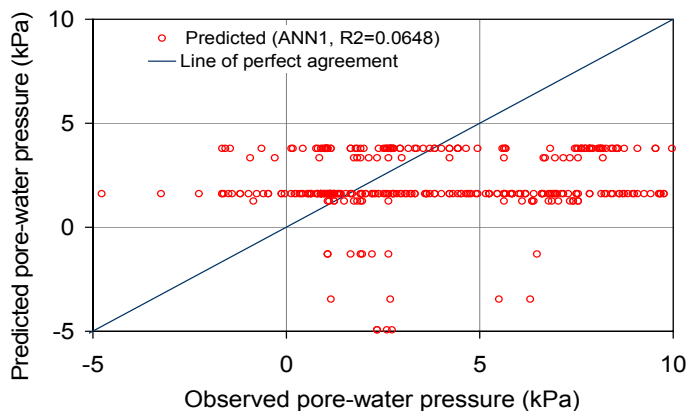
Figure 5a. Comparison between observed and predicted pore-water pressures of ANN1 model
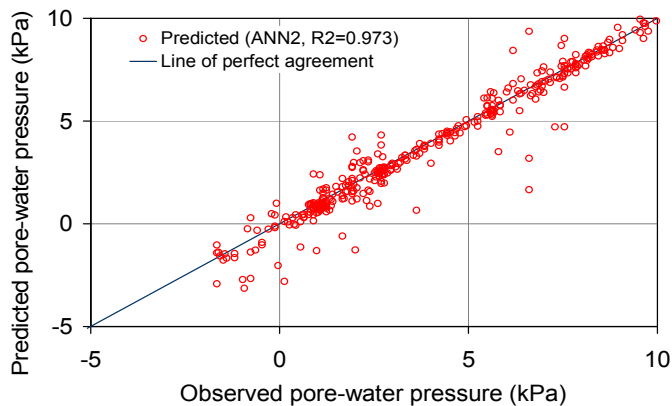
Figure 5b. Comparison between observed and predicted pore-water pressures of ANN2 model

Hybrid Projective Dislocated Synchronization of Liu Chaotic System Based on Parameters Identification

Yanfei Chen

College of Science, Guilin University of Technology

Guilin 541004, China

Tel: 86-139-7838-5785   E-mail: chenyanfei2010@126.com

Zhen Jia (Corresponding author)

College of Science, Guilin University of Technology

Guangxi Key Laboratory of Spatial Information and Geomatics, Guilin University of Technology

Guilin 541004, China

Tel: 86-159-0787-8165   E-mail: jjjzzz0@163.com

Abstract

This letter discusses hybrid projective dislocated synchronization of Liu chaotic system with five uncertain parameters. Based on adaptive technique, the hybrid projective dislocated synchronization of Liu chaotic system is achieved by designing a novel nonlinear controller. Furthermore, the parameters identification is realized simultaneously. A sufficient condition is given and proved theoretically by Lyapunov stability theory and LaSalle's invariance principle. Finally, the numerical simulations are provided to show the effectiveness and feasibility of the proposed method.

Keywords: Hybrid projective dislocated synchronization, Parameters identification, Liu chaotic system, Adaptive technique

1. Introduction

Since the pioneering work on chaos synchronization by Pecora and Carroll in 1990 (Pecora, 1990), chaos synchronization has attracted much attraction due to its potential applications in many practical engineering fields, such as secure communication, information processing, chemical reaction, and so on. In the past two decades, many types of synchronization phenomena have been studied, namely, complete synchronization (Lu, 2005), generalized synchronization (Jia, 2008), phase synchronization (Ho, 2002), lag synchronization (Chen, 2007), etc. Meanwhile, many schemes for chaos synchronization have been proposed, including linear and nonlinear feedback approach (Wang, 2006; Jia, 2007), adaptive technique (Jia, 2007), coupled method (Chen, 2011), impulsive control method (Luo, 2008), among many others.

Mainieri and Rehacek considered a type of chaos synchronization, called projective synchronization (Mainieri, 1999), where the corresponding state vectors of drive-response systems could be synchronized up to a constant scaling factor. In Ref. (Hu, 2007), Hu et al. proposed a dislocated synchronization method. In this paper, we investigate the hybrid projective dislocated synchronization and parameters identification of Liu chaotic system. In this scheme, every state variable of drive system synchronizes other mismatched state variables of response system with different scaling factors. Based on the adaptive technique, a novel controller and parameter adaptive laws are designed such that parameters identification is realized, and hybrid projective dislocated synchronization of Liu chaotic system is achieved simultaneously.

This work is organized as follows. The drive and response systems are described and hybrid projective

dislocated synchronization errors are theoretically analyzed in section 2. In section 3, a general scheme for hybrid projective dislocated synchronization of Liu chaotic system and parameters identification is proved. Section 4 presents some numerical simulations to show the effectiveness of the proposed scheme. Finally, conclusions are shown.

2. Problem Formulation

The Liu chaotic system (Liu, 2004) as the drive system is given by

$$\begin{cases} \dot{x}_1 = a(x_2 - x_1), \\ \dot{x}_2 = bx_1 - kx_1x_3, \\ \dot{x}_3 = -cx_3 + hx_1^2, \end{cases} \tag{1}$$

having a chaotic attractor when $a = 10, b = 40, c = 2.5, h = 4, k = 1$. Here the Lyapunov exponents of system (1) are found to be $L_1 = 1.64328, L_2 = 0, L_3 = -14.42$. The phase portrait is shown in Figure 1.

Considering the drive system (1), the response system is controlled Liu chaotic system as following

$$\begin{cases} \dot{y}_1 = a_s(y_2 - y_1) + u_1, \\ \dot{y}_2 = b_s y_1 - k_s y_1 y_3 + u_2, \\ \dot{y}_3 = -c_s y_3 + h_s y_1^2 + u_3, \end{cases} \tag{2}$$

where the system parameters a_s, b_s, c_s, h_s, k_s of (2) are unknown, $U = [u_1, u_2, u_3]^T$ is the controller which should be designed. Therefore, the goal of parameters identification and hybrid projective dislocated synchronization is to find an appropriate controller $U = [u_1, u_2, u_3]^T$ and parameter adaptive laws of a_s, b_s, c_s, h_s, k_s, such that the synchronization errors

$$e_1 = y_1 - \lambda_2 x_2 \to 0, e_2 = y_2 - \lambda_3 x_3 \to 0, e_3 = y_3 - \lambda_1 x_1 \to 0 \text{ as } t \to \infty \tag{3}$$

and the unknown parameters

$$\lim_{t \to \infty} a_s = a, \lim_{t \to \infty} b_s = b, \lim_{t \to \infty} c_s = c, \lim_{t \to \infty} h_s = h, \lim_{t \to \infty} k_s = k. \tag{4}$$

where $\lambda_1, \lambda_2, \lambda_3$ are the scaling factors.

Remark 1 When $\lambda_1 \neq \lambda_2$ or $\lambda_1 \neq \lambda_3$, the hybrid projective dislocated synchronization will appear. When $\lambda_1 = \lambda_2 = \lambda_3$, projective dislocated synchronization will appear. More in general, dislocated synchronization and dislocated anti-synchronization will appear when $\lambda_i = 1$ and $\lambda_i = -1, i = 1, 2, 3$, respectively.

Remark 2 Here are another four types of hybrid projective dislocated synchronization errors

$$(\text{I}) \begin{cases} e_1 = y_1 - \lambda_1 x_1, \\ e_2 = y_2 - \lambda_3 x_3, \\ e_3 = y_3 - \lambda_2 x_2. \end{cases} (\text{II}) \begin{cases} e_1 = y_1 - \lambda_2 x_2, \\ e_2 = y_2 - \lambda_1 x_1, \\ e_3 = y_3 - \lambda_3 x_3. \end{cases} (\text{III}) \begin{cases} e_1 = y_1 - \lambda_3 x_3, \\ e_2 = y_2 - \lambda_1 x_1, \\ e_3 = y_3 - \lambda_2 x_2. \end{cases} (\text{IV}) \begin{cases} e_1 = y_1 - \lambda_3 x_3, \\ e_2 = y_2 - \lambda_2 x_2, \\ e_3 = y_3 - \lambda_1 x_1. \end{cases}$$

For these cases, the discussions are similar to the method given in this paper.

3. Hybrid Projective Dislocated Synchronization of Liu Chaotic System

In this section, based upon the nonlinear adaptive feedback control technique, a systematic design process of parameters identification and hybrid projective dislocated synchronization of Liu chaotic system under the situation of response system with unknown parameters is provided.

According to the systems (1) and (2), the errors dynamical system can be obtained as follows.

$$\begin{cases} \dot{e}_1 = -ae_1 - (a_s - a)y_1 + a_s y_2 + k\lambda_2 x_1 x_3 - b\lambda_2 x_1 - a\lambda_2 x_2 + u_1, \\ \dot{e}_2 = -ce_2 + (b_s - b)y_1 - (k_s - k)y_1 y_3 - ky_1 y_3 + by_1 + cy_2 - h\lambda_3 x_1^2 + u_2, \\ \dot{e}_3 = -ae_3 - (c_s - c)y_3 + (h_s - h)y_1^2 + hy_1^2 - (c - a)y_3 - a\lambda_2 x_2 + u_3. \end{cases} \tag{5}$$

Obviously, hybrid projective dislocated synchronization of systems (1) and (2) appears if the errors dynamical system (5) has an asymptotically stable equilibrium point $e = 0$, where $e = [e_1, e_2, e_3]^T$.

Thus, we design the controller and parameter adaptive laws as the following theorem.

Theorem Assuming that the Liu chaotic system (1) drives the controlled Liu chaotic system (2), take

$$\begin{cases} u_1 = -a_s y_2 - k\lambda_2 x_1 x_3 + b\lambda_2 x_1 + a\lambda_2 x_2, \\ u_2 = ky_1 y_3 - by_1 - cy_2 + h\lambda_3 x_1^2, \\ u_3 = -hy_1^2 + (c-a)y_3 + a\lambda_1 x_2, \end{cases} \tag{6}$$

and parameter adaptive laws

$$\begin{cases} \dot{a}_s = y_1 e_1, \\ \dot{b}_s = -y_1 e_2, \\ \dot{c}_s = y_3 e_3, \\ \dot{h}_s = -y_1^2 e_3, \\ \dot{k}_s = y_1 y_3 e_2. \end{cases} \tag{7}$$

Systems (1) and (2) can realize hybrid projective dislocated synchronization and the unknown parameters will be identified, i.e., Eqs. (3) and (4) will be achieved.

Proof Eq. (5) can be converted to the following form under the controller (6)

$$\begin{cases} \dot{e}_1 = -ae_1 - (a_s - a)y_1, \\ \dot{e}_2 = -ce_2 + (b_s - b)y_1 - (k_s - k)y_1 y_3, \\ \dot{e}_3 = -ae_3 - (c_s - c)y_3 + (h_s - h)y_1^2. \end{cases} \tag{8}$$

Consider the following Lyapunov function

$$V = \frac{1}{2}\left[e_1^2 + e_2^2 + e_3^2 + (a_s - a)^2 + (b_s - b)^2 + (c_s - c)^2 + (h_s - h)^2 + (k_s - k)^2\right],$$

Obviously, V is a positive definite function. Taking its time derivative along with the trajectories of Eqs. (8) and (7) leads to

$$\begin{aligned} \dot{V} &= e_1\dot{e}_1 + e_2\dot{e}_2 + e_3\dot{e}_3 + (a_s - a)\dot{a}_s + (b_s - b)\dot{b}_s + (c_s - c)\dot{c}_s + (k_s - k)\dot{k}_s + (h_s - h)\dot{h}_s \\ &= -ae_1^2 - ce_2^2 - ae_3^2 = -e^T Pe \le 0, \end{aligned} \tag{9}$$

It is obvious that $\dot{V} = 0$ if and only if $e_i = 0, i = 1, 2, 3$, namely the set $M = \{e = 0, a_s = a, b_s = b, c_s = c, \ h_s = h, k_s = k\}$ is the largest invariant set contained in $E = \{\dot{V} = 0\}$ for Eq. (8). So according to the LaSalle's invariance principle (Lasalle, 1960), starting with arbitrary initial values of Eq. (8), the trajectory converges asymptotically to the set M, i.e., $e \to 0, a_s \to a, b_s \to b, c_s \to c, h_s \to h$ and $k_s \to k$ as $t \to \infty$. This indicates that the hybrid projective dislocated synchronization of Liu chaotic system is achieved and the unknown parameters a_s, b_s, c_s, h_s, k_s can be successfully identified by using controller (6) and parameter adaptive laws (7). Now the proof is completed.

Remark 3 Taking our adaptive synchronization method, we can not only achieve synchronization but also identify the system parameters.

4. Numerical Simulation

In this section, some numerical simulations about the hybrid projective dislocated synchronization and parameters identification between systems (1) and (2) are given to verify the effectiveness and feasibility of the proposed technique. In the numerical simulations, all the differential equations are solved by using the fourth-order Runge-Kutta method.

We assume that the drive signals are from the Liu chaotic system (1) with system parameters $a = 10, b = 40, c = 2, 5, h = 4, k = 1$ and the initial values $x(0) = [2.2, 2.4, 38]^T$, the initial values of controlled Liu chaotic system (2) is $y(0) = [9, -2, -15]^T$ and the unknown parameters have zero initial condition. The three scaling factors are chosen as $\lambda_1 = -2, \lambda_2 = 1, \lambda_3 = 2.8$. The simulation results are shown in Figures 2 and 3. Figure 2 (a)-(c) display the errors state response of systems (1) and (2), Figure 3 shows the identification results of unknown parameters a_s, b_s, c_s, h_s, k_s.

5. Conclusion

In this letter, we introduce an adaptive hybrid projective dislocated synchronization and parameters identification scheme for the Liu chaotic system with the response system parameters unknown. With this scheme we can achieve hybrid projective dislocated synchronization and parameters identification simultaneously. Theoretical proof and numerical simulations demonstrate the effectiveness of the proposed scheme.

It should be pointed out that, although this process is focused on the Liu chaotic system, the systematic design process could be used for many other complex dynamical systems with unknown parameters.

References

Chen, Y., Chen, X., & Chen, S. (2007). Lag synchronization of structurally nonequivalent chaotic systems with time delays. *Nonlinear Analysis,* 66, 1929-1937. http://dx.doi.org/10.1016/j.na.2006.02.033

Chen, J., Lu, J., & Wu, X. (2011). Bidirectionally coupled synchronization of the generalized Lorenz system. *J Syst Sci Complex*, 24, 443-448. http://dx.doi.org/10.1007/s11424-010-8323-2

Ho, M. C., Hung, Y. C., & Chou, C. H. (2002). Phase and anti-phase synchronization of two chaotic systems by using active control. *Phys. Lett. A.*, 296, 43-48. http://dx.doi.org/10.1016/S0375-9601(02)00074-9

Hu, M., & Xu, Z. (2007). Nonlinear feedback mismatch synchronization of Lorenz chaotic sysytems. *Syst Eng Electr*, 29(8), 1346-1348.

Jia, Z. (2008). Linear generalized synchronization of chaotic systems with uncertain parameters. *J Syst Eng Electr,* 19(4), 779-784. http://dx.doi.org/10.1016/S1004-4132(08)60153-X

Jia, Z., Lu, J. A., & Deng, G. M. (2007). Nonlinear state feedback and adaptive synchronization of hyperchaotic Lü systems. *Syst Eng Electr*, 29(4), 598-600.

Lasalle, J. P. (1960). The extent of asymptotic stability. *Proc. Natl. Acad. Sci. U.S.A.*, 46(3), 363-365. http://dx.doi.org/10.1073/pnas.46.3.363

Liu, C., Liu, T., Liu, L., & Liu, K. (2004). A new chaotic attractor. *Chaos, Solitons & Fractals*, 22, 1031-1038. http://dx.doi.org/10.1016/j.chaos.2004.02.060

Luo, R. Z. (2008). Impulsive control and synchronization of a new chaotic system. *Phys .Lett. A,* 372, 648-653. http://dx.doi.org/10.1016/j.physleta.2007.08.010

Lu, J., & Cao, J. (2005). Adaptive complete synchronization of two identical or different chaotic (hyperchaotic) systems with fully unknown parameters. *Chaos*, 15(4), 043901. http://dx.doi.org/10.1063/1.2089207

Mainieri, R., & Rehacek, J. (1999). Projective synchronization in three-dimensional chaotic systems. Phys. Rev. Lett., 82(15), 3042-3045. http://dx.doi.org/10.1103/PhysRevLett.82.3042

Pecora, L. M., & Carroll, T. L. (1990). Synchronization in chaotic systems. *Phys. Rev. Lett.,* 64(8), 821-824. http://dx.doi.org/10.1103/PhysRevLett.64.821

Wang, F., & Liu, C. (2006). A new criterion for chaos and hyperchaos synchronization using linear feedback control. *Phys.Lett.A*, 360, 274-278. http://dx.doi.org/10.1016/j.physleta.2006.08.037
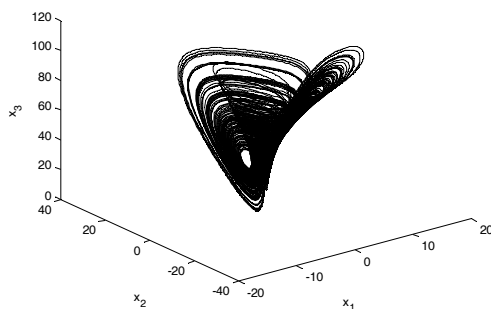
Figure 1. The phase portrait of Liu chaotic system (1) with parameter values

$$a = 10, b = 40, c = 2.5, h = 4, k = 1$$

(a)

(b)

(c)
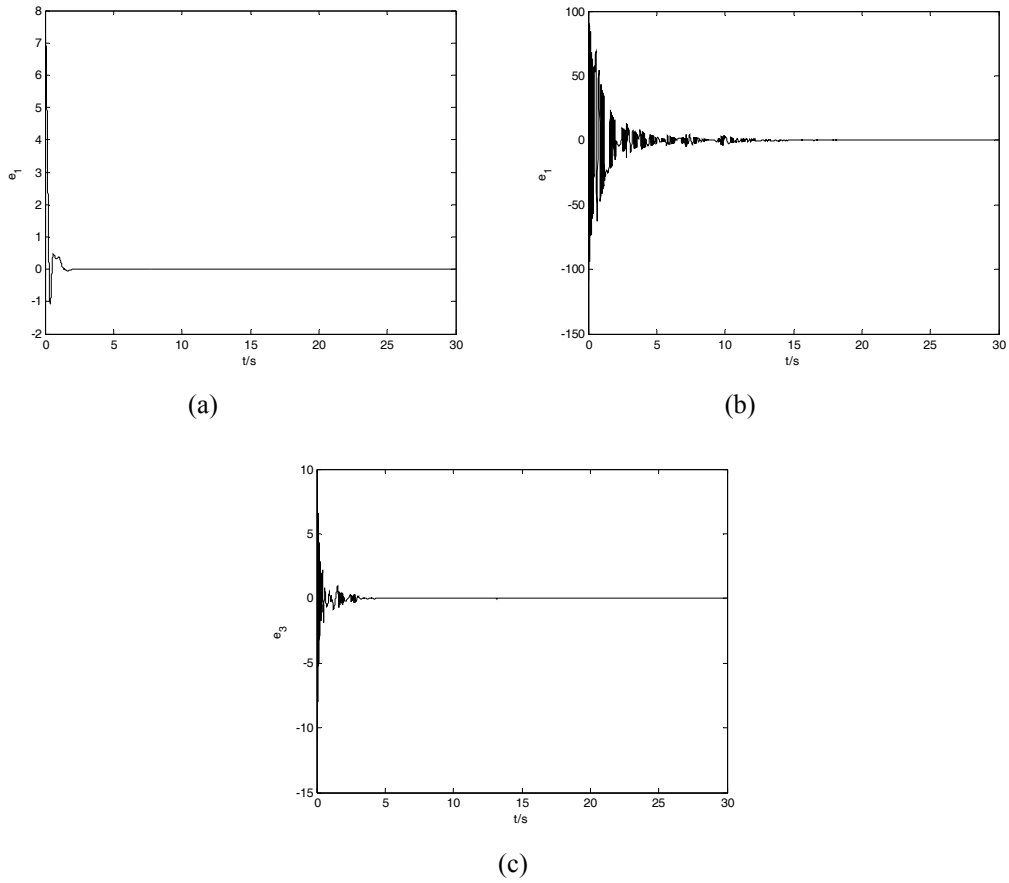
Figure 2. The synchronization error evolutions of systems (1) and (2):

(a) $e_1 = y_1 - x_2$; (b) $e_2 = y_2 - 2.8x_3$; (c) $e_3 = y_3 + 2x_1$

(a)

(b)

(c)

(d)

(e)
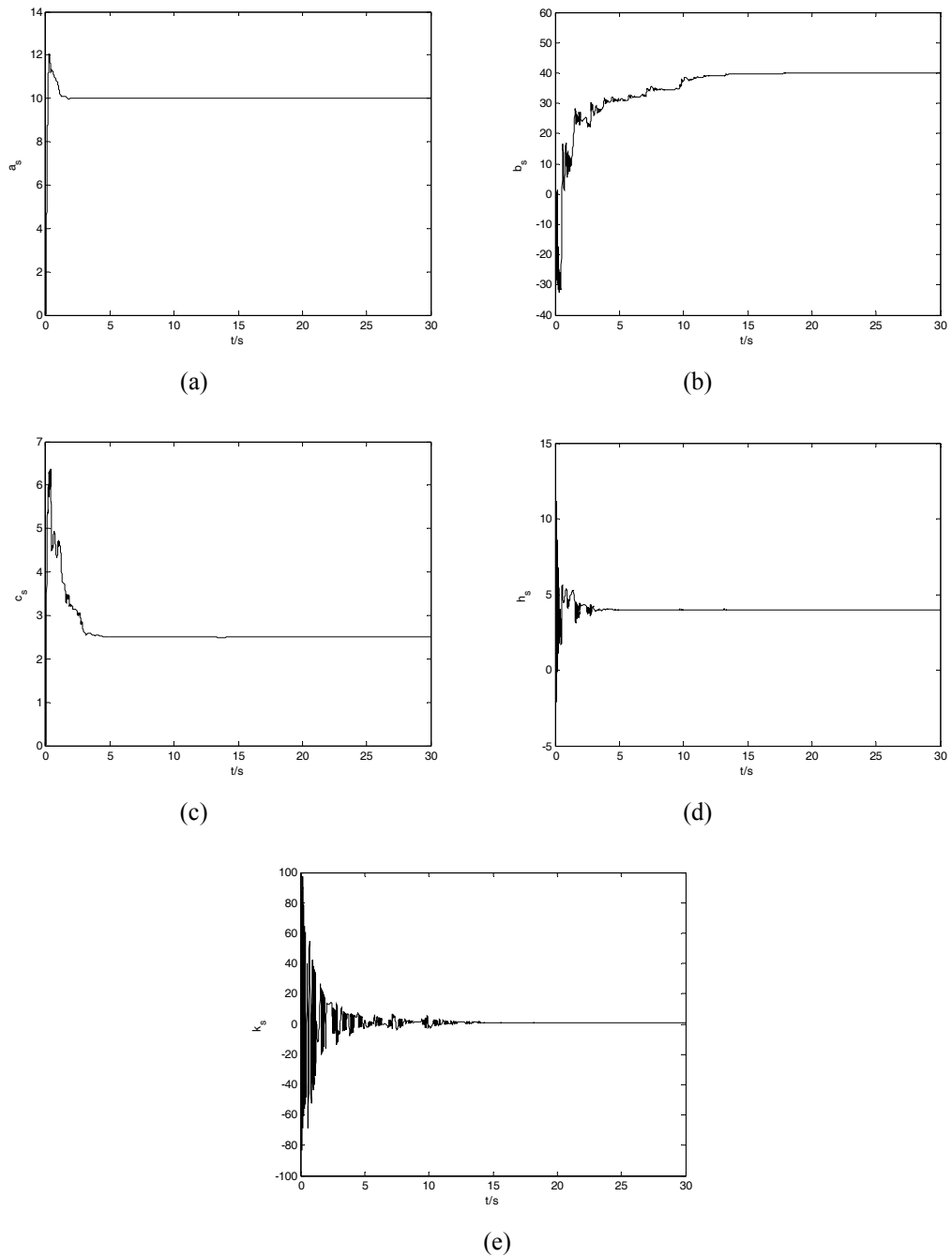
Figure 3. The parameters identification results of response system (2):

(a) $a_s = 10$; (b) $b_s = 40$; (c) $c_s = 2.5$; (d) $h_s = 4$; (e) $k_s = 1$

A Fuzzy Based Solution for Improving Power Quality in Electric Railway Networks

Mohammad Ali Sandidzadeh

School of Railway Engineering, Iran University of Science & Technology, Tehran, Iran

Tel: 98-21-7749-1030   E-mail: sandidzadeh@iust.ac.ir

Saleh Akbari

School of Railway Engineering, Iran University of Science & Technology, Tehran, Iran

E-mail: Sakbari118@gmail.com

Abstract

There are many fundamental differences between electric traction networks and other industrial supply networks in terms of dynamic behavior and static characteristics. For example, the time variation of a load causes voltage variations in a supply network, which results in variations of power flow in the supply network. Today, reactive power compensators are the most practical solutions for keeping voltage levels in normal boundaries. In this paper, with the aim of fuzzy logic, a method for compensating reactive power losses in electrical traction networks is proposed. The proposed method has many advantages such as decreasing the reactive power compensation costs, determining the optimum switching step of capacitor banks and deducing the losses in electric traction networks.

Keywords: Reactive Power, Electric Traction Networks, Railway Electrification, Fuzzy Logic

1. Introduction

Reactive power creates numerous problems in electric railway supply networks. Because of the particular characteristics of electric traction loads, the problems have higher intensity in railway supply networks than other types of electric supply networks. Reactive power can be compensated by implementation of active or static methods. Nowadays a common method, in most electric substations, is to use shunt capacitors (Chin H. C., & Lin Wh. M., 1994; Baghzouz Y., & Ertem S., 1995). The advantages and disadvantages of this method are explained in Table 1.

Allocation of these shunt capacitors in the network shall be according to the power network topology. Electric railway networks has individual characteristic such as time variant and location variant trains' power demand. So, this paper proposed improving power quality based on optimization of capacitor allocation in electric railway power supply network. In next sections, this solution is expressed.

2. Calculation of the Capacitor Power for Power Factor Correction

In three phase circuits, the power factor correction capacitor is installed as shown in Figure 1. The capacitor power can be calculated from equation (1) (Chin Hong-Chan, & Lin Whei-min, 1996).

$$Q_C = P_L \left(\tan\phi_o - \tan\phi_C \right) \tag{1}$$

In Figure1, phases a and b are the supplying overhead lines in both sides and C_1 and C_2 are the shunt capacitors. In a traction substation, the power factor is obtained from

$$Cos\varphi = \frac{W_{P\varepsilon}}{\sqrt{W_{P\varepsilon}^2 + W_{Q\varepsilon}^2}} \tag{2}$$

Where $W_{P\varepsilon}$ is the measured active power (kWh) and $W_{Q\varepsilon}$ is the measured reactive power (kvarh) (Baghzouz Y., & Ertem S., 1990). In the electric railway supply circuit, by considering the circuit, the capacitor power can be calculated from

$$Q_C = P_L (\tan \phi_O - \tan \phi_C) \frac{1}{1 - P_O} \tag{3}$$

Where P_o is the circuit no-load probability. Generally, implantation of capacitors in three phases (between the lag, lead or no-load phases) is not necessary. Capacitors are usually installed in circuits in the following ways (Shirmohamadi D., et al., 1988):

  I.   If $I_{lead} \gg I_{lagging}$ capacitor in lag and lead phases

  II. If $I_{lead} \ll I_{lagging}$ capacitor in no-load and lag phases

  III. If $I_{lead} = I_{lagging}$ capacitor in the lag phase

In case II, it is also possible to install the capacitor in the lead phases; however, this would be harmful to the network power factor.

3. Cost Equation

After calculating the loss and considering the required capacitor for reactive power compensations, the cost value (Chin Hong-Chan, & Lin Whei-min, 1994) can be acquired from

$$f = K_p P_{Loss} + \sum_{j=1}^{k} K_j Q_j \tag{4}$$

where K_P is the cost of the reactive losses, P_{loss} is the total losses of the overhead network in each step of capacitor allocation, J $(=1,2,...,K)$ is the selected bus for capacitor installation, K_j is the minimum cost of possible circumstance coefficients plus the installation and maintenance, and Q_j is the total power of the existing capacitors.

4. Problems' Constraints

Each optimization problem usually includes constraints. The operational constraint is the voltage amplitude in traction substations, which must be kept in the permitted limits of

$$v \min \leq |v_i| \leq v \max \tag{5}$$

where V_i is the voltage of substation i, and V_{max} and V_{min} are the maximum and minimum permitted voltages, respectively.

5. Determining the Required Capacitor Power via Fuzzy Logic

Various capacitor allocation methods are implemented for minimization of the reactive power losses. One of the implemented methods is based on Fuzzy logic that can assign sensitive points for capacitor installation. A Fuzzy-logic based solution benefits from high accuracy, response rate and μp (Chin Hong-Chan, & Lin Whei-min, 1996).

In this research, the active power losses are used as the static input data to the fuzzy sensitive system of voltage in the electric train location (or bus).

It should be noted that the minimum membership functions of the reactive power and bus voltage sensitiveness have assigned the required capacitor power in each operation period. Thus any increase in the losses results in an increase in the value of the membership function. Also, any decrease in the losses results in a decrease in the value of the membership function. One of the useful equations for demonstration of the function is

$$\mu_p(i) = e^{-\frac{wP(Li)}{P_{Loss}}} \tag{6}$$

where w is the weight coefficient obtained from

$$w = \frac{P(Li)}{P_t} \tag{7}$$

where $P(L_i)$ is the active power losses in the train to the substation circuit, P_t is the total active power of other trains and P_{Loss} is the sum of the active power losses.

In order to find a solution for the bus voltage sensitiveness problem, in case of large voltage deviations, a low membership function is taken into account. Thus, the relative membership function can be expressed as

$$\mu_v(i) = e^{-w\left[\frac{v(i)-1}{v\max - v\min}\right]^2} \tag{8}$$

where $v(i)$ is the voltage of bus i, V_{max} is the maximum voltage limit, V_{min} is the minimum voltage limit and w is the weight coefficient acquired from equation 7. Generally for calculating the required capacitor power, both the bus voltage sensitiveness (as in Figure 2) and the active losses (as in Figure 3) factors should be considered. Therefore it becomes necessary to define a decision function that contains μs.

For finding the candidate locations for capacitor installation, both the active losses and the voltage sensitiveness factor are vital. Thus, considering the mentioned factors, a comprehensive decision function can be defined as

$$\mu_s(i) = \min\{\mu_v(i), \mu_p(i)\} \quad i=1, 2, \ldots, m \tag{9}$$

The minimum point of the membership function is selected as the candidate location for capacitor installation. The low value of μ_s indicates that the point of the overhead network has a very high sensitiveness to voltage deviations and power losses.

6. Explanation of the Fuzzy-based Procedure

Figure 4 explains the Flowchart of the Optimum Capacitor Allocation Procedure in the Electric Railway Overhead Network.

The main steps of this procedure are (Ng H. N., et.al, 2000):

    i.   Calculating the network load flow, determining voltages and losses of the buses, and calculating μ_p and μ_v.

    ii.   Distinguishing the candidate point (i.e. bus M) by considering the minimum decision function.

    iii.   Determining the capacitor power, which satisfies both the voltage and the cost constraints, after performing the capacitor installation steps in bus M and running the load flow. If any capacitor power value does not satisfy voltage constraints of a selected bus, the bus should be eliminated from the list of candidate buses.

    iv.   After eliminating bus M from the decision function and setting the calculated capacitor on it, the load flow is run and a new decision function is formed without considering bus M.

    v.   Distinguishing the new candidate bus from the new decision function, then jumping to step iii.

    vi.   The flowchart should be taken into account until it satisfies the voltage constraints. Also decreasing the cost value in an instant step from proceeding is lower than the defined minimum value for all buses.

One of the advantages of the demonstrated flowchart is that it considers the voltage constraints, while minimizing the active losses and therefore the corresponding cost function. In addition, the introduced procedure is capable of solving minimization of active losses problem (i.e. minimization of the cost function). The procedure can also determine the location and rate of the required capacitor for installation in the overhead network, provided that the bus voltages are in the permitted limits.

7. Simulation Results and Comparisons

7.1 The Required Information

A radial supply feeder is considered and presented in Figure 5. The feeder has 9 load buses (an electric train per block), a nominal voltage of 25 kV and a rated power of 15 MVA.

The loads and the feeder data of the assumed overhead network are shown in Tables 2 and 3. Other data presented are: V_{min} =0.9 p.u., V_{max} =1.1 p.u. and kp =168 \$/kW.

In Table 2, the maximum capacitor power should not exceed the total reactive power (i.e. 4186 VAR). Therefore, regarding the existing capacitor and the minimum cost conditions (including the maintenance, installation and purchase costs), the capacitor step value and the corresponding cost coefficients can be acquired from Table 4. The network load flow results before compensation via the presented procedure are shown in Table 5.

It is clear from Table 6 that the costs and total losses in the presented procedure have more appropriate values than the referenced value in (Chin H. C., & Lin Wh. M., 1994).

8. Flowchart Implementation Results

According to Table 7, the probable rates of the capacitors are obtained by considering the corresponding cost coefficients in every step of the calculations. The voltage magnitudes for each selected item are shown in Table 8.

9. Conclusion

An appropriate method for determining the capacitors rates in each step, by considering the voltage magnitude constraints and the cost of losses, was proposed. In the proposed method, by setting the capacitor conditions in each period of operation and considering the absorbed power from each substation and the number of trains in each line, it became possible to ensure the improvement of the power quality index of the electric railway networks. In addition, the proposed Fuzzy-based solution had many advantages such as optimization of the compensation steps and reduction of the compensation costs.

Acknowledgement

References

Baghzouz, Y., Ertem, S. (1990). Shunt Capacitor Sizing for Radial Distribution Feeders with Disturbed Substation Voltages. *IEEE Trans. on Power Delivery,* 5(2), 650-657. http://dx.doi.org/10.1109/61.53067

Chin, H. C., Lin, W. M. (1994). Capacitor Placements for Distribution Systems with Fuzzy Algorithm. *Theme frontiers of computer technology.* TECON94, IEEE Region 10's, Ninth annual international conference, Proceedings of Aug., pp. 22-26.

Ng, H. N., et al. (2000). Capacitor Allocation by Approximate Reasoning: Fuzzy Capacitor Placement. *IEEE Trans. on Power Delivery,* 15(1), 393-398. http://dx.doi.org/10.1109/61.847279

Ng, H. N., Salama, M. M. A., Chikhani, A. Y. (1996). Capacitor Placement in Distribution System Using Fuzzy Technique. *IEEE electrical and computer conference,* 2, 26-29.

Shirmohamadi, D., et al. (1988). A Compensation-based Power Flow Method for Weakly Meshed Distribution and Transmission Networks. *IEEE Trans. on Power Systems,* 3(2), 753-762. http://dx.doi.org/10.1109/59.192932

Table 1. Advantages and disadvantages of compensating the reactive power via shunt capacitors

Disadvantages	Advantages
-Insufficient life cycle	-Improvements of network utilization coefficient
-Instability during faulty conditions	-Deduction of losses
-Increased switching over voltages	-Power supply quality improvement
-Accretion in shunt resonance occurrence probability	-Deduction of negative sequence component
	-Improvement of Total Harmonic Distortion (THD) factor
	-Simple installation

Table 2. Load data of assumed overhead network

Number of Bus	P (KW)	Q (KVar)
1	460	1840
2	340	980
3	446	1790
4	1840	1598
5	600	1610
6	110	780
7	60	1150
8	130	980
9	200	1640

Table 3. Feeder data of assumed overhead network

Primary Bus (i)	Final Bus (i+1)	R(Ω)	X(Ω)
0	1	0.1233	0.4127
1	2	0.014	0.6051
2	3	0.7463	1.205
3	4	0.6984	0.6084
4	5	1.9831	1.7276
5	6	1.905	0.7886
6	7	2.0552	1.164
7	8	4.7953	2.716
8	9	5.3434	3.0264

Table 4. Variable choices of capacitor rates and corresponding cost coefficients

J	Q	K_i($/kvar)	J	Q	K_i($/kvar)
1	150	0.5	15	2250	0.197
2	300	0.5	16	2400	0.17
3	450	0.253	17	2550	0.189
4	600	0.22	18	2700	0.187
5	750	0.276	19	2850	0.183
6	900	0.183	20	3000	0.18
7	1050	0.228	21	3150	0.195
8	1200	0.17	22	3300	0.174
9	1350	0.207	23	3450	0.188
10	1500	0.201	24	3600	0.17
11	1650	0.193	25	3750	0.183
12	1800	0.187	26	3900	0.182
13	1950	0.211	27	4050	0.179
14	2100	0.176	---	---	---

Table 5. Bus voltage results

J	Q	Voltage (the defined method in this paper)
1	0.993	0.9929
2	0.987	0.9874
3	0.963	0.967
4	0.984	0.9482
5	0.917	0.9175
6	0.907	0.908
7	0.889	0.8892
8	0.859	0.8593
9	0.838	0.8382

Table 6. The results of comparing the presented procedure with reference value

Reference (Chin H. C., 1994)			Defined method in this paper					
119,736			119007.4					Total losses($/kvar)
707			701.66					Total losses(kW)
9	5	4	9	8	5	4	3	Compensated buses
900	2500	2100	900	300	1800	450	2400	Q_c(kvar)

Table 7. Variable choices of capacitor rates and the corresponding cost coefficients

J	Q	Kj($/kvar)
1	150	0.5
2	300	0.5
3	450	0.253
4	600	0.22
5	750	0.276
6	900	0.183
7	1050	0.228
8	1200	0.170
9	1350	0.207

Table 8. The voltages of the bus after capacitor placement

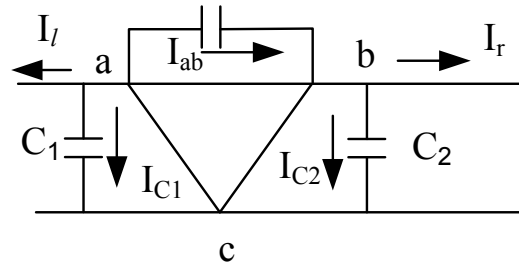| Scenario	Voltage
1	0.993
2	0.9874
3	0.967
4	0.948
5	0.917
6	0.908
7	0.889
8	0.859
9	0.834

Figure 1. Power factor correction in a three-phase circuit by using shunt capacitors
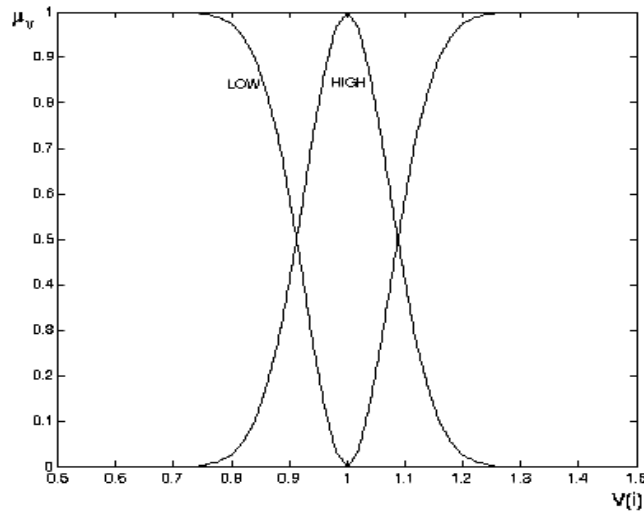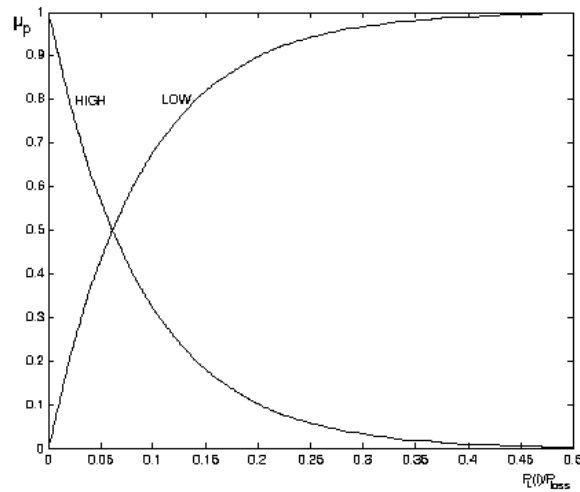

Figure 2. Voltage sensitivity membership function(μv)

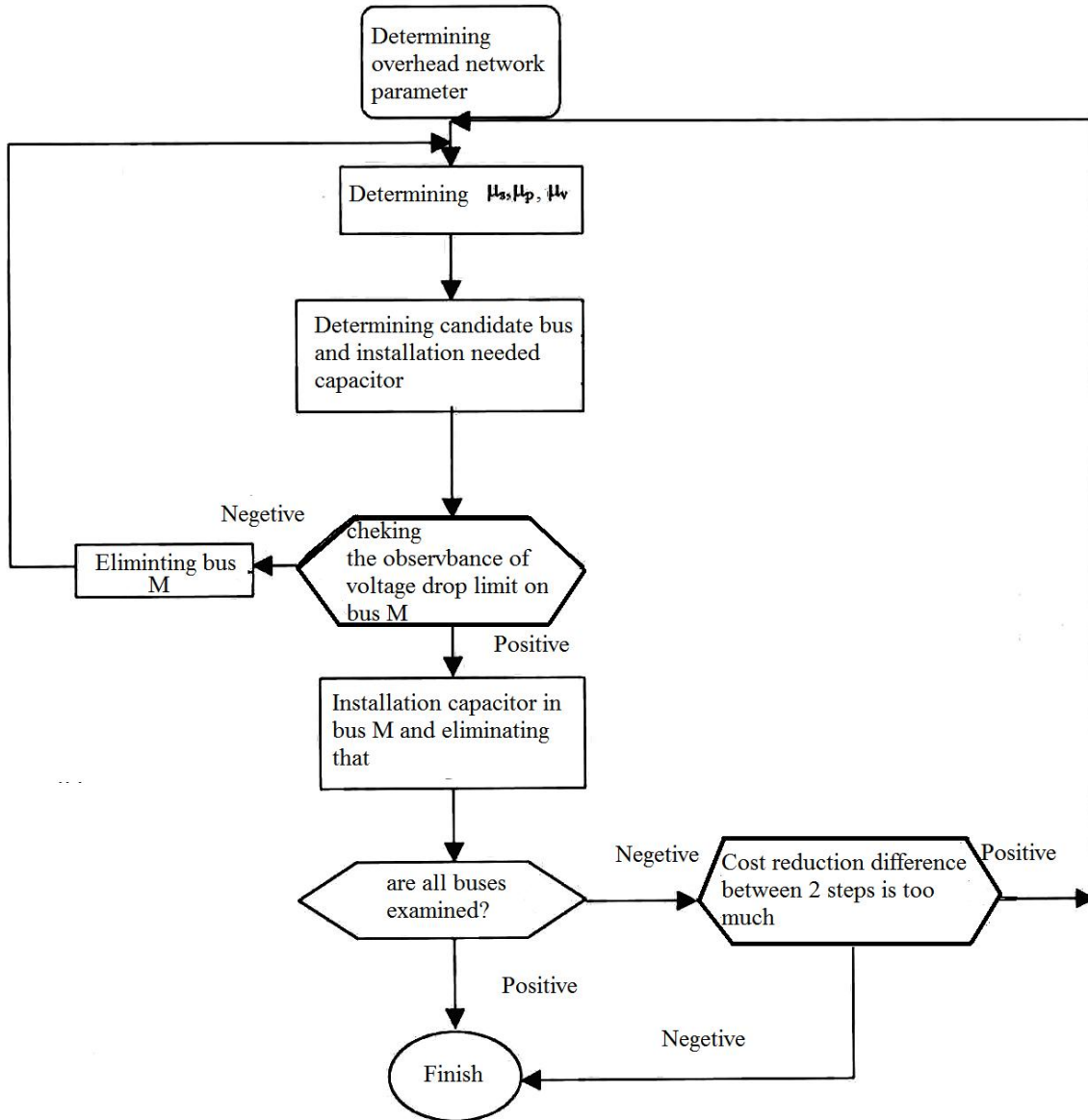Figure 3. Loss membership function(μp)

Figure 4. Flowchart of the optimum capacitor allocation procedure in the electric railway overhead network
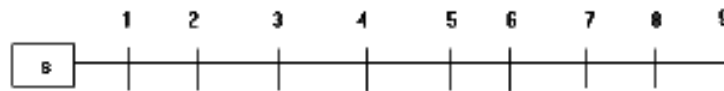

Figure 5. Single line diagram of radial feeder of the assumed overhead network

Biosynthesis of Bacitracin in Stirred Fermenter by *Bacillus Licheniformis* Using Defatted Oil Seed Cakes as Substrate

Iman Zarei

Department of Chemistry, Division of biochemistry

University of Pune Ganeshkhind

Pune 411007, Maharashtra, India

Tel: 91-20-2569-6061   E-mail: iman.zarei@gmail.com

Abstract

Bacitracin is being imported in India involving substantial amount of foreign exchange for its incorporation in poultry feed. The raw material for its production is readily available and cheap such as soybean meal, sunflower meal & wheat bran. Thus development of this technology in this country would result in saving a reasonable amount of foreign exchange by utilizing our resources. The present study is concerned with the biosynthesis of antibioticBacitracin by *Bacillus licheniformis*on laboratory to scale up studies in StirredFermenter using defatted oil seed cakes of agricultural bye-products as startingmaterial for maximum production of the antibiotic Bacitracin. In stirred fermenter, antibiotic formation reached maximum (342 i.u. ml^{-1}), 30 hours after inoculation at 37 °C using different natural media such as defattedsoybean meal, glucose and metal ions.In solid-state fermentation, wheat bran, soybean meal, sunflower meal, rice hulls and their different combinationswere used. The antibiotic activity 48 hours after inoculation was 4540 i.u/g when only soybean was used.

Keywords: Antibiotics, Bacitracin, Defatted oil seed, Fermenter, Inoculation

1. Introduction and Literature Survey

Bacitracin is derived from cultures of *Bacillussubtilis* (Tracey). It is a white to pale buff, hygroscopic powder, odorless or having a slight odor. It is freely soluble in water; insoluble in acetone, chloroform, and ether. While soluble in alcohol, methanol, and glacial acetic acid, there is some insoluble residue. It is precipitated from its solutions and inactivated by many of the heavy metals.

The molecular formula is: $C_{66}H_{103}N_{17}O_{16}S$. *Bacitracin* is comprised of a polypeptide complex and *Bacitracin* A is the major component in this complex. The molecular weight of *Bacitracin* A is 1422.71.

Bacitracin consists of one or more of the antimicrobial polypeptides produced by certain strains of *Bacillus licheniformis* and *Bacillus subtilis* var Tracy and yields the Amino acids L-cysteine, D-glutamic acid, Lhistidine, D-phenylalanine, L-lysine, L-isoleucine, L-leucine, D-ornithine and DL-Aspartic acid on hydrolysis (BP 2002) and functions as an inhibitor of cell wall biosynthesis (Azevedo, 1993). Bacitracin of other micro-organism is an antibiotic as well as non-ribosomally produced by *Bacillus licheniformis* (Ohki, 2003).

Different types of Bacitracin like A, A1, B, C, D, E, F, F1, F2, F3 and G have been isolated. The most potent antibiotic is Bacitracin A, whereas Bacitracin B and C are less potent and the rest possess a very little antibacterial activity. This antibiotic is the most effective against Gram +ve and a few Gram –ve species of bacteria. It is almost exclusively used as a topical preparation in the treatment of infections (Brunner, 1965).

Bacillus licheniformis is a bacterium that is commonly found in soil and bird feathers. Birds that tend to stay on the ground more than the air (i.e. sparrows) and on the water (i.e. ducks) are common carriers of this bacterium; it is mostly found around the bird's chest area and back plumage.

B. licheniformis is part of the subtilis group along with Bacillus subtilis and Bacillus pumilus. These bacteria are commonly known to cause food poisoning and food spoilage. B. licheniformis also is known for contaminating dairy products. Food borne outbreaks usually involve cases of cooked meats and vegetables, raw milk, and industrially produced baby food contaminated with B. licheniformis.

This bacterium, although detrimental, can be modified to become useful. Researchers are trying to turn bird feathers into a nutritious livestock feed by fermenting non-digestible proteins on bird feathers with B. licheniformis. There is also research about the possibility that B. licheniformis causes changes in color in birds' feathers; this will provide information on the evolution of molting. Also, cultures of B. licheniformis are made to retain its protease, which is in turn used in laundry detergent.

Bacillus licheniformis, a Bacitracin producer, has an ABC transporter system which is hypothesized to pump out Bacitracin for self-protection (Podlesek, 1995). Bacitracin holds considerable importance. It is also widely used as supplement in poultry nutrition. Its addition to the feed increases feed efficiency and the incidence of infectious diseases are greatly reduced (Shalak, 1971; Smekal, et al., 1979). Zinc Bacitracin and Bacitracin methyl disalicylate (feed grade) are widely used for growth promotion. Addition of Bacitracin to the feed may affect the activity and synthesis of certain liver enzymes (Rybinska, 1977) and increase the level of proteases and amylases in the digestive tract of laying hens.

2. Materials and Methods

2.1 Organism

Bacillus licheniformis (ATCC 9945, 10716, 11945, 11946 and 14580- PCSIR 89 locally isolate) were collected from National Chemical Laboratory (N.C.L) in Pune-India and used for the production of antibiotic Bacitracin.

2.2 Gram Staining

Gram staining was carried out before Inoculum Preparation to ensure whether collected *Bacillus licheniformis*from N.C.L was pure.

2.3 Inoculum Preparation

The bacterial growth was aseptically scrapped from 48 hours old cultures lants and transferred to 50 ml sterilized basal medium (Table 1) in 250 ml conical flask and then shaken on rotary shaker at 150 rpm for 24 hours at 37 °C. The vegetative culture thus obtained was used for inoculation into fermentation media. 4% v/v inoculum was used in this study.

2.4 Fermentation Media for Bacitracin Production

Fermentation media used for the production of Bacitracin by *Bacilluslicheniformis*is given in Table 2.

3. Fermentation Technique (Method)

10 g of the substrate was taken in 250 ml of conical flask. It was wetted by 10 ml of distilled water previously adjustedto pH 7 or phosphate buffer of pH 7 was used. Medium (Table 2) was autoclaved at 121 ^{o}C for 15 minutes; it was allowed to cool and then was inoculated with 1ml of seed culture. After inoculation, the flasks were shaken well and then incubated at 37 ^{o}C for 48 hours. At the end offermentation period, the fermented material was soaked in N/100 HCl for 1 hour and then centrifuged. The supernatant layer was assayed for calculation of antibiotic activity.

Rate of production of bacitracin by *Bacillus licheniformis* in wheat bran by solid-state fermentation is given in the following Table 3.

3.1 Effect of Different Oil Seed Cake on the Production of Bacitracin

Bacitracin consists of a group of closely related peptides. Thus effect of different defatted oil seed cakes as a source ofamino acids, vitamins, minerals and sugars were investigated as in Table 4.

The production of Bacitracin on laboratory scale was carried out in 30-L Glass Stainless Steel Fermenter (B.E. Marubishi – MSJ – N2, Japan). It was connected with bioprocess operator-MSSD-1 and bioprocess controller-MEDIAC-93. The basal medium was sterilized inside the fermenter automatically. Temperature, pH, agitation and foaming were controlled automatically. The fermentation medium (Table 2) which gave the best results in shake flasks was used. The fermenter was run for 48 hours. The antibiotic activity during fermentation was determined from time to time.

Fermentation phenomenon can be occurred in simple condition. A rotary shaker is required. The fermentation medium would be a flask which is plugged by cotton. Note that transfer of inoculum (basal) medium to fermentation flask must be done in absolute sterilized environment.

3.2 Assay

The activity of the antibiotic Bacitracin present in the fermented material was determined by agar diffusion method (Table 5).

The pH of the medium was adjusted to 7.0 with 1N NaOH/HCl before the addition of agar. The medium was sterilized at 121 °C for 15 minutes. Approximately 20 ml of the medium was aseptically poured into the sterile Petri-plates and allowed to solidify. Then, 4 ml of melted assay medium which was previously inoculated with the pre-determined concentration of test organisms i.e. *Staphylococcus aureus* and *Escherichia coli* were spread uniformly over the first layer and were allowed to congeal. After setting the second layer, four holes 0.8 cm of diameter were made in the plates aseptically with stainless steel borer of uniform edge and size.

Two opposite holes were filled with working standard of 1:4 dilution (S1, S2) and the remaining two were filled with sample to be determined of 1:4 dilution (T1, T2) using micropipette. 0.12 ml solution was poured in each digged hole. The plates were then very carefully placed in incubator for 24 hours at 37 °C. Clear zones of inhibition were developed both by standards and samples. Diameters of zones of inhibition were measured and compared with the known standard.

The potency of the sample was determined by the following formulae:

1. Difference due to dose (E): $E = \frac{1}{2}(T2 + S2) - (T1 + S1)$
2. Difference due to sample (F): $F = \frac{1}{2}(T2 + T1) - (S2 + S1)$
3. Log ratio of doses (I): $I = \log 4 = 0.602$
4. Slope (B): $B = E / I$
5. Potency ratio = Antilog of M, where $M = F / B$
6. Potency of sample = Antilog of M x Potency of standard

Where

S1 = Standard High (in concentration)

S2 = Standard Low (in concentration)

T1 = Test High

T2 = Test Low

3.3 Units of Bacitracin

One unit of Bacitracin activity is the amount of antibiotic in 0.2 ml of culture supernatant broth that will cause a 1 mm inhibition zone outside the cylinder (Bernlohr, & Novelli, 1960). One unit of Bacitracin is equivalent to 26 μg of USP standard (Harvey, 1980). The USP Unit of Bacitracin is the Bacitracin activity exhibited by the weight of USP Bacitracin Reference Standard indicated on the label of the Standard. It has a potency of not less than 40 USP Units of Bacitracinmg-1 (Nichols, 2000).

3.4 Isolation of Bacitracin by Centrifugation

The fermented broth was centrifuged at 10,000 rpm for 15 minutes in a refrigerated centrifuge at 4 °C in order to remove cells and solid suspended particles. The clear supernatant solution was used for the isolation of antibiotic.

3.5 Partitioning

Physical separation may be used for isolation, purification, identification and determination of organic compounds. It is, of course, generally a two-phase process, and can be classified into solid-liquid, liquid-liquid, gas-liquid and gas-solid systems. An exception is electrophoresis, which takes place in a single phase. Applications of physical separation may cut across these categories- for example; phase titrations may result in separation of a solid or a liquid phase from the initial liquid phase. Similarly, some of the factors associated with physical separation have implications for figurative separation.

4. Results and Discussion

The production of antibiotic by solid state fermentation involves less consumption of energy compared to stirred fermenters where continuous aeration, agitation and control of foaming are necessary.

The rate of production was determined by using wheat bran as solid substrate. The antibiotic activity was determinedafter every 12 hours during the course of fermentation (Table 3). The antibiotic activity reached maximum (3287 i.u/g), 48 hours after inoculation. Further increases in fermentationperiod resulted in decline of bacitracin activity. It may be attributed to inhibition of "Bacitracin Synthetase" enzyme by bacitracin itself by feedback mechanism.

Data of Table 4 shows that synthesis of bacitracin was maximum in of soybean meal (4540 i.u/g) while amount of bacitracin produced in sunflower meal was 1330 i.u/g. wheat bran also gave good antibiotic titre i.e. 3287 i.u/g but rice hulls only produced 562 i.u/g. The reason of low antibiotic production by rice hulls may be of its

being poor source of carbon and nitrogen while soybean and wheat bran are ideal substrate providing all the nutrients required by *Bacillus licheniformis.*

4.1 Screening of Culture Media

The composition of the basal medium (Table 1) greatly influence theproduction of antibiotics. Replacing soybean meal with sunflower meal and/or wheat bran of same quantity (Table 2) in fermenting medium wasused for the screening purpose. The nutritional studies were carried out.

The antibiotic activity in the fermented broth was determined, 44-48 hours after inoculation with 4% v/v bacterial cell suspension obtained from theslant surface. Of the medium tested, soybean meal medium (Table 2) gave the best results of antibiotic titer.

K_2HPO_4 and KH_2PO_4 were used as buffering agents, $MnSO_4.7H_2O$ and $MgSO_4.4H_2O$ as co-factors of enzymes while $FeSO_4.7H_2O$ was used toassist the action of Manganese ion. Addition of citric acid leads to theformation of soluble coordinate complex with the metal ion thus makingthem available to the microorganism at adequate time (Haavik, 1976).

Organic and inorganic matter content is considered as an indicator of richresources of media for Nitrogen source (Varvel, 1994). The conditions like pH, temperature, aeration, different ratio of substrates as nitrogen sources and other parameters were optimized (Shabbir, 2001).

References

[Online] Available: http://biology.kenyon.edu/Microbial_Biorealm/bacteria/gram-positive/ bacillus/ bacillus.htm

Azevedo, E. C. (1993). Bacitracin production by a new strain of Bacillus Subtilis.Extraction, purification and characterization. *Appl. Biochem Biotechnol.,* 42, 1-7. http://dx.doi.org/10.1007/BF02788897

Barnes, D., Beicher, R., & Zuman, P. (1967). Talanta, 14, 1197.

Bernlohr, R. W., & Novelli, G. D. (1960). Some characteristics of Bacitracin production by Bacillus licheniformis. *Archives of Biochem And Biophysics,* 87, 232-238. http://dx.doi.org/10.1016/0003-9861(60)90166-1

Berdy, J. (1974). Recent developments of antibiotic research and classification of antibiotics according to chemical structure. *Adv. Appl. Microbiol.,* 18, 309-406. http://dx.doi.org/10.1016/S0065-2164(08)70573-2

Bottone, E. J., & Peluso, R. W. (2003). Production by Bacillus pumilus (MSH) of an antifungal compound that is active against Mucoraceae and Aspergillus species: preliminary report. *J. Med. Microbiol.,* 52, 69-74. http://dx.doi.org/10.1099/jmm.0.04935-0

British Pharmacopoeia. (2002). pp 201.

Brunner, R. (1965). Polypeptide. In: R. Brunner and G. Machek (Eds.), Di Antibiotica, VerlagCari, Nurnberg, pp 167-214, 702-707.

Buchanan, J. R., & Gibbons, N. E. (1974). *Bergey's Manual of Determinative Bacteriology*, 8th ed., The Williams and Wilkins Company, Baltimore.

Chang, S. C., Wei, Y. H., Wei, D. L., Chen, Y. Y., & Jong, S. C. (1991). Factors affecting the production of eremofortin C and PR toxin in *Penicilliumroqueforti*. *Appl. Environ. Microbiol*., 57, 2581- 2585.

Claus, G. W., & Balckwill, D. (1989). Antibiotic Evaluation by Kirby-Bauer Method. *Understanding Microbes: A Laboratory Textbook for Microbiology*, U.S.A., pp. 405.

Craig, L. C., & Konigsberg, W. (1957). Further studies with the Bacitracin polypeptides. *J. Org. Chem.*, 22, 1345-1353. http://dx.doi.org/10.1021/jo01362a013

Datta, A. R., & Kothary, M. H. (1993). Effects of glucose, growth temperature and pH on listeriolys in O. *Listeriamonocytogenes*. *Appl. Environ. Microbiol*., 59, 3495–3497.

Defuria, M. D., & Claridge, C. A. (1976). Aminoglycoside antibiotics produced by the genus *Bacillus*.*Microbiology*. (Ed.): M. Schlessinger, pp 421-436. American Society of Microbiology, Washington, D.C.

De Mondena, J. A., Guttierrez, S. A. J., Falchini, R. A., Gallazo, J. L., Hughes, D. E., Bailey, J. E., & Martin, J. F. (1993). Intracellular expression of vitreoscilla haemoglobin improves cephalosporin C production by *Acremonium chrysogenum. Biotech*., 11, 926-929. http://dx.doi.org/10.1038/nbt0893-926

Egorov, N. S., Loriia, Z., Vybornykh, S. N., & Khamrun, R. (1986). Effect of culture medium composition on bacitracin synthesis and sporulation in *Bacillus licheniformis* 28 KA. *Prikl. Biokhim. Mikrobiol*., 22, 107-111.

Eppelmann, K., Doekel, S., & Marahiel, M. A. (2001). Engineered Biosynthesis of the Peptide Antibiotic Bacitracin in the Surrogate Host *Bacillus subtili*s. *J. Biol. Chem*., 276, 34824-34831. http://dx.doi.org/10.1074/jbc.M104456200

Espeso, E. A., Tilburn, J., Arts, H. N., & Peñalva, M. A. (1993). PH regulation is a major determinant in expression of a fungal penicillin biosynthetic gene. *EMBO J.* 12, 3947-3956.

ë1Jta, F. (September 1961). Paper at Symposium on Teaching of Analytical Chemistry, Aberdeen University.

Fukuda, N., Kobayashi, H., & Ueno, K. (1969). Talanta, in press. 6 A. K. De, S. M. T. Fujinaga, Talanta, 16, 1225.

Glenn, A. L. (1967). Lecture to Scottish Section, Society for Analytical Chemistry, Glasgow. Proc. Soc. Anal. *Chem.,* 4, 116. http://dx.doi.org/10.1039/sa9670400116

Gordon, L. (May 1961). Lecture to Czechoslovak Chemical Society, Prague.

Gordon, L., Salutsky, M. L., & Willard, H. H. (1959). Precipitation from Homogeneous Solution, Chaps. 8 and 10, Wiley: New York.

Haavik, H. I. (1975). Bacitracin production by the neotype; bacillus licheniformis ATCC 14580. *ActaPathol. Microbiol. Scand. Suppl.*, 83, 534-540.

Haavik, H. I. (1974). Studies on the formation of bacitracin by *Bacillus licheniformis*: Role of catabolite repression and organic acids. *J. Gen. Microbiol*., 84, 321-326.

Haavik, H. I. (1976). Studies on the formation of Bacitracin by *Bacillus Licheniformis*: Role of catabolite repression and organic acids. *J. Gen. Microbiol*., 84, 221-236.

Harvey, S. C. (1980). Antimicrobial Drugs: Bacitracin. In: A. Osol, (Ed.), *Remington Pharmaceutical Sciences*, 16, Mack Publishing Co., p. 1144.

Iglewski, W. J., & Gerhardt, N. B. (1978). Identification of an antibiotic-producing bacterium from the human intestinal tract and characterization of its antimicrobial product. *Antimicrob. Agents Chemother*., 13, 81-89.

Katz, E., & Demain, A. L. (1977). The peptide antibiotics of *Bacillus*; chemistry, biogenesis, and possible functions. *Bacteriol. Rev*., 41, 449-474.

Khopkar, & Chalmers, R. A. (1970). Solvent Extraction of Metals, Chap. 11, Van Nostrand Reinhold: London.

Kugler, M., Loeffler, W., Rapp, C., Kern, A., & Jung, A. G. (1990). Rhizocticin A, an antifungal phosphono-oligopeptide of *Bacillus subtilis* ATCC 6633: biological properties. *Arch. Microbiol*., 153, 276-281. http://dx.doi.org/10.1007/BF00249082

Lebbadi, M. A., Galvez, M., Maqueda, M., Martinez, B., & Valihuia, E. (1994). Fungicin M4: a narrow spectrum peptide antibiotic from *Bacillus licheniformis*M-4. *J. Appl. Bacteriol*., 77, 49-53. http://dx.doi.org/10.1111/j.1365-2672.1994.tb03043.x

Maraheil, M. A., Stachelhaus, T., & Mootz, H. D. (1997). Modular peptide synthetases involved in non-ribosomal pepetidesyhtesis. *Chem. Rev*., 97, 2651-2673.

Mendo, S., Faustino, N. A., Sarmento, A. C., Amado, F., & Moir, A. J. (2004). Purification and characterization of a new peptide antibiotic produced by a thermotolerant *Bacillus licheniformis* strain. *Biotechnol. Lett*., 26, 115.

Nichols, W. K. (2000). Anti-infectives: Bacitracin. In: Daniel Limmer (Ed.), *Remington Pharmaceutical Sciences*, 20, Lippincott Williams and Wilkins, p. 1536.

Ohki, R. (2003). A Bacitracin – Resistant *Bacillus subtilis* Gene Encodes a Homologue of the Membrane-spanning subunit of the *Bacillus licheniformis* ABC Transporter. *J. Bact*., 185(1), 51-59. http://dx.doi.org/10.1128/JB.185.1.51-59.2003

Pfann, W. G. (1966). Zone Melting, 2nd ed., Wiley: New York.

Podlesek, Z. (1995). *Bacillus licheniformis* Bacitracin-resistance ABC transporter: Relationship to mammalian multidrug resistance. *Mol. Microbiol*., 16, 969-976 (Medline). http://dx.doi.org/10.1111/j.1365-2958.1995.tb02322.x

Priest, F. G. (1992). Biology of *Bacilli.* In: *Bacilli: applications to industry*. (Eds.): R.H. Doi and M. Mcgloughlin. pp. 293- 320. Butterworth- Heinemann, Boston, Mass.

Robinson, J. W., Hailey, D. M., & Barnes, H. M. (1969). Talanta, 16, 1109.

Rogers, D. W., & Scher, J. (1969). Talanta, 16, 1579.

Robbers, E. J., Marilyn, S. K., & Varro, T. E. (1996). Antibiotics. In: *Pharmacognosy* and *Pharmacobiotechnology*, University School of Pharmacy and pharmaceutical Sciences, pp. 219- 220. West Lafayette, Indiana.

Rybinska, K. (1977). Effect of Zinc Bacitracin on the activity of certain enzymes in rats. Part I: Determination of aspartate and alanine aminotransferases in the liver and kidney of test animal. *Rocz. Panstw. Zakl. Hlg.*, 28, 133-140.

Sawicki, E. (1969). Talanta, 16, 1231.

Schallmey, M., Singh, A., & Ward, O. P. (2004). Developments in the use of *Bacillus* species for industrial production. *Can. J. Microbiol.*, 50, 1-17. http://dx.doi.org/10.1139/w03-076

Sen, K. S., Haque, F. S., & Pal, C. S. (1995). Nutrient optimization for production of broad-spectrum antibiotics by *Streptomyces* antibioticus Str. 15. 4. *Acta Microbial. Hung.*, 42, 155-162.

Shabbir, G. (2001). Salt Tolerance Potential of some selected fine rice Cultivars.*Online Journal of Biological Sciences*, 1(12), 1175-1177.

Shalak, M. V. I. (1971). Bacitracin-a new preparation in poultry farming. *Tr. Beloruses. Set'ShokhozAkad.*, 90, 42.

Sun, S. K. (1970). Talanta, 17, 577.

Smekal, F., et al. (1979). Fermentation Production of Bacitracin. *Czech.*, 175, 992 (C1-C12 D9/22).

Silo-Suh, L. A., Lethbridge, B. J., Raffel, S. J., Clardy, J., & Handelsman, J. (1994). Biological activities of two fungistatic antibiotics produced by *Bacillus cereus* UW 85.*Appl. Environ. Microbiol.*, 60, 2023-2030.

Snell, N., Ijichi, K., & Lewis, J. C. (1955). *Paper Chromatographic Identification of Polypeptide Gram Positive Inhibiting Antibiotics*. Western Utilization Research Branch, U.S Departmentof Agriculture, Albany, California.

Solé, M., Francia, A., Rius, N., & Lorén, J. G. (1997). The role of pH in the "glucose effect" on prodigiosin production by non-proliferating cells of *Serratiamarcescens*. *Lett. Appl. Microbiol.*, 25, 81-84. http://dx.doi.org/10.1046/j.1472-765X.1997.00171.x

Solé, M., Rius, N., Francia, A., & Lorén, J. G. (1994). The effect of pH on prodigiosin production by non-proliferating cells of *Serratiamarcescens*. *Lett. Appl. Microbiol.*, 19, 341-344. http://dx.doi.org/10.1111/j.1472-765X.1994.tb00470.x

Tipson, R. S. (1950). Crystallization and recrystallization, in Techniques of Organic Chemistry, Vol. III (Ed. A. Weissberger), Interscience: New York.

Todar, K. (2002). *Antimicrobial Agents used in the treatment of infectious disease*. Department of Bacteriology University of Wisconsin-Madison.

Varvel, E. G. (1994). Rotation and Nitrogen fertilization effect on changes in soil Carbon and Nitrogen. *Agronomy J.*, 86, 319-320. http://dx.doi.org/10.2134/agronj1994.00021962008600020021x

Yousaf, M. (1997). *Studies on the cultural conditions for the production of antibiotic bacitracin by B. licheniformis*. PhD Thesis, Islamia University, Bahawalpur.

Yamamoto, Y., Kukamaru, T., & Hayashi, Y. (1967). Talanta, 14, 611.

Zinsser, H. (1988). Antimicrobial Agents. In: *Zinsser Microbiology*. (Eds.): H. Zinsser, W.K. Joklik, H. P. Willett, D. B. Amos and C. Wilfert. pp. 128- 160. Prentice Hall International, UK.

Table 1. Composition of basal medium

Materials	Content (g /L)
Peptone	10.0
Glucose	5.0
Beef Extract	5.0
Sodium Chloride	2.5
Manganese Chloride	0.167

Table 2. Composition of fermentation media

Materials	Content (g/L)
Citric Acid	1.0
Glucose	0.5
KH_2PO_4	0.5
K_2HPO_4	0.5
$MgSO_4 \cdot 7H_2O$	0.2
$MnSO_4 \cdot 4H_2O$	0.01
$FeSO_4 \cdot 7H_2O$	0.01
Soybean meal/Sunflower/or Wheat bran	45.0

The media was sterilized at 121 °C for 15 minutes at pH 7. All media were prepared in distilled water.

Table 3. Rate of production of bacitracin by Bacillus licheniformisin wheat bran

No. of observation	Fermentation period (Hours)	Potency (i.u/g)
1	12	135.0
2	24	411.0
3	36	2001.0
4	48	3287.0
5	60	3000.0
6	72	2133.0

Table 4. Effect of different substrate on the production of bacitracin by solid-state fermentation

Substrate	Quantity (g/flask)	Incubation temp.	Duration (hrs.)	Potency (i.u/g)
Soybean meal	10	37°C	48	4540
Wheat bran	10	37°C	48	3287
Sunflower meal	10	37°C	48	1330
Rice hulls	10	37°C	48	562

Table 5. Composition of nutrient agar media

Materials	Content (g/L)
Beef extract	1.0
Yeast extract	2.0
Sodium Chloride	5.0
Peptone	5.0
Agar	25.0

Note: Nutrient broth powder can be used instead of beef extract, yeast extract, Sodium Chloride and peptone, because it contains all mentioned components. It will be sufficient to dissolve Nutrient broth and agar powder in distilled water and sterilize it.

Treatment of Dye Wastewater Using Granular Activated Carbon and Zeolite Filter

Syafalni S.

School of Civil Engineering, Universiti Sains Malaysia

Engineering Campus, Seri Ampangan, Nibong Tebal 14300, Pulau Pinang, Malaysia

E-mail: cesyafalni@eng.usm.my

Ismail Abustan, Irvan Dahlan, & Chan Kok Wah

School of Civil Engineering, Universiti Sains Malaysia

Engineering Campus, Seri Ampangan, Nibong Tebal 14300, Pulau Pinang, Malaysia

Genius Umar

Faculty of Agriculture, Cokroaminoto Palopo University, Indonesia

Abstract

Dye wastewater sample contains moderate concentration of chemical oxygen demand (COD), ammonia (NH_3) and color. This work evaluates the removal of COD, ammonia and color in dye wastewater using granular activated carbon (GAC) and zeolite in the column studies. Different surface loading rates, height of adsorbent and empty bed contact time were used to investigate the efficiency of the adsorption process. The maximum removal efficiency was found at the surface loading rate of 2.84 ml/cm^2.min and bed height of 10 cm. Due to the characteristics of GAC and zeolite, a sequence of combination with both adsorbents produces a better removal of contaminants. The best removal of the contaminants among the all adsorption treatment was found using GAC (bottom layer) and zeolite (upper layer) in 6.35 cm diameter column with 59.46% removal of COD, 60.82% removal of ammonia and 58.4% removal of color. For the adsorption with zeolite as the bottom layer and GAC as the upper layer, the data fitted well with the Langmuir model. While for the adsorption with zeolite as the upper layer and GAC as the bottom layer, the data fitted well for both Langmuir and Freundlich isotherms.

Keywords: Dye wastewater, Granular activated carbon (GAC), Zeolite, Adsorption, Isotherm model

1. Introduction

Textile dyeing is one of the important industries in Malaysia. Different steps in the dyeing and finishing processes in textile dyeing industry, however, results in the generation of large quantities of colored dye wastewater (Babu, et al., 2007). The release of untreated colored wastewaters into the ecosystem can be very damaging to the receiving water bodies. Typically, untreated dyes wastewaters from dyestuff production and dyeing industries have a great variety of colors and difficult to biodegrade due to complex chemical structures. Furthermore, dyes used in the textile industry may be toxic to aquatic organisms and some of these dyes are suspected carcinogens (Erdem, et al., 2005; Hameed, 2009a; Pinheiro, et al., 2004; Babu, et al., 2007).

The environmental concern of these untreated dyes wastewaters has drawn the awareness of many research studies. Accordingly, various treatment processes have been employed for the removal of dyes from wastewater, such as coagulation/ flocculation process (Butt, et al., 2005), cation exchange membranes (Wu, et al., 2008), electrochemical degradation (Fan, et al., 2008), advanced oxidative process (Banerjee, et al., 2007; Mahmoud, et al., 2007; Fathima, et al., 2008), Fenton-biological treatment (Lodha, & Chaudhari, 2007; Garcia-Montano, et al., 2008), and adsorption (Allen, et al., 2004; Erdem, et al., 2005; Hameed, 2009a; Hameed, et al., 2009).

Until now, adsorption technique using many types of adsorbents is still the most favorable method in the removal of contaminants from wastewaters due to its efficiency; high adsorption capacity and low operational

cost method. Adsorbent such as activated carbon is very suitable for reducing the organic substances (such as COD/BOD) and color (Alvares, et al., 2001; Kalderis, et al., 2008; Ahmad, et al., 2009). On the other hands, zeolite was found very effective in reducing ammoniacal nitrogen and COD (Lee, et al., 1996; Chang, et al., 2001; Jung, et al., 2004; Otal, et al., 2005) since it have high cationic exchange capacities, large surface areas and high residual carbon contents.

The purpose of the present work was to evaluate the removal efficiency of ammonia, COD and color in dye wastewater using granular activated carbon (GAC) and zeolite, as well as to compare the performance of the sequence arrangement between GAC and zeolite as filter media in different surface diameter of column sizes. Apart from that, adsorption isotherms were also analyzed using equilibrium data for the combination of GAC and zeolite at different sequences.

2. Materials and Methods

2.1 Materials

The dye wastewater was taken from Penfabric Mill 3, Bayan Lepas, Penang. The dye wastewater mainly consists of dying ingredients, sodium sulphate anhydride (Na_2SO_4) and PVA (polyvinyl alcohol). Table 1 presents the characteristics of the raw dye wastewater sample. Granular activated carbon (GAC) and zeolite were used as the media treatment (adsorbent) for dye wastewater. GAC and zeolite were supplied by Fudojaya Sdn. Bhd. GAC and zeolite were sieved to obtain the required particle size range of 1.18 mm – 2.00 mm. Zeolite was immersed into 1 M of NaCl for 24 h (Ilyas, 2007). Both adsorbents were rinsed with distilled water for several times to remove dust and others impurities. After that, both adsorbents were then placed in an oven at 105 °C for 24 h and subsequently dried in a desiccator for 2 h and it was ready to use.

2.2 Analytical Methods

The concentration of COD, ammoniacal nitrogen, and color were analyzed in accordance with the Standard Methods for the Examination of Water and Wastewater (APHA, 1992). Calorimetric method with HACH DR/2010 spectrometer (set at 620 nm wavelength) was used in measuring COD concentration. Ammonia concentrations was measured by Nesslerization Method (4500 NH_3) using a HACH DR/2010 spectrometer (set at 425 nm wavelength). While color was measured by APHA Platinum-Cobalt Method using HACH DR/2010 spectrometer (set at 455 nm wavelength) and distilled water was used as a blank. The unit that used for the color test is platinum cobalt (PtCo).

2.3 Laboratory Column Studies

The removal efficiency of COD, ammonia and color from dye wastewater was investigated using laboratory plastic column filled with GAC and zeolite. In this study, four set of experiments (shown in Figure 1 and Table 2) were conducted to determine the effectiveness of the adsorbents and it consists of column with surface diameter of 1.91 cm, 3.81 cm and 6.35 cm, respectively. Columns were mounted vertically and the adsorbent (bed height of 6 cm, 8 cm and 10 cm) was supported on a perforated net. A total sample of 500 ml dye wastewater was used/prepared and drained from the holding tank to the specific flow rate using a control valve. The operation was down plug flow mode. Effluent samples were collected into a beaker after the adsorption treatment. All the sorption experiments were carried out at room temperature.

2.4 Surface Loading Rate (SLR) & Empty Bed Contact Time (EBCT)

Three different flow rates (90 ml/min, 270 ml/min and 510 ml/min) were used for column filled with GAC (Figure 1a). While for column filled with zeolite (Figure 1b) and columns with sequences arrangement of GAC and zeolite (Figures 1c & 1d), the flow rate used was 90 ml/min. The surface loading rate (SLR) was calculated by,

$$\text{Surface Loading Rate (SLR)} = \frac{\text{Volumetric Flow Rate (ml / min)}}{\text{Column Cross Sectional Area (cm}^2)} \quad (1)$$

The SLR calculated ranges from 2.84 to 178.95 ml/cm^2.min. The void volume for GAC and zeolite was found to be 58% and 52%, respectively through the column experiment. It means that empty bed contact time (EBCT) is about twice the true contact time between the fluid being treated and the GAC particles. The EBCT for GAC and zeolite can be calculated based on these void volume of the wastewater sample in the desired bed height and flow rate that are given by Eqs. (2) and (3), respectively.

$$\text{EBCT}_{GAC} = \frac{(\frac{\pi D^2}{4}) \times \text{bed height} \times 0.58 \times 60}{\text{Volumetric Flow Rate}} \quad (2)$$

$$\text{EBCT}_{zeolite} = \frac{(\frac{\pi D^2}{4}) \times \text{bed height} \times 0.52 \times 60}{\text{Volumetric Flow Rate}} \tag{3}$$

While the EBCT for the sequences arrangement of GAC and zeolite will be the sum of both EBCT according to the bed height in the treatment.

2.5 Isotherm Models

Freundlich and Langmuir isotherm models were applied in this study to analyze adsorption capacity of GAC and zeolite. The Freundlich isotherm is based on an assumption of adsorption onto heterogeneous surfaces, multilayer adsorption which is different with the Langmuir isotherm that based on assumption of monolayer adsorption. Experiment was carried out with different arrangement of adsorbent sequence in order to differentiate the adsorption capacity. The experiment was conducted using the same length of adsorbent but varying the diameter of the surface column (from 1.91 cm to 6.35 cm). The dye wastewater was treated at the maximum condition (flow rate of 90 ml/min and bed height of 10 cm). The amount of adsorption at equilibrium, q_e (mg/g), was calculated by the following equation,

$$q_e = \frac{(C_o - C_e).V}{W} \tag{4}$$

where C_o and C_e (mg/L) are the liquid-phase concentrations of sample at initial and equilibrium, respectively. W (g) is the mass of composite media used and V (L) is the volume of the solution. The removal efficiency of parameters studied can be calculated as follows,

$$\text{Removal Efficiency (\%)} = \frac{C_o - C_e}{C_o} x100 \tag{5}$$

Adsorption isotherm is fundamentally essential to explain how solutes interact with adsorbents, and is critical in optimizing the use of adsorbents (Hameed, 2009b). The Langmuir (Langmuir, 1916) and the Freundlich (Freundlich, 1906) were employed in the present study. The linearized forms of the two isotherms are as follows,

$$\frac{1}{q_e} = \frac{1}{K_a q_m C_e} + \frac{1}{q_m} \tag{6}$$

$$\ln q_e = \ln K_F + \frac{1}{n} \ln C_e \tag{7}$$

The Langmuir constants, q_m (mg/g) and K_a (L/mg), are related to adsorption capacity and energy of adsorption, respectively. While K_F and n are Freundlich constants.

2.6 Data Precision

Every analysis and experimental run was repeated at least two to three times to increase the precision of the results, and only the average value was reported throughout this study. The repeatability of the experimental data was found to be sufficiently high with relative error between repeated runs less than 5%.

3. Results and Discussion

3.1 Effects of SLR on the GAC and Zeolite Adsorption Processes

The effect of SLR on the removal of COD, ammonia and color using GAC adsorbent are shown in Figures 2 to 4 at various surface diameter and bed height. It can be seen from these figures the maximum reduction for all parameters were recorded at 10 cm of GAC height and SLR of 31.58 ml/cm^2.min, 7.89 ml/cm^2.min, and 2.84 ml/cm^2.min. The maximum COD reductions for surface column diameter of 1.91 cm, 3.81 cm and 6.35 cm were 11.88%, 28.89% and 40.31%, respectively. For ammonia, the maximum reduction of 12.08%, 27.03% and 40.79% were obtained at surface column diameter of 1.91 cm, 3.81 cm and 6.35 cm, respectively. The same trend was also observed for color removal. The adsorption rate is controlled by two intraparticle diffusion mechanisms, i.e. diffusion within the pore volume (pore diffusion) and diffusion along the surface of pores (surface diffusion) (Tien, 1994). Adsorption at low SLR may provide more adequate contact time for impurity to transport from liquid to the pores of adsorbent. Based on this result, it can be concluded that higher removal of COD, ammonia and color could be obtained at a lower SLR and higher bed of GAC adsorbent. The maximum removal condition for all the parameters using GAC was obtained at SLR of 2.84 ml/cm^2.min and adsorbent height of 10 cm.

On the other hand, the effect of various SLR and bed height on the removal of COD, ammonia and color using zeolite adsorbent are shown in Figure 5. It was shown that the removal percentage for all parameters increase with

increasing the height of zeolite column and decreasing the SLR values. The maximum COD, ammonia and color reduction of 20.53%, 45.62% and 39.86%, respectively were obtained using 10 cm zeolite height and SLR of 2.84 ml/cm^2.min. The increase in the removal percentage for all parameters leads to decrease in the solute concentration in the effluent. Consequently, the effluent concentration might be reduced with further increase in the bed height of zeolite.

3.2 Effects of EBCT on the GAC and Zeolite Adsorption Processes

Figure 6 depicts the effect of contact time (EBCT) on the removal of COD, ammonia and color at various GAC heights. The contact times used were varied (ranges from 7 – 123 seconds) by the increment of the surface diameter of the column from 1.91 cm to 6.35 cm, depending on the total volume of GAC used. When the adsorption process was carried out at 6 cm GAC height (Figure 6a), the reduction of COD, ammonia and color was only about 5.28%, 5.42% and 16%, respectively at lower contact time. However, the amount of all parameters adsorbed increases with time and reaches a constant value after 20 s. After the equilibrium time, the amount of all parameters adsorbed did not alter with time. However, when GAC column was filled with higher bed, especially with 10 cm bed height, different results were obtained. It was shown that the removal percentage for all parameters increase with increasing the contact time between dye and GAC. Eventually, a saturation curves were not reached in all curves of Figures 6b and 6c (except COD reduction curve in Figure 6b) indicating that the adsorbent was not saturated in this level of contact time studied. From the figures, it was observed that the maximum removal was found to be at 123 s (Figure 6c) with a total of 40.31%, 40.79% and 49.46% reduction of COD, ammonia and color, respectively.

At the same time, the experiment was also carried out to study the effect of contact time (EBCT) on the removal of COD, ammonia and color using various heights of zeolite. It was observed from Figure 7 that the maximum removal for all parameters was found at the maximum contact time. This indicates that higher contact time between dye and zeolite will lead to higher removal efficiency till the equilibrium time is reached. From the Figures, it was observed that the maximum removal was found to be at 110 s using 10 cm height of zeolite.

3.3 Effects of EBCT toward the Sequence Arrangement of GAC and Zeolite

Sequence arrangement of activated carbon-zeolite formed by the zeolite growth on porous carbon supports can possess the bifunctional properties of both carbon and zeolite, which have the potential to remove the contaminants from dye wastewater (Zhang et al., 2004). In this study, the sequence arrangement of GAC and zeolite for dye wastewater treatment was carried out, whereby zeolite was filled at the lower part and GAC was filled at the upper part of the column and visa versa. It was found from Figure 8 that the removal percentage for all parameters increases with increasing the contact time for both sequence arrangements. The maximum reduction of COD, ammonia and color of 42.95%, 55.71% and 55.83, respectively were obtained using zeolite-GAC sequence arrangement with a total of 233 s of contact time. The result shows that the removal percentage for all parameters was increased as compared to the column filled with only GAC or zeolite.

3.4 Adsorption Isotherm

In this study, the Freundlich and Langmuir adsorption models, which have been successfully applied to many adsorption processes, were used to study the COD, ammonia, and color adsorption behaviour of GAC and zeolite combination. The Freundlich isotherm is based on an assumption of adsorption onto heterogeneous surfaces, multilayer adsorption which is different with the Langmuir isotherm that based on assumption of monolayer adsorption. The maximum performance of the media (SLR of 2.84 ml/cm^2.min, 7.89 2.84 ml/cm^2.min and 31.58 2.84 ml/cm^2.min; adsorbent height of 10 cm for each GAC and zeolite) was chosen in order to compare the effectiveness in changing the sequence of the adsorbents for every different surface diameter of surface columns.

3.5 Freundlich Isotherm

Figures 9 and 10 shows the linear plot (ln qe versus ln Ce) of Freundlich isotherm for zeolite-GAC and GAC-zeolite arrangements, respectively using experimental data obtained. The applicability of the model suggests multilayer of the adsorbate at the outer surface of the adsorbent is significant. Values of K_f and $1/n$ calculated from the plot shown in Figures 9 and 10 are listed in Table 3. From the isotherm above, the correlation coefficient (R^2) is in the range of 0.768 to 0.894 for zeolite-GAC arrangement. Whereas for GAC-zeolite arrangement, high R^2 values of 0.984 and 0.992, respectively were obtained for COD and color removal. On the other hand, the R^2 for ammonia is only 0.756. K_f value shows the combination of both adsorbents represents beneficial adsorption. Therefore, the adsorption (by both sequence arrangement) was favorable for COD, ammonia and color, whereby new adsorption sites are available and the adsorption capacity increases as the value of $1/n < 1$.

3.6 Langmuir Isotherm

The linear plot of specific adsorption ($1/q_e$) against the equilibrium concentration ($1/C_e$) (Figures 11 and 12) shows that the adsorption also obeys the Langmuir model. The Langmuir constants q_m and K_a were determined from the slope and intercept of the plot and are presented in Table 4. The value of the coefficient of correlation (R^2) range from 0.897 to 0.923 (for zeolite-GAC arrangement) and from 0.869 to 0.991 (for GAC-zeolite arrangement) obtained from Langmuir expression indicates that Langmuir expression provided a better fit to the experimental data.

Since the value of coefficient of determination (R^2) in Langmuir isotherm is almost the same with Freundlich isotherm in COD, ammonia and color removal for adsorption with GAC and zeolite, therefore, the results show the Langmuir isotherm is also fitted with the Freundlich model.

4. Conclusion

The treatment of dye wastewater using GAC and zeolite adsorbents was investigated under different experimental conditions in column process. The criteria of determining the reduction of contaminants are basically found that depend on the surface loading rate (SLR), bed depth of adsorbent, the empty bed contact time and the type of adsorbent used. The different in the length of adsorbent and surface diameter column will yield different contact time. In addition, the particle size of adsorbent will also affect the performance of adsorbent. Among the SLR that have been conducted in 1.91 cm, 3.81 cm and 6.35 cm diameter of surface column, the maximum SLR in removing contaminants was 2.84 ml/min.cm^2. The lower SLR and longer in adsorbent depth will increase the volume of adsorption process. The higher volume of the contact bed adsorbent yield the longer contact time and better removal will be produced. At the higher SLR will decrease the EBCT and lesser of contaminants will be adsorbed in GAC and zeolite. In relation to the characteristics of GAC and zeolite, a sequence of combination with both adsorbents may produce a better removal of contaminants. From the data that obtained, the arrangement of GAC as the bottom layer and zeolite as the upper layer produce better result in all parameters. The maximum removal of the contaminants among the all adsorption treatment was found using 10 cm of GAC (bottom layer) and 10 cm of zeolite (upper layer) in 6.35 cm diameter column with 59.46% removal of COD, 60.82% removal of ammonia and 58.4% removal of color. The Freundlich and Langmuir isotherm models were used to express the sorption phenomena of dye wastewater removal using sequence of combination of GAC and zeolite. Linear regression of the experimental data showed that the Freundlich and Langmuir isotherm models can be used to describe COD, ammonia and color removal.

Acknowledgement

References

Ahmad, A. A., & Hameed, B. H. (2009). Reduction of COD and color of dyeing effluent from a cotton textile mill by adsorption onto bamboo-based activated carbon. *Journal of Hazardous Materials,* 172, 1538-1543. http://dx.doi.org/10.1016/j.jhazmat.2009.08.025

Allen, S. J., Mckay, G., & Porter, J. F. (2004). Adsorption isotherm models for basic dye adsorption by peat in single and binary component systems. *Journal of Colloid and Interface Science,* 280, 322–333. http://dx.doi.org/10.1016/j.jcis.2004.08.078

Alvares, A. B. C, Diaper, C., & Parsons, S. A. (2001). Partial oxidation of hydrolysed and unhydrolysed textile azo dyes by ozone and the effect on biodegradability. *Process Safety and Environmental Protection,* 79(2), 103-108. http://dx.doi.org/10.1205/09575820151095184

APHA. (1992). Standard Methods for the Examination of Water and Waste Water, 19th ed. American Public Health Association, Washington, D.C.

Babu, B. R., Parande, A. K., Raghu, S., & Prem Kumar, T. (2007). Cotton textile processing: Waste generation and effluent treatment. *Journal of Cotton Science,* 11, 141–153.

Banerjee, P., Dasgupta, S., & De, S. (2007). Removal of dye from aqueous solution using a combination of advanced oxidation process and nanofiltration. *Journal of Hazardous Materials,* 140, 95-103. http://dx.doi.org/10.1016/j.jhazmat.2006.06.075

Butt, M. T., Arif, F., Shafique, T., & Imtiaz, N. (2005). Spectrophotometric estimation of colour in textile dyeing wastewater. *Journal of the Chemical Society of Pakistan*, 27(6), 627-630.

Chang, W., Hong, S., & Park, J. (2001). Effect of zeolite media for the treatment of textile wastewater in a biological aerated filter. *Process Biochemistry*, 37, 693–698. http://dx.doi.org/10.1016/S0032-9592(01)00258-8

Erdem, E., Çölgeçen, G., & Donat, R. (2005). The removal of textile dyes by diatomite earth. *Journal of Colloid and Interface Science,* 282, 314–319. http://dx.doi.org/10.1016/j.jcis.2004.08.166

Fan, L., Zhou, Y., Yang, W., Chen, G., & Yang, F. (2008). Electrochemical degradation of aqueous solution of Amaranth azo dye on ACF under potentiostatic model. *Dyes Pigments,* 76, 440–446. http://dx.doi.org/10.1016/j.dyepig.2006.09.013

Fathima, N. N., Aravindhan, R., Rao, J. R., & Nair, B. U. (2008). Dye house wastewater treatment through advanced oxidation process using Cu-exchanged Y zeolite: A heterogeneous catalytic approach. *Chemosphere,* 70, 1146–1151. http://dx.doi.org/10.1016/j.chemosphere.2007.07.033

Freundlich, H. M. F. (1906). Over the adsorption in solution. *Journal of Physical Chemistry*, 57, 385-470.

Garcia-Montano, J., Perez-Estrada, L., Oller, I., Maldonado, M. I., Torrades, F., & Peral, J. (2008). Pilot plant scale reactive dyes degradation by solar photo-Fenton and biological processes. *Journal of Photochemistry and Photobiology A: Chemistry*, 195, 205–214. http://dx.doi.org/10.1016/j.jphotochem.2007.10.004

Hameed, B. H. (2009a). Spent tea leaves: A new non-conventional and low-cost adsorbent for removal of basic dye from aqueous solutions. *Journal of Hazardous Materials,* 161, 753–759. http://dx.doi.org/10.1016/j.jhazmat.2008.04.019

Hameed, B. H. (2009b). Evaluation of papaya seeds as a novel non-conventional low-cost adsorbent for removal of methylene blue. *Journal of Hazardous Material*s, 162, 939–944. http://dx.doi.org/10.1016/j.jhazmat.2008.05.120

Hameed, B. H., Krishni, R. R., & Sata, S. A. (2009). A novel agricultural waste adsorbent for the removal of cationic dye from aqueous solutions. *Journal of Hazardous Materials*, 162, 305–311. http://dx.doi.org/10.1016/j.jhazmat.2008.05.036

Ilyas, H. (2007). Penyerapan besi dan ammonium dalam air oleh zeolite Lampung. MSc Thesis, Universitas Islam Negeri Syarif Hidayatullah, Jakarta.

Jung, J., Chung, Y. C., Shin, H. S., & Son, D. H. (2004). Enhanced ammonia nitrogen removal using existent biological regeneration and ammonium exchange of zeolite in modified SBR process. *Water Research*, 38, 347–354. http://dx.doi.org/10.1016/j.watres.2003.09.025

Kalderis, D., Koutoulakis, D., Paraskeva, P., Diamadopoulos, E., Otal, E., del Valle, J. O., & Fernández-Pereira, C. (2008). Adsorption of polluting substances on activated carbons prepared from rice husk and sugarcane bagasse. *Chemical Engineering Journal*, 144(1), 42-50. http://dx.doi.org/10.1016/j.cej.2008.01.007

Langmuir, I. (1916). The constitution and fundamental properties of solids and liquids, Part I. Solids. *Journal of the American Chemical Society*, 38(11), 2221–2295. http://dx.doi.org/10.1021/ja02268a002

Lee, J. H., Kim, D. S., Lee, S. O., & Shin, B. S. (1996). Treatment of municipal landfill leachates using artificial zeolite. *Chawon Risaikring*, 5, 34-41.

Lodha, B., & Chaudhari, S. (2007). Optimization of Fenton-biological treatment scheme for the treatment of aqueous dye solutions. *Journal of Hazardous Materials*, 148, 459-466. http://dx.doi.org/10.1016/j.jhazmat.2007.02.061

Mahmoud, A. S., Brooks, M. S., & Ghaly, A. E. (2007). Decolorization of remazol brilliant blue dye effluent by advanced photo oxidation process (H_2O_2/UV system). *American Journal of Applied Sciences*, 4(12), 1054-1062. http://dx.doi.org/10.3844/ajassp.2007.1054.1062

Otal, E., Vilches, L. F., Moreno, N., Querol, X., Vale, J., & Fernández Pereira, C. (2005). Application of zeolitised coal fly ashes to the depuration of liquid wastes. *Fuel,* 84, 1440-1446. http://dx.doi.org/10.1016/j.fuel.2004.08.030

Pinheiro, H. M., Touraud, E., & Thomas, O. (2004). Aromatic amines from azo dye reduction: status review with emphasis on direct UV spectrophotometric detection in textile industry wastewaters. *Dyes and Pigments*, 61, 121–139. http://dx.doi.org/10.1016/j.dyepig.2003.10.009

Tien, C. (1994). Adsorption Calculations and Modeling. Butterworth-Heinemann, Boston

Wu, J. S., Liu, C. H., Chu, K. H., & Suen, S. Y. (2008). Removal of cationic dye methyl violet 2B from water by cation exchange membranes. *Journal of Membrane Science*, 309, 239-245. http://dx.doi.org/10.1016/j.memsci.2007.10.035

Zhang, X., Zhu, W., Liu, H., & Wang, T. (2004). Novel tubular composite carbon-zeolite membranes. *Material Letters,* 58, 2223–2226. http://dx.doi.org/10.1016/j.matlet.2004.01.027

Table 1. Characteristics of the raw dye wastewater

Parameter	Unit	Average Value
pH	-	9.0-10.18
Turbidity	FAU	63-74
COD	mg/L	298-360
Suspended solid	mg/L	0.0076
Zinc	mg/L	< 0.2
Manganese	mg/L	0.5-0.6
Iron	mg/L	0.13-0.15
Copper	mg/L	0.03
Ammonia	mg/L	2.10-3.8
True Color	PtCo	680-750

Table 2. The arrangement of the experiment studies

Experiment	Bottom Layer	Upper Layer
Experiment 1	GAC	
Experiment 2	Zeolite	
Experiment 3	Zeolite	GAC
Experiment 4	GAC	Zeolite

Table 3. Freundlich isotherm for COD, ammonia and color removal

Parameters	COD	Ammonia	Color
Zeolite-GAC arrangement:			
R^2	0.894	0.768	0.793
K_f	1.293×10^{-9}	6.382×10^{-6}	2.862×10^{-11}
1/n	0.383	0.336	0.310
Freundlich equation	$q_e = 1.293 \times 10^{-9} C_e^{0.383}$	$q_e = 6.382 \times 10^{-6} C_e^{0.336}$	$q_e = 2.862 \times 10^{-11} C_e^{0.310}$
GAC-Zeolite arrangement:			
R^2	0.984	0.756	0.992
K_f	3.171×10^{-7}	6.866×10^{-6}	3.124×10^{-11}
1/n	0.641	0.425	0.269
Freundlich equation	$q_e = 3.171 \times 10^{-7} C_e^{0.641}$	$q_e = 6.866 \times 10^{-6} C_e^{0.425}$	$q_e = 3.124 \times 10^{-11} C_e^{0.269}$

Table 4. Langmuir isotherm for COD, ammonia and color removal

Parameters	COD	Ammonia	Color
Zeolite-GAC arrangement:			
R^2	0.923	0.897	0.911
K_a (L/g)	-0.264	-0.750	-0.003
q_m (mg/g)	-1.54×10^{-3}	-1.89×10^{-6}	-4.28×10^{-4}
Langmuir Equation	$q = \dfrac{4.066 \times 10^{-4} C_e}{1 - 0.264 C_e}$	$q = \dfrac{1.418 \times 10^{-6} C_e}{1 - 0.750 C_e}$	$q = \dfrac{1.284 \times 10^{-6} C_e}{1 - 0.003 C_e}$
GAC-Zeolite arrangement:			
R^2	0.976	0.869	0.991
K_a (L/g)	0.0043	0.6494	0.00369
q_m (mg/g)	5.4×10^{-4}	3.2×10^{-6}	3.3×10^{-4}
Langmuir Equation	$q = \dfrac{2.322 \times 10^{-6} C_e}{1 - 0.0043 C_e}$	$q = \dfrac{2.078 \times 10^{-6} C_e}{1 - 0.6494 C_e}$	$q = \dfrac{1.218 \times 10^{-6} C_e}{1 - 0.00369 C_e}$

Figure 1. Column studies

(a)

(b)

(c)

Figure 2. Removal efficiency of (a) COD, (b) ammonia and (c) color in dye wastewater using GAC column
(with surface diameter of 1.91 cm) at different SLR and bed height

(a)

(b)

(c)
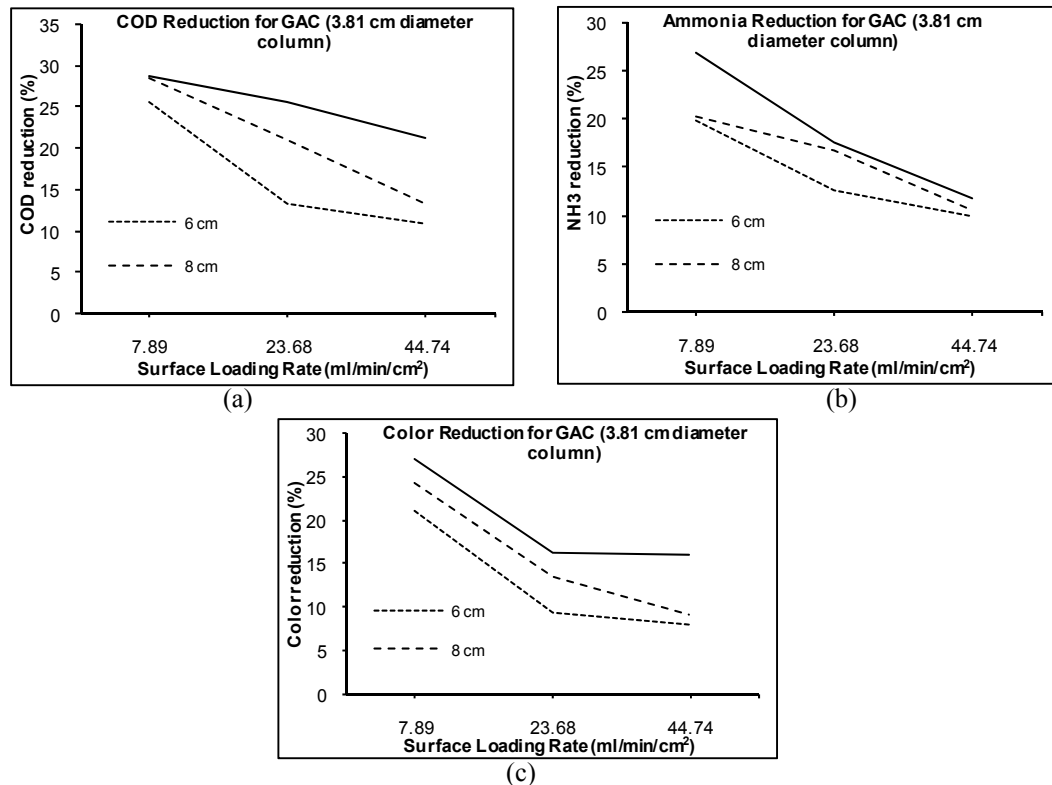
Figure 3. Removal efficiency of (a) COD, (b) ammonia and (c) color in dye wastewater using GAC column
(with surface diameter of 3.81 cm) at different SLR and bed height

(a)

(b)

(c)
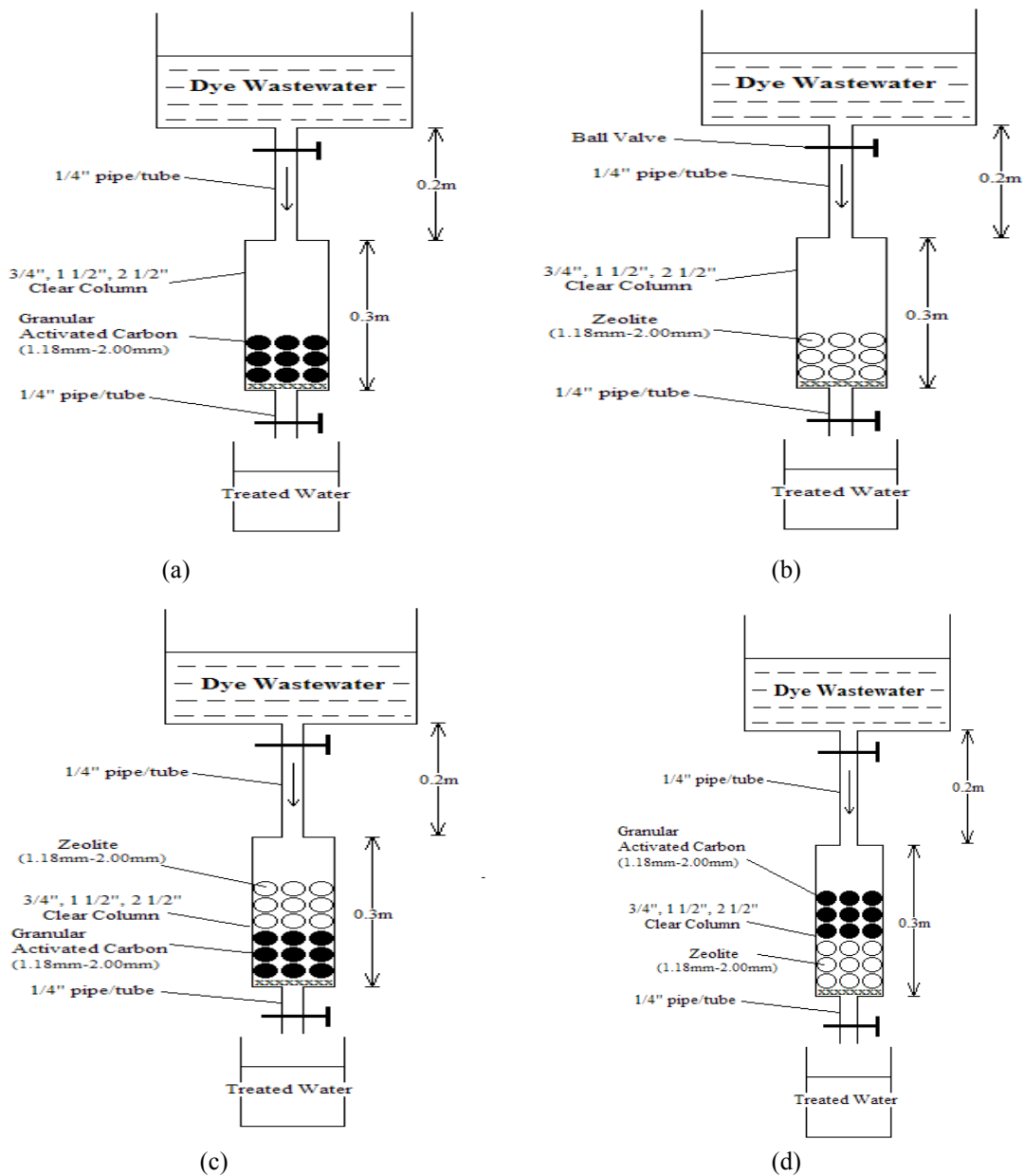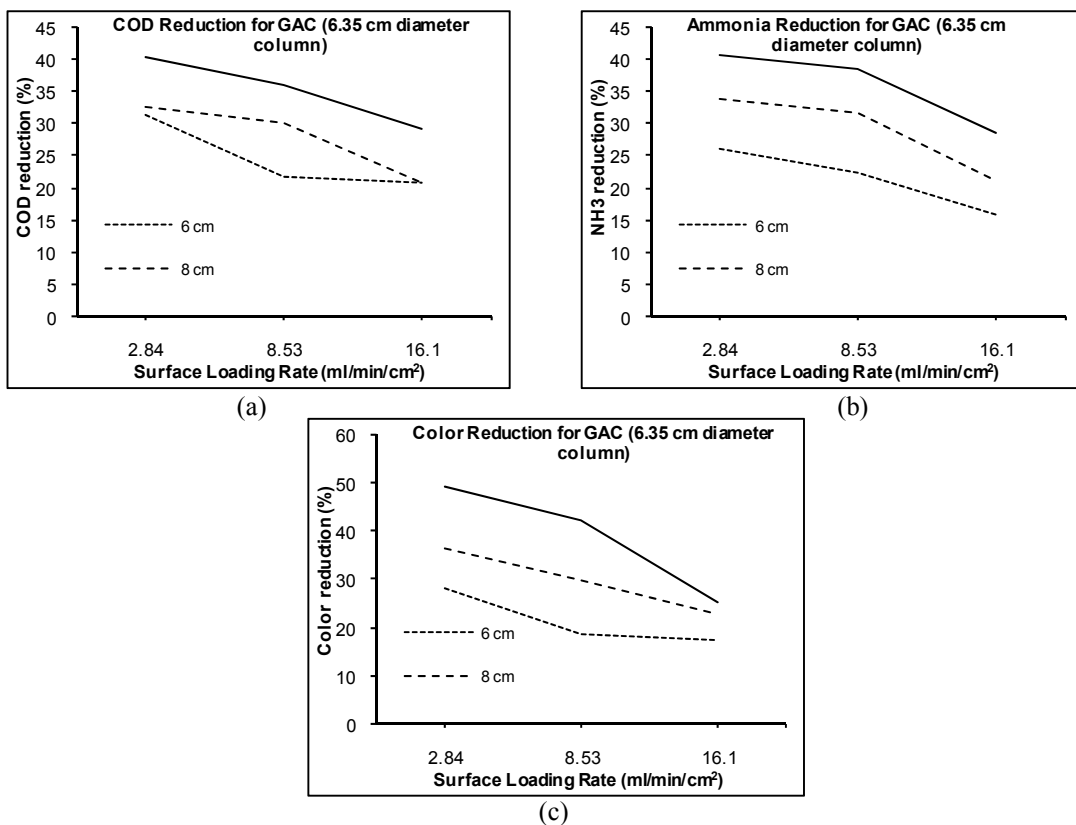
Figure 4. Removal efficiency of (a) COD, (b) ammonia and (c) color in dye wastewater using GAC column
(with surface diameter of 6.35 cm) at different SLR and bed height

(a)
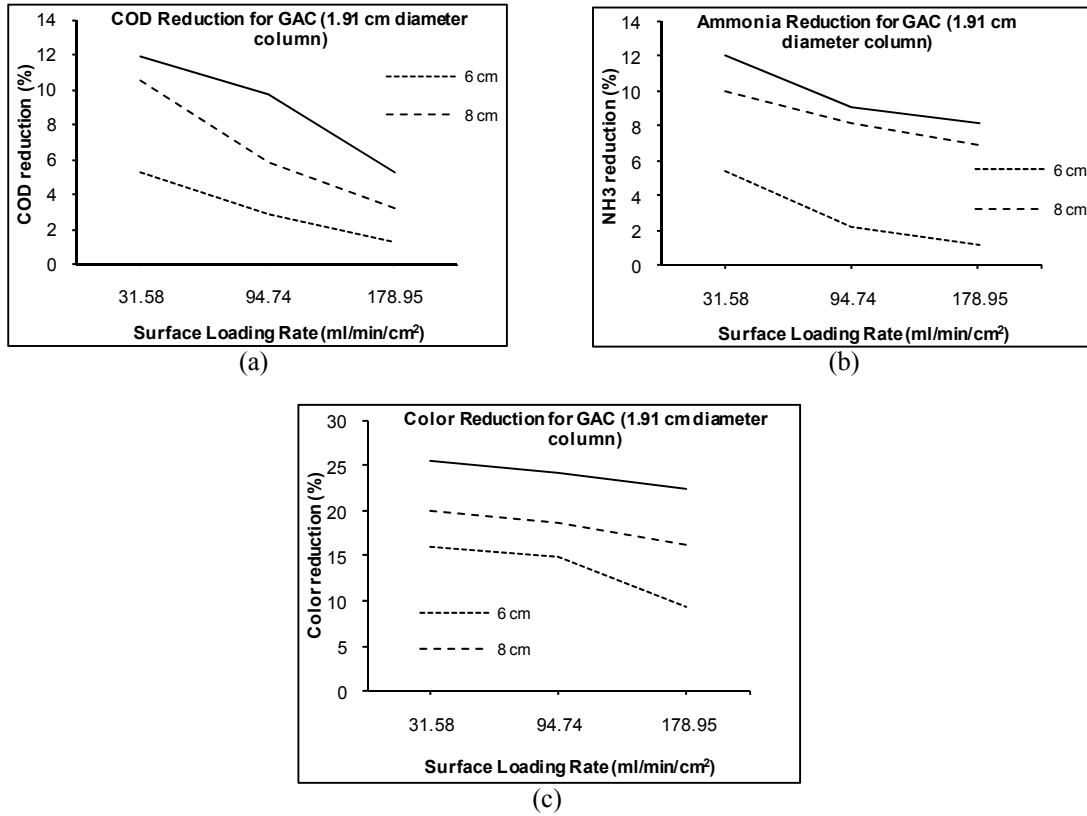

(b)

(c)
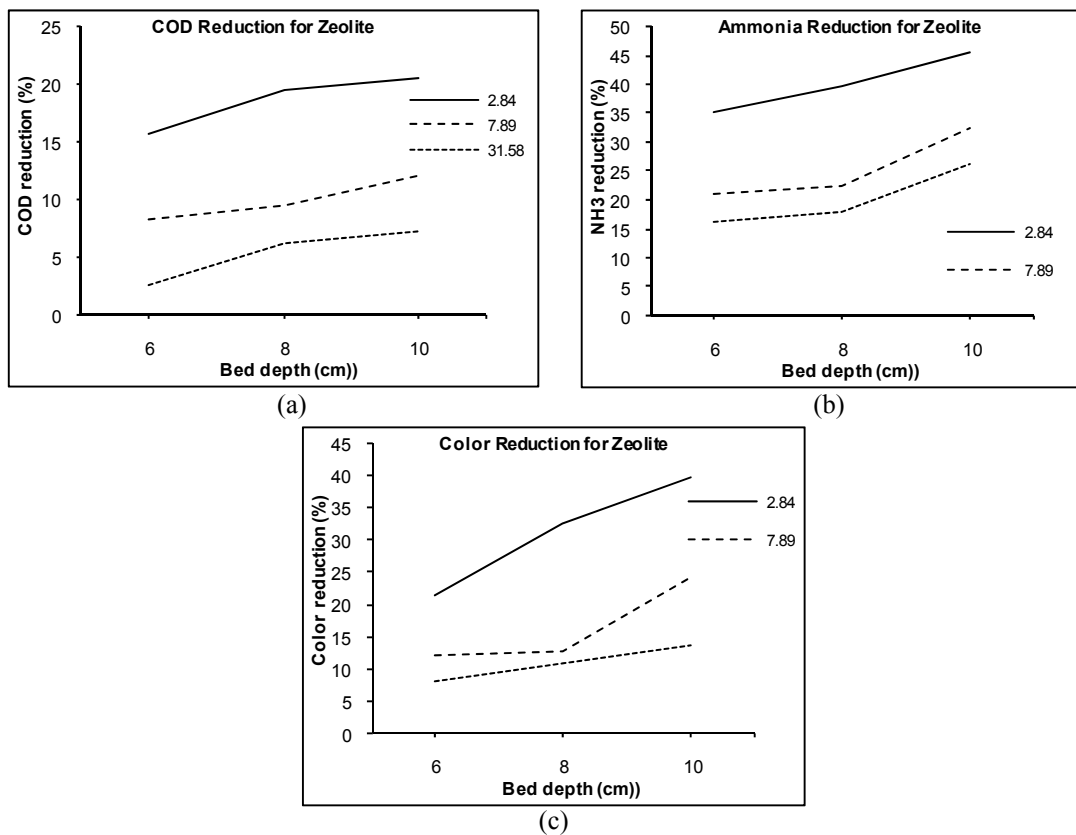
Figure 5. Removal efficiency of (a) COD, (b) ammonia and (c) color in dye wastewater using zeolite column
(with surface diameter of 1.91 cm) at different SLR and bed height

(a)

(b)

(c)
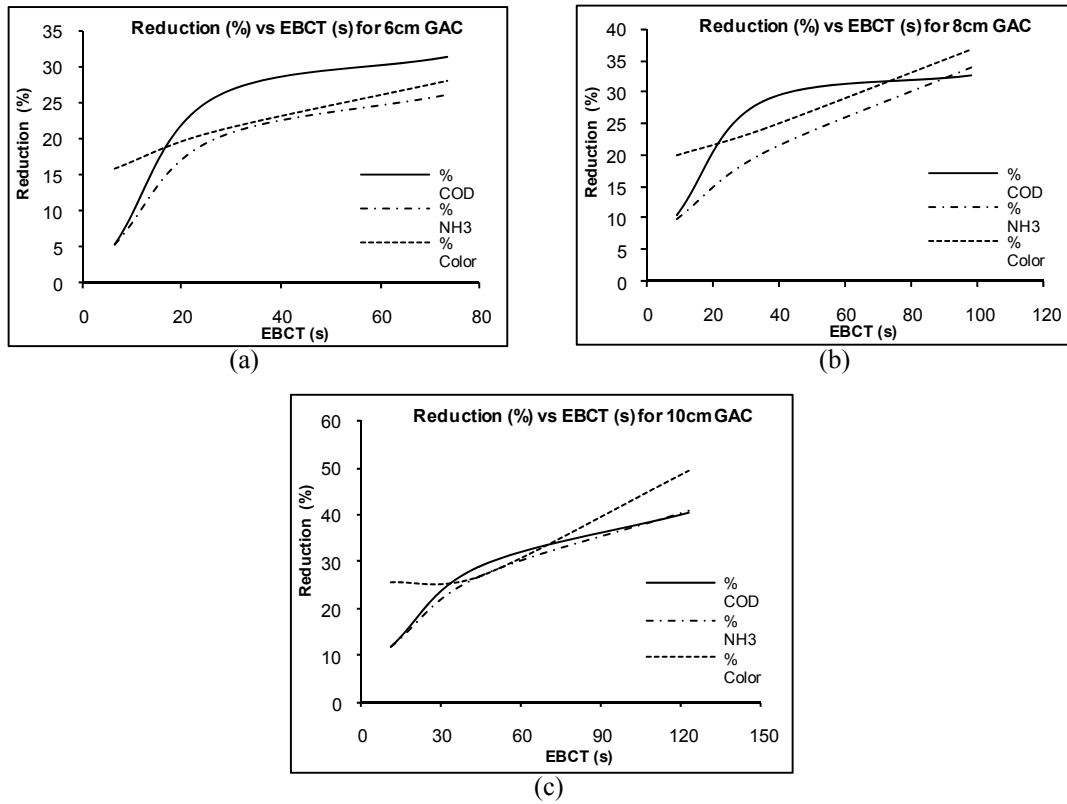
Figure 6. Removal efficiency of COD, ammonia and color in dye wastewater using (a) 6 cm (b) 8 cm and (c) 10 cm GAC height at different contact time (EBCT)

(a)

(b)

(c)
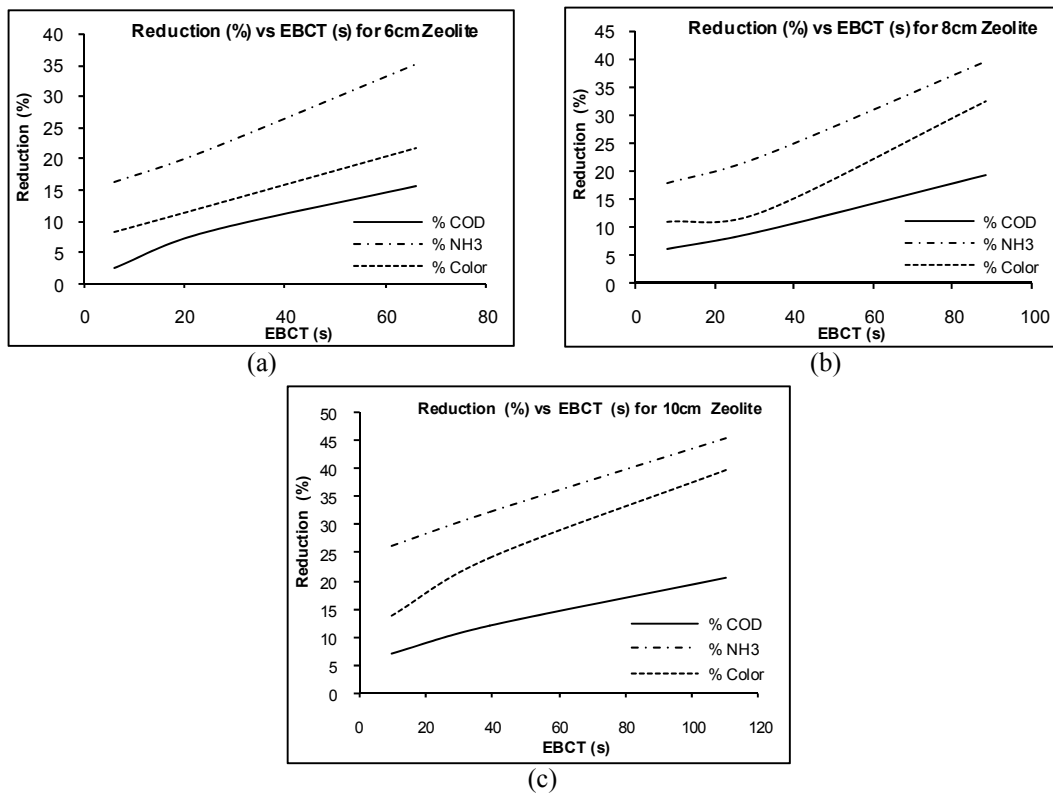
Figure 7. Removal efficiency of COD, ammonia and color in dye wastewater using (a) 6 cm (b) 8 cm and (c) 10 cm zeolite height at different contact time (EBCT)

(a)   (b)
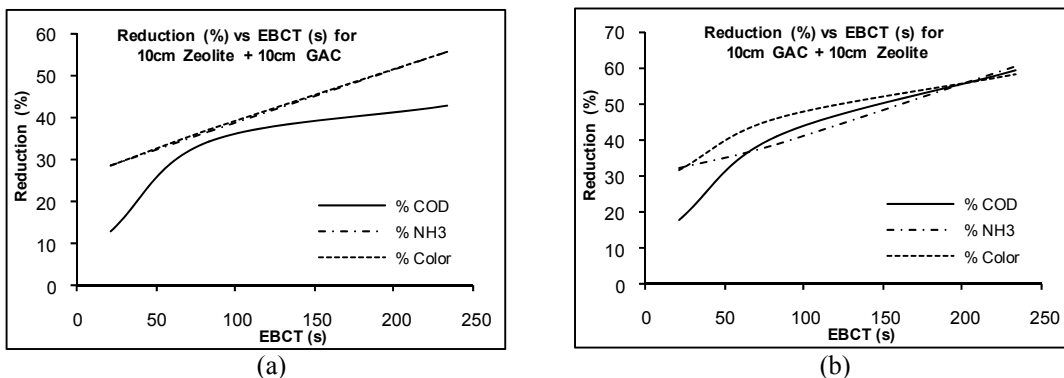
Figure 8. Removal efficiency of COD, ammonia and color in dye wastewater using (a) zeolite-GAC and (b) GAC-zeolite sequence arrangements at different contact time (EBCT)

(a)   (b)

(c)
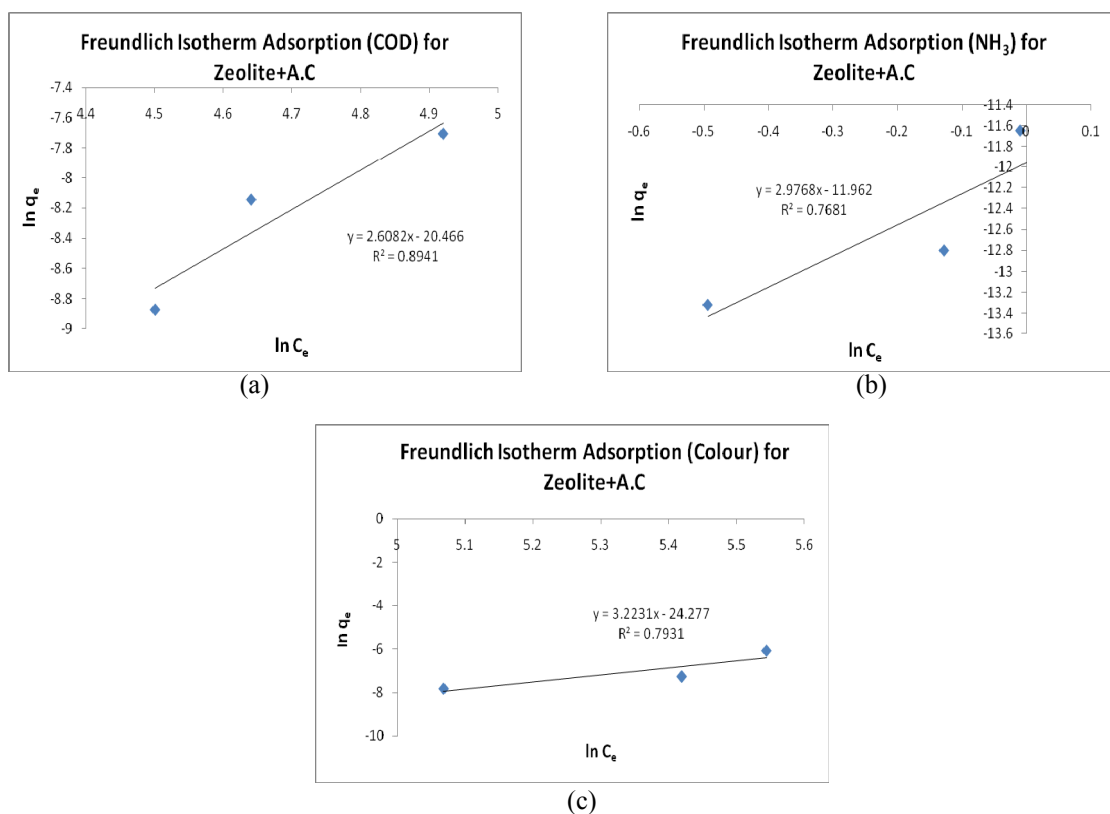
Figure 9. Freundlich isotherm for (a) COD, (b) ammonia and (c) color removal for dye wastewater treatment with zeolite as bottom layer and GAC as upper layer

(a)   (b)

(c)
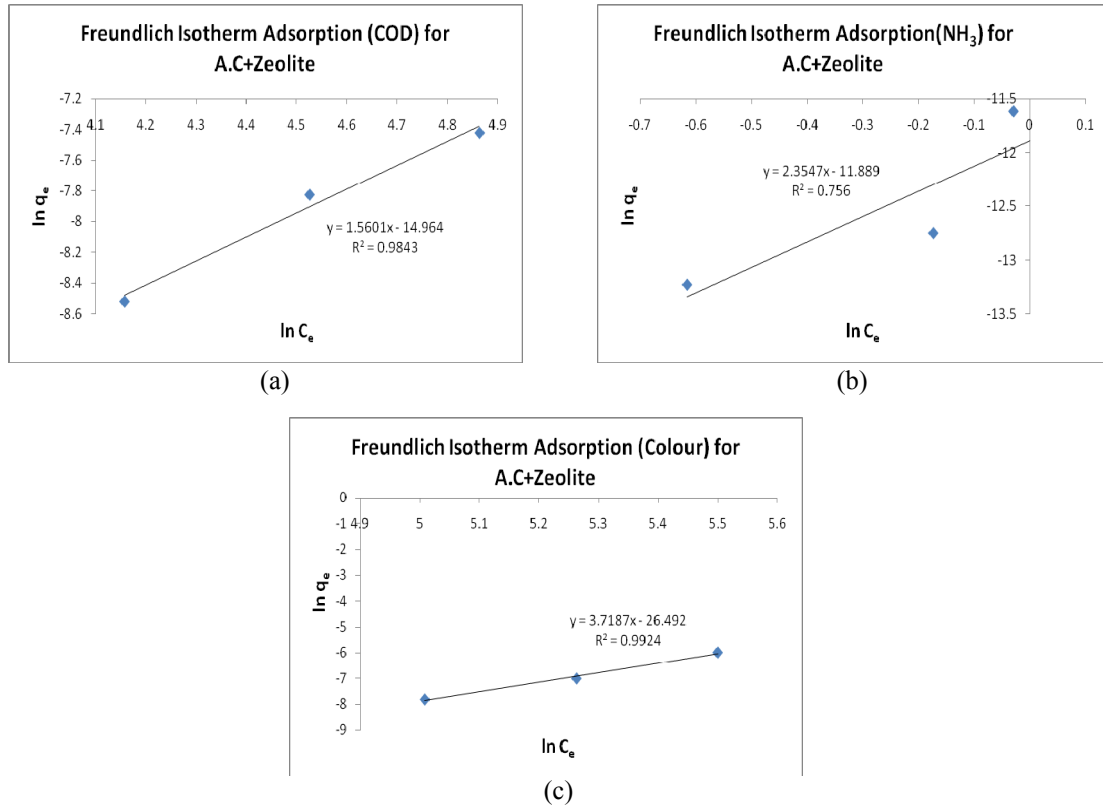
Figure 10. Freundlich isotherm for (a) COD, (b) ammonia and (c) color removal for dye wastewater treatment with GAC as bottom layer and zeolite as upper layer

(a)   (b)

(c)
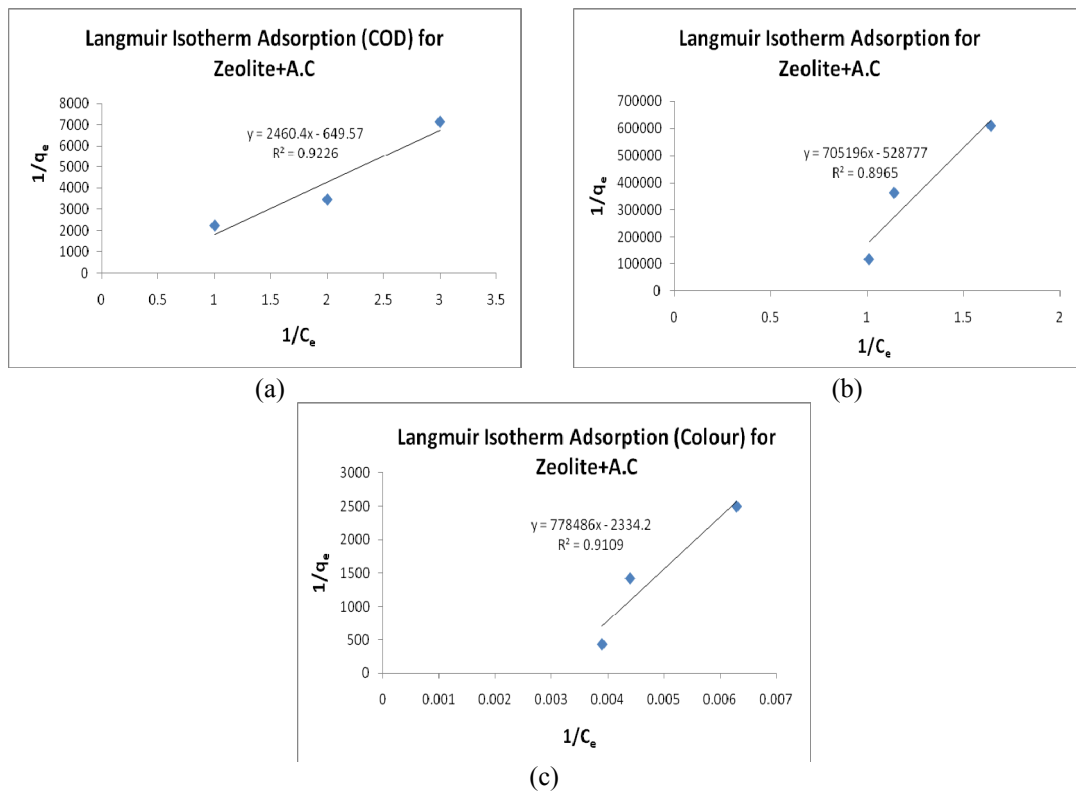
Figure 11. Langmuir isotherm for (a) COD, (b) ammonia and (c) color removal for dye wastewater treatment with zeolite as bottom layer and GAC as upper layer

(a)

(b)

(c)
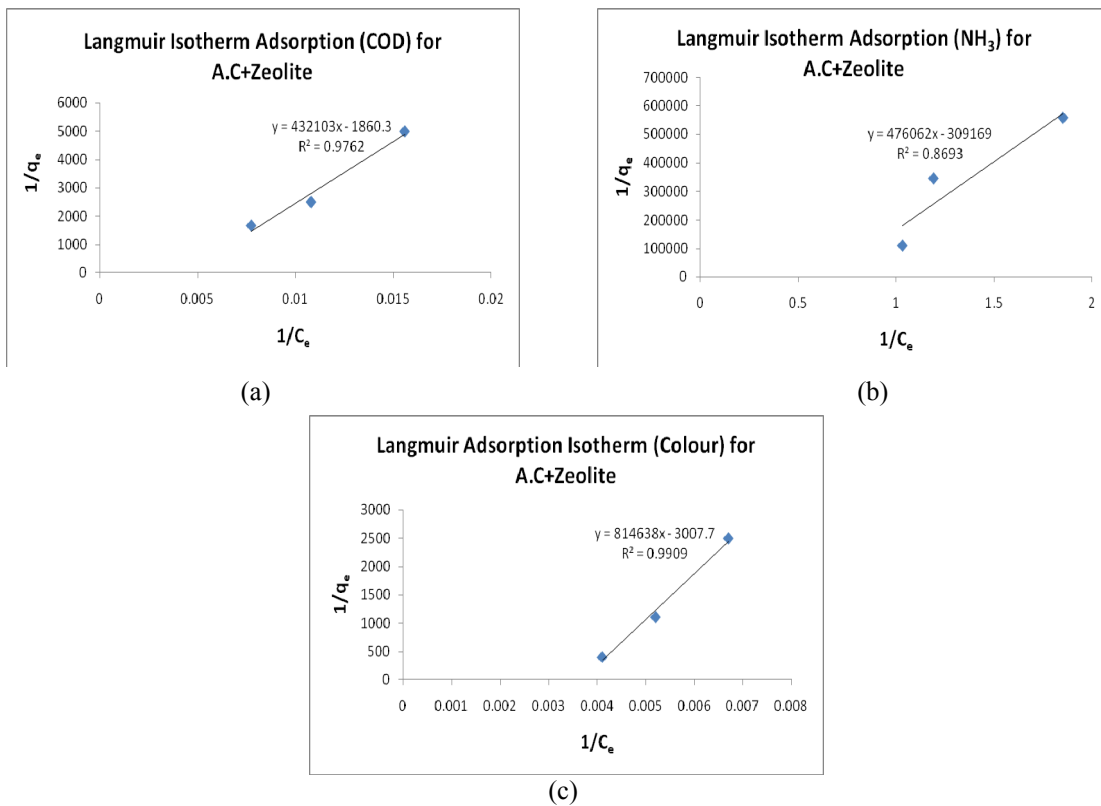
Figure 12. Langmuir isotherm for (a) COD, (b) ammonia and (c) color removal for dye wastewater treatment with GAC as bottom layer and zeolite as upper layer

Review Power Quality Issues

Mahmoud S. Awad

Faculty of engineering Technology, Al-Balqa' Applied University

Amman, Jordan Amman, PO box 15008, Marka Ashamalia

Tel: 962-7738-7901   Email: dr_awad_m@yahoo.com,

Abstract

This paper introduces the terminology and various issues related to 'power quality'. The interest in power quality is explained in the context of a number of much wider developments in power engineering: deregulation of the electricity industry, increased customer-demands, and the integration of renewable energy sources. After an introduction of the different terminology power quality disturbances are discussed in detail: voltage dips and harmonic distortion. For each of these two disturbances, a number of other issues are briefly discussed, which are characterisation, origin, mitigation, and the need for future research.

Keywords: Power quality, Harmonic distortion, Voltage dips

1. Introduction

Power Quality (PQ) has become increasingly important for industrial and commercial electric power customers, particularly as today's manufacturing and control processes rely on computerized equipment which is sensitive to power system interruptions and disturbances. Power Quality is simply the characteristic of the energy or electrical supply by the utility which might affect the load (electrical equipments that are connected for an electrical supply) or vise versa (Faisal, 2005).

Power quality issues have in recent years received an increasing attention both by the end users and utilities alike. This paper aims to elaborate power quality issues and the impact it may have to the users and utilities as utilities are bound in most cases to a pre-determined quality supply agreement.

2. Effects of Power Quality to Industrial Users

Electrical power is perhaps the most essential raw material used by commerce and industry today. It is an unusual commodity because it is required as a continuous flow it cannot be conveniently stored in quantity and it cannot be subject to quality assurance checks before it is used. It is, in fact, the epitome of the 'Just in Time' philosophy in which components are delivered to a production line at the point and time of use by a trusted and approved supplier with no requirement for 'goods in' inspection. Thus, it is necessary for end customer to have good control of the onwards supply component specification. The reliability of the supply must be known and the resilience of the process to variations must be understood. In reality, of course, electricity is very different from any other product it is generated far from the point of use, is fed to the grid together with the output of many other generators and arrives at the point of use via several transformers and many kilometers of overhead and possibly underground cabling. Where the industry has been privatized, these network assets will be owned, managed and maintained by a number of different organizations. Assuring the quality of delivered power at the point of use is no easy task and there is no way that sub-standard electricity can be withdrawn from the supply chain or rejected by the customer.

From the consumers' point of view the problem is even more difficult. There are some limited statistics available on the quality of delivered power, but the acceptable quality level as perceived by the supplier (and the industry regulator) may be very different from that required, or perhaps desired, by the consumer. The most obvious power defects are complete interruption (which may last from a few seconds to several hours) and voltage dips or sags where the voltage drops to a lower value for a short duration. Naturally, long power interruptions are a problem for all users, but many operations are very sensitive to even very short interruptions. Examples of sensitive operation are (Mertens Jr., et al., 2004):

- Continuous process operations, where short interruptions can disrupt the synchronization of the machinery and result in large volumes of semi-processed product. A typical example is the paper making industry where the clean-up operation is long and expensive.

- Multi-stage batch operations, where an interruption during one process can destroy the value of previous operations. An example of this type is the semiconductor industry, where the production of a wafer requires a few dozen processes over several days and the failure of a single process is catastrophic.

- Data processing, where the value of the transaction is high but the cost of processing is low, such as share and foreign exchange dealing. The inability to trade can result in large losses that far exceed the cost of the operation

3. Common Power Quality Problems

So, what do we mean by 'power quality'? A perfect power supply would be one that is always available, always within voltage and frequency tolerances, and has a pure noise free sinusoidal wave shape (Felce, et al., 2004; Pirjo, & Matti 2003). Just how much deviation from perfection can be tolerated depends on the user's application, the type of equipment installed and his view of his requirements. Power quality defects the deviations from perfection fall into six categories:

1. Voltage Fluctuation (flicker)

2. Harmonic Distortion

3. Power Frequency Variation

4. under or over voltage

5. Voltage Dips (or sags) and Surges

6. Transients

Each of these power quality problems has a different cause. Some problems are a result of the shared infrastructure. For example, a fault on the network may cause a dip that will affect some customers and the higher the level of the fault, the greater the number affected, or a problem on one customer's site may cause a transient that affects all other customers on the same subsystem. Other problems, such as harmonics, arise within the customer's own installation and may or may not propagate onto the network and so affect other customers. Harmonic problems can be dealt with by a combination of good design practice and well proven reduction equipment (Arrilaga, & Chen, 2001). Electricity utilities argue that critical users must bear the costs of ensuring supply quality themselves rather than expect the supply industry to provide a very high reliability supply to every customer everywhere on the network (Mertens Jr., et al., 2003). Such a guaranteed quality supply would require a very substantial investment in additional network assets for the benefit of relatively few customers (in numerical, not consumption, terms) and would be uneconomic. It is also doubtful whether it would be technically feasible within the current social and legal framework in which any customer is normally entitled to be connected to the supply and utility providers have the right to excavate roadways with the risk of cable damage. It is therefore a growing trend that critical industry consumer take steps to ensure that the quality of power delivered to his process is good enough, with the clear implication that this quality level may well be higher than that delivered to the plant by the utilities.

3.1 Transients

AC and DC drives, along with other electronic loads, can be very sensitive to transient voltages. The tolerance levels of these devices are often less than other loads such as standard motors. A major concern for transient voltages occurs with possible magnification of utility capacitor switching transients at low-voltage capacitor locations on customer power systems. Transient disturbances are high frequency events with durations much less than one cycle of the supply (Arrilaga, & Chen, 2001). Causes include switching or lightning strikes on the network and switching of reactive loads on the consumer's site or on sites on the same circuit. Transients can have magnitudes of several thousand volts and so can cause serious damage to both the installation and the equipment connected to it. Electricity suppliers and telecommunications companies go to some effort to ensure that their incoming connections do not allow damaging transients to propagate into the customers' premises. Nevertheless, non-damaging transients can still cause severe disruption due to data corruption. The generation and influence of transients is greatly reduced and the efficacy of suppression techniques greatly enhanced where a good high integrity earthing system has been provided. Such an earthing system will have multiple ground connections and multiple paths to earth from any point, so ensuring high integrity and low impedance over a wide frequency band.

3.2 Voltage Sags and Momentary Interruptions

Voltage sag is widely recognized as one of the most important power quality disturbances (Wahab, & Alias, 2006). These can be caused by the utility or by customer loads. When sourced from the utility, they are most commonly caused by faults on the distribution system. Voltages sag as shown in Figure 1 is a short reduction in *rms* voltage from nominal voltage, happened in a short duration, about 10 ms to seconds (Dugan, et al., 2003).

Can be single or three phases, Depending on the design of the distribution system, a ground fault on one phase can cause a simultaneous swell on another phase. The IEC 61000-4-30 defines the voltage sag (dip) as a temporary reduction of the voltage at a point of the electrical system below a threshold (IEEE, 1993). According to IEEE Standard 1159-1995, defines voltage sags as an *rms* variation with a magnitude between 10% and 90% of nominal voltage and duration between 0.5 cycles and one minute (IEEE Working Group P1346, 1994).

Voltage sag normally happens at the feeder adjacent to an unhealthy feeder. This unhealthy feeder are caused by two factors which are short circuits due to faults in power system networks and starting motor which draw very high lagging current. Both of these factors are the main factor creating voltage sag as power quality problem in power system.

Increased sensitivity of power electronic equipment such as programmable logic controller (PLC), adjustable speed drive (ASD), coupled with the high likelihood of voltage sags and interruptions, has resulted in these being the most visible power quality events. Adjustable-speed drives, computers, office equipment, programmable controllers, and induction heating furnaces can be extremely sensitive to these events. Typically, sags occur when there are temporary faults on the utility power system, resulting in a reduction in the voltage level (McGranaghan, et al., 1993). Equipment sensitivity to these events is important because nuisance tripping of sensitive industrial loads can cause equipment downtime, reduce productivity, and hurt your bottom line. There are many ways in order to mitigate voltage sag problem. One of them is minimizing short circuits caused by utility directly which can be done such as with avoid feeder or cable overloading by correct configuration planning. Another alternative is using the flexible ac technology (FACTS) devices which have been used widely in power system nowadays because of the reliability to maintain power quality condition including voltage sag (Bollen, 2000). There are many devices have been created with purpose to enhance power quality such as Dynamic Voltage Restorer (DVR), Distribution Static Compensator (D-STATCOM) and Uninterruptible Power Supply (UPS). All of these devices are also known as custom power devices.

3.3 Harmonics Distortion

Harmonic distortion of the voltage and current results from the operation of nonlinear loads and devices on the power system, the nonlinear loads that cause harmonics can often be represented as current sources of harmonics (Dugan, et al., 1996). The system voltage appears stiff to individual loads and the loads draw distorted current waveforms. Table 1 illustrates some example current waveforms for different types of nonlinear loads. The weighting factors indicated in the table are being proposed in the Guide for Applying Harmonic Limits on the Power System for preliminary evaluation of harmonic producing loads in a facility.

Harmonic voltage distortion results from the interaction of these harmonic currents with the system impedance. The harmonic standard (IEEE 519-1992), has proposed two way responsibilities for controlling harmonic levels on the power system.

1. End users must limit the harmonic currents injected onto the power system.

2. The power supplier will control the harmonic voltage distortion by making sure system resonant conditions do not cause excessive magnification of the harmonic levels.

Harmonic distortion levels can be characterized by the complete harmonic spectrum with magnitudes and phase angles of each individual harmonic component. It is also common to use a single quantity, the Total Harmonic Distortion, as a measure of the magnitude of harmonic distortion. For currents, the distortion values must be referred to a constant base (e.g. the rated load current or demand current) rather than the fundamental component. This provides a constant reference while the fundamental can vary over a wide range

Harmonic distortion is a characteristic of the steady state voltage and current. It is not a disturbance. Therefore, characterizing harmonic distortion levels is accomplished with profiles of the harmonic distortion over time (e.g. 24 hours) and statistics. Figure 2 illustrates a typical profile of harmonic voltage distortion on a feeder circuit over a one month period.

3.4 Voltage Fluctuation

Flicker is the impression of unsteadiness of visual sensation induced by a light stimulus, the luminance or spectral distribution of which fluctuates with time. Usually, it applies to cyclic variation of light intensity of lamps caused by fluctuation of the supply voltage. Flicker is symptoms of voltage fluctuation which can be caused by disturbances introduced during power generation, transmission or distribution, but are typically caused by the use of large fluctuating loads, i.e. loads that have rapidly fluctuating active and reactive power demand (Power Quality' Working Group WG2, 2000). The following sections examine the nature of voltage fluctuations, their causes, and effects, methods of measurement, mitigation and applicable standards.

3.4.1 Causes of Voltage Fluctuations

The classification of *rms* voltage variations is shown in Figure 3 as a plot of voltage against duration of disturbance. The hatched areas correspond to the voltage changes considered in this paper.

For any supply line, the voltage at the load end is different from that at the source. This can be demonstrated from the per-phase equivalent circuit in Figure 4a. The relationship (1, below) illustrates how the value of the voltage difference ΔU, defined in Figure 4b, can be derived from the phasor diagram and simple geometrical rules.

$$\frac{E - U_0}{U_0} \approx \frac{\Delta U}{U_0} = R_S \frac{P}{U_0^2} + X_S \frac{Q}{U_0^2} = \approx R_S \frac{P}{U_0^2} + \frac{Q}{S_{ZW}} \tag{1}$$

Where:

E	= The source voltage
U_0	= The voltage at the load terminal
I_0	= Current
Z_S, X_S, R_S	=Equivalent impedance, reactance and resistance of the line respectively
P, Q	=active and reactive power of the load
S_{ZW}	=short-circuit power at the point of load connection (SSC).

Assuming that the equivalent resistance of the line is negligibly small compared with its reactance ($XS > 10RS$), which holds true for practical MV and HV supply systems, the following relationship defines the relative value of voltage change at the load-end of the line:

$$\frac{\Delta U}{U_0} \cong \frac{Q}{S_{ZW}} \tag{2}$$

Depending on its cause, voltage change ΔU can take the form of a voltage drop having a constant value over a long time interval, a slow or rapid voltage change, or a voltage fluctuation. Voltage fluctuation is defined as a series of *rms* voltage changes or a cyclic variation of the voltage waveform envelope as shown in Figure 5.

The defining characteristics of voltage fluctuations are:

- The amplitude of voltage change (difference of maximum and minimum *rms* or peak voltage value, occurring during the disturbance),
- The number of voltage changes over a specified unit of time, and
- The consequential effects (such as flicker) of voltage changes associated with the disturbances.

4. Conclusion

To overcome the negative impact of poor power quality on equipment and businesses, suitable power quality equipment can be invested. Identifying the right solution remains the first step. Many power quality problems are easily identified once a good description of the problems is obtained. Unfortunately, the tensions caused by power problems often result in vague or overly dramatic descriptions of the problem. A power quality audit can help determine the causes of your problems and provide a well-designed plan to correct them. The power quality audit checks the facility's wiring and grounding to ensure that it is adequate for your applications and up to code. The auditor normally will check the quality of the AC voltage itself, and consider the impact of the utility's power system. Many businesses and organizations rely on computer systems and other electrical equipment to carry out the mission critical functions, but they aren't safeguarding against the dangers of an unreliable power supply. It is time utilities as well as businesses engage in more proactive approach to power quality treats by engaging in power quality analysis.

References

Arrilaga, J., & Chen, S. (2001). Power System Quality Assessment. (2nd ed.) *John Wiley & Sons,* Britain.

Bollen, M. H. J. (2000). *Understanding Power Quality Problems: Voltage Sags and Interruptions.* IEEE Press, New York.

Dugan, R. C., McGranaghan, M. F., & Beaty, H. W. (1996). Electric Power Systems Quality, McGraw-Hill, New York

Dugan, R. C., McGranaghan, M. F., & Beaty, H. W. (2003). Electrical Power Systems Quality, McGraw-Hill, 2nd Ed.

Electrical Power System Compatibility with Industrial Process Equipment - Part 1. (1994). Voltage Sags, Paper by the IEEE Working Group P1346, Proceedings of the Industrial and Commercial Power Systems Conference, 94CH3425-6, May.

Faisal, M. F. (2005). Power quality management program: TNB's Experience. Distribution Engineering Department, TNB.

Felce, A., Matas, G., & Silva, Y. D. (2004). Voltage Sag Analysis and Solution for an Industrial Plant with Embedded Induction Motors. Inelectra S.A.C.A., Caracas, Venezuela.

Heine, P., & Lehtonen, M. (2003). Voltage Sag Distributions caused by Power System Faults. *IEEE Transactions on Power Systems,* 18(4). http://dx.doi.org/10.1109/TPWRS.2003.818606

IEEE Std. 519-1992. (1993). IEEE Recommended Practices and Requirements for Harmonic Control in Electrical Power Systems, IEEE, New York.

Mertens Jr., E. A., Bonatto, B. D., & Dias, L. F. S. (2004). Evaluation of the electric system on short-duration voltage variation (in Proceedings). XVI National Seminar on Electric Energy Distribution (XVI SENDI), Brasilia, DF, Brazil, November, 21-24.
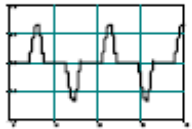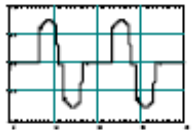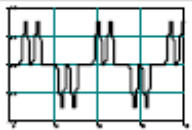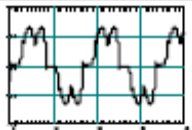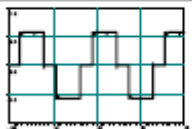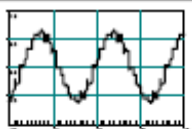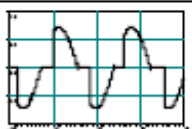
McGranaghan, M., Mueller, D., & Samotyj, M. (1993). Voltage Sags in Industrial Plants. *IEEE Transactions on Industry Applications,* 29(2). http://dx.doi.org/10.1109/28.216550

Mertens Jr., E. A., da Silva, E. S., Bonatto, B. D., & Dias, L. F. S. (2003). Impact of frequency variations versus short-duration voltage variations (in Proceedings). XVII National Seminar on Production and Transmission of Electric Energy (SNPTEE), Uberlandia-MG, Brazil, October, 19-24.

Power Quality' Working Group WG2. (2000). Guide to Quality of Electrical Supply for Industrial Installations, Part 5, Flicker and Voltage Fluctuations.

Wahab, W. W, & Alias, M. Y. (2006). Voltage Sag and Mitigation Using Dynamic Voltage Restorer (DVR) System. Faculty of Electrical Engineering, University Technology Malaysia. *Elektrika,* 8, 32-37.

Table 1. Example current waveforms for various nonlinear loads

Type of Load	Typical Waveform	Current Distortion	Weighting Factor (W_i)
Single Phase Power Supply		80% (high 3rd)	2.5
Semiconverter		high 2nd,3rd, 4th at partial loads	2.5
6 Pulse Converter, capacitive smoothing, no series inductance		80%	2.0
6 Pulse Converter, capacitive smoothing with series inductance > 3%, or dc drive		40%	1.0
6 Pulse Converter with large inductor for current smoothing		28%	0.8
12 Pulse Converter		15%	0.5
ac Voltage Regulator		varies with firing angle	0.7

Figure 1. Voltage sag waveform

Figure 2. Example profile of harmonic voltage distortion on a distribution feeder circuit

Figure 3. Classification of voltage variations

Figure 4a. Per phase equivalent circuit of supply network

Figure 4b. Per phase equivalent circuit of phasor diagram for a resistive inductive load E U_0

Figure 5. Example of rms voltage fluctuation

Improving Solid Waste Management in Gulf Co-operation Council States: Developing Integrated Plans to Achieve Reduction in Greenhouse Gases

Mohammed Saleh Al.Ansari (Corresponding author)

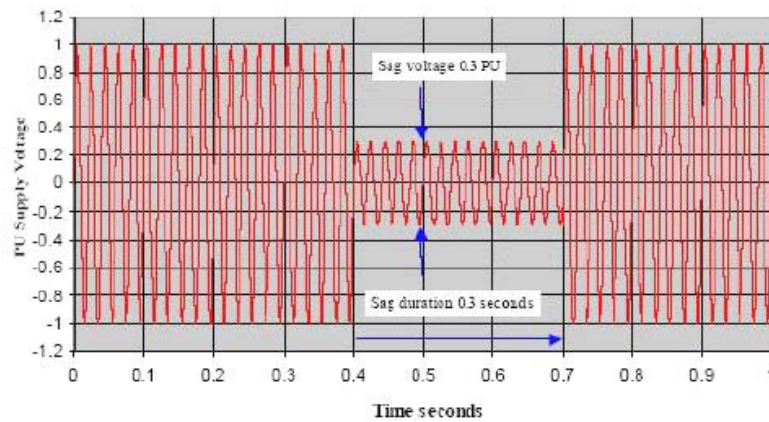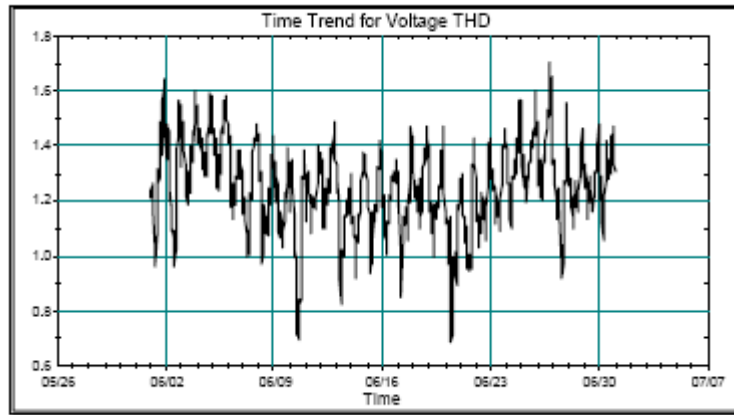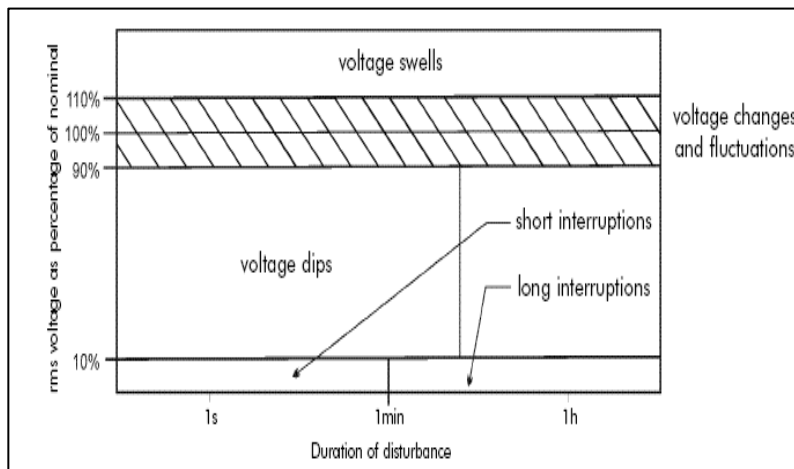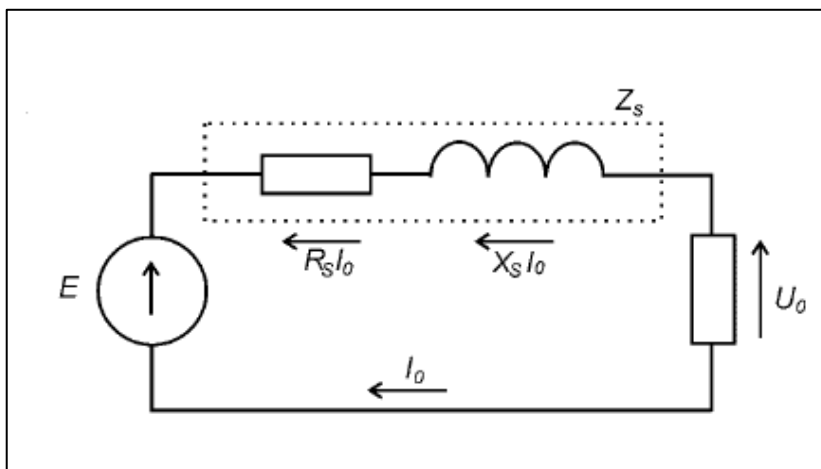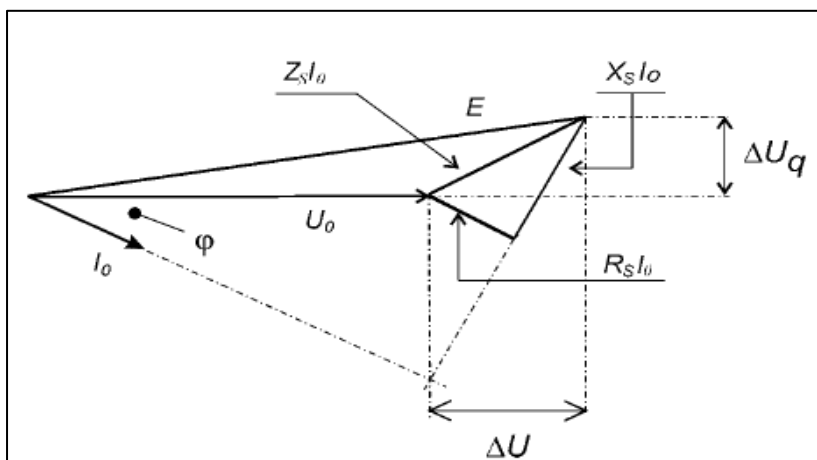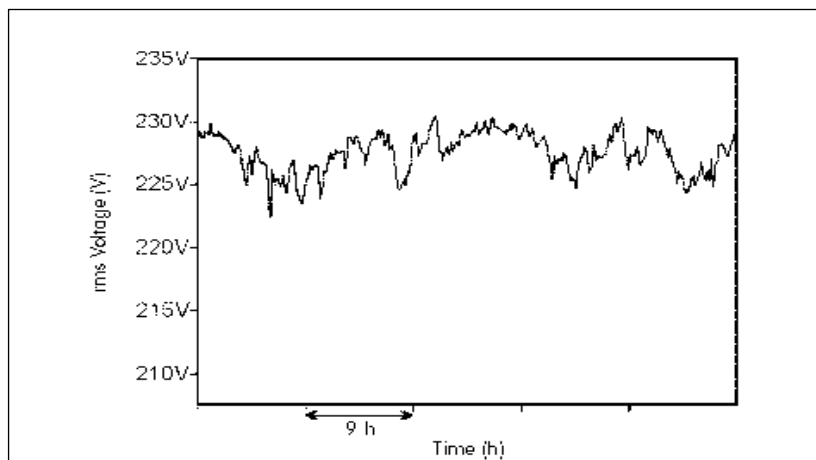Department of Chemical Engineering, College of Engineering, University of Bahrain

PO box 32038, Sukhair Campus, Kingdom of Bahrain

Tel: 973-3944-1110　　　E-mail: malansari@uob.edu.bh

Abstract

Landfills are a significant source of greenhouse gases, which contribute to the process of global warming. In the region covered by the Gulf Co-operation Council (GCC), changes in consumption patterns have led to an excessive dump of municipal solid waste (MSW). Thus, it is clearly an important time to re-evaluate conventional waste management protocols in order to establish methods that not only deal with increased demand but also minimize greenhouse gas emissions and improve efficiency of resource management, in general. Here, I advocate the use of a new hierarchy in integrated municipal solid waste schemes, with the aim of designing more eco-friendly management plans for use in GCC states.

Keywords: Municipal solid waste, Global warming, Greenhouse gases, Gulf Co-operation Council

1. Introduction

Global warming is driven by increase in greenhouse gases (GHGs)—predominantly water vapour, nitrous oxide, carbon dioxide (CO_2), and methane (CH_4)—in the Earth's atmosphere. This has led to major environmental changes worldwide, including (1) rising sea levels that may flood coastal and river delta communities; (2) shrinking mountain glaciers and reduced snow cover that may diminish freshwater resources; (3) the spread of infectious diseases and increased heat-related mortality; (4) possible loss of biological diversity and other impacts on ecosystems; and (5) agricultural shifts that may impact crop yields and productivity (McCarthy, et al., 2001). Current projections suggest that the rate of climate change attributable to GHGs will exceed any natural climate changes that occurred from 1900 to 2010 (Chen, & Lin, 2008; Liamsanguan, & Gheewala, 2007).

One major source of GHGs is landfills, which account for 3.4–3.9% of total annual GHG emissions worldwide (Figure 1) (Chen, & Lin, 2008; Baumert, et al., 2003; Forbes, et al., 2001). This is because large quantities of carbon dioxide and methane are produced by decomposition of the organic fraction of solid wastes in landfills. Methane is particularly problematic, because it has 21 times the global warming potential of carbon dioxide, and according to the Intergovernmental Panel on Climate Change, methane emissions from landfills account for 18% of all methane added to the atmosphere each year, ranging from 9 to 70 Tg (megatonnes) annually. In fact, landfills are the largest source of atmospheric methane in the world (Hansen, et al., 2005b). Thus, in order to reduce GHG emissions, it will be essential to reform solid waste management practices so that solid waste can be used as a resource for generation of new useful products or can be recycled (Forbes, et al., 2001).

In 2010, the Gulf countries generated in excess of 22.2 million tonnes of municipal waste and approximately 4.6 million tonnes of industrial solid waste. Today, many of the Gulf Co-operation Council (GCC) countries (the Kingdom of Bahrain, State of Kuwait, Sultanate of Oman, State of Qatar, Kingdom of Saudi Arabia, and United Arab Emirates) rank higher than developed countries in terms of per capita waste generation. However, GCC countries have also been active in symposia, conferences, and initiatives aimed at combating global warming. These states are in a unique position to enhance their public images by leading the global charge to reduce GHG emissions.

Current models of waste management assume that waste already exists and needs to be managed. In other words, waste management is simply a reaction to the presence of something that needs to be eliminated (Figure 2). However, resource efficiency and sustainable waste management are maximized by preventing the accumulation

of waste. Thus, the current definition of waste may become a barrier to an efficient and sustainable waste management system, as it impacts decisions related to the transport, reuse, and sale of materials.

A waste management hierarchy has been developed for use by governments, industry, educators, and environment groups as they make decisions about waste policies and programmes (Table 1). The conventional waste management hierarchy includes 5 stages: (1) reduce (source reduction, using recycled products, and controlling the material to reduce final waste), (2) re-use, (3) recycle, (4) incinerate (energy recovery), and (5) safe transport of remaining waste to landfills (AlAnsari M., 2008; Forbes, et al., 2001). An optimal approach to waste management would be an integrative plan that provides control over processes that generate waste, waste handling, and waste utilization. This more integrated, whole-system approach would enable managers to minimize waste generation from the beginning (Intergovernmental Panel on Climate Change, 2007; Gentil, et al., 2009), a goal that has been pursued by industrial scientists and developers over the past decade. Since good waste management reflects good management in general, the amount of waste minimization can be used as an indicator by financial institutions looking to identify companies that are unlikely to face costs associated with environmental liability (Forbes, et al., 2001; European Commission: Sustainable Development Task Force, 2001; Honkasalo, 1998). Waste policies can significantly influence product characteristics, leading to less waste generation (Figure 3). Thus, some policies have advocated reducing waste and thus reducing pollution and increasing resource efficiency by changing products. However, the changes in products may be defined by contradictory policy objectives. For instance, recycling costs are cheaper when glass packaging is used instead of plastic packaging for beverages; however, this substitution increases packaging weight. To tackle these possible contradictions, waste policies will need to establish an unambiguous hierarchy of different objectives. This includes changes in product design or characteristics leading to at least one of the following three consequences: first, that start with the reduction in the quantity of waste generated by consumption; second, reduction of toxicity of generated waste; and third, facilitation of recycling or re-use (Intergovernmental Panel on Climate Change, 2007; Gentil, et al., 2009; Seadon, 2006).

Although it is preferable to avoid the creation of waste altogether, alternative management tactics include re-use of materials, recycling, thermal treatment with energy recovery, thermal treatment without energy recovery, and landfilling. Unfortunately, the waste management hierarchy has a poor scientific and/or technical basis. For instance, it is always preferable to recycle materials rather than attempt energy recovery, and its utility is greatly improved when a combination of the aforementioned options is used. Thus, it is important to conduct an assessment of the whole system, by considering not only different waste management techniques but also costs (in order to determine the economic affordability of different waste systems) and the wide variety of specific local situations in which the waste management systems must operate effectively.

As applied to manufacturing, the Zero Waste concept involves the design and implementation of industrial processes and products that are beneficial to the environment but are also competitive in the market. To achieve sustainable development, it will be necessary to make fundamental changes in production and consumption patterns and to make these changes in all developed and developing countries. This will have social, economic, and environmental benefits (USEPA, 2005a; Vesilund, 2002; ACT NOWaste, 2005)

2. Brief Overview of Solid Waste Management

Solid waste profiles vary spatially and are dependent on diverse variables, including urbanization, commercial enterprises, manufacturing, and service sector activities. Likewise, attitudes about waste management practices also vary. This is often referred to as the *waste management ethic* and includes feelings towards *recycling* and *littering*. The diversity of practices and opinions has made it difficult to develop a single approach to implement waste management practice worldwide (Gentil, 2009).

Despite these differences, there are some recurring waste management issues in many communities. For instance, one common problem is the increased availability of single-use packaging and disposable items, which add to the quantity of waste produced. The most common method of disposal is licensed landfilling. However, landfills only provide a short-term solution to waste management, as additional plans must be made to manage old, abandoned, and often hazardous dumps. Thus, a variety of innovative strategies are required to deal with the waste we produce today to prevent it from causing problems for future generations (Seadon, 2006).

3. Current Climate of SWM in GCC Countries

Because of fast-paced industrial growth, recent booms in construction, increasing population sizes, rapid urbanisation, and lifestyle improvements, GCC countries have some of the highest per capita waste generation rates worldwide. GCC countries implemented a uniform waste management system and a monitoring mechanism for waste production, collection, sorting, treatment, and disposal in December 1997. Most of the waste

management regulations and strategies adopted are based on the universally accepted scientific approach enumerated in the Integrated Waste Management Hierarchy. Although most of the MSW produced in these countries is largely decomposable and recyclable, most waste is disposed in landfills. This is not likely to be sustainable over the long term, as preliminary estimates put the total volume of solid waste generated in the GCC region at ~120 million tons/year. A huge proportion of this is expected to be waste generated from construction and demolition activities; municipal waste is the second largest source of waste (Grant, et al., 2003).

Increased population density and land scarcity are not as problematic in the GCC states as in other industrialised, developed countries around the world. Thus, the dominant method of waste disposal in GCC countries is landfilling (Table 2), and all landfill sites in the GCC region are governmental premises. Although some of the GCC countries have targeted recycling as the main concern in their solid waste management strategies, the landfill and availability of land, usually old quarries, became an impediment to recycling programs. The only comprehensive form of recycling available within the GCC member states is for paper and cartons. Unlike the European Union, which has planned to meet a recycling goal of 1.7 million tonnes per year, the majority of the GCC states have never set national or regional recycling targets. This is likely to be particularly problematic in countries such as Kuwait and Bahrain, where land is limited. Throughout the region, but particularly in these areas, it is important to encourage not only recycling but also composting and incineration. Moreover, for this region, it is also essential to develop more waste management infrastructure to handle the increased amount of waste generated annually (Gautam, 2009; Grant, et al., 2003).

Table 2 lists waste management land requirements calculated per country, both with and without the presence of a recycling policy. If recycling rates are 19% and land is worth US$ 661 per m^2, recycling efforts could save over US$ 478 million annually. Many researchers suggest that these savings could be used for the research and development studies on recycling.

4. Developing Sustainable Solid Waste Management Plans for GCC Countries

'Waste' includes both products that have reached the end of their shelf life and by products of processes such as manufacturing, commercial use, and construction. These waste products will also be associated with materials that were used to process and transport the product throughout its life cycle. Cumulatively, all these materials are known as the 'ecological rucksack' or 'ecological footprint' (Moisio, et al., 2008; UNESCO, 2008). Additionally, each product 'embodies' other ecological impacts made during its manufacturing, such as land degradation, use of materials and energy, and air and water emissions (Forbes, et al., 2001; Snow, 2003; Hawken, 1999). Typically, MSW materials in GCC states have been produced through many steps, starting with extraction and processing of raw materials; manufacture or processing of products; transportation of materials and products to markets or agents; and finally, use and disposal by consumers (AlAnsari M., 2008).

Even waste management itself has environmental impacts, such as air emissions from garbage and recycling trucks collecting wastes and water used in reprocessing. It also has social and economic impacts. Thus, it is important to consider the 'embodied environmental value' (EEV) when relating sustainability and waste, and to evaluate the broader impacts of each waste management option (including not just actual impacts but also those that might be avoided) when developing a 'waste hierarchy.' It may also be useful to consider the concept of 'biomimicry,' which examines ways in which nothing is wasted in nature, wherein the waste from one process becomes the raw material for another in continuous closed cycles. In human terms, this can be achieved through recycling and composting. Cumulatively, these considerations will promote an organisational and technical shift from a hierarchy dominated by resource recovery to a hierarchy emphasising prevention and avoidance.

The new waste hierarchy should aim to achieve several goals:

1. Avoid or reduce generation of waste; 'do more with less' and/or improve resource use efficiency by using closed cycles that maximise the value of materials (in both environmental and socioeconomic terms).

2. In recovery efforts, attempt to maximise EEV; engage in energy recovery only when materials have no higher end use than to be converted to energy; where possible, eliminate this practice altogether.

3. When selecting recovery options, consider not only the impacts on waste, but also those on socioeconomics, sustainability, and environmental health (e.g., whether the technology generates greenhouse gases, requires water consumption, produces waterborne wastes, etc.) (Gautam, 2009; Grant, et al., 2003; Lewis, et al., 2010).

Cultural and socioeconomic practices are likely to cause challenges for the GCC waste management sector, but this offers unique and exciting opportunities for a variety of private players to use their technical knowledge and experience to make significant contributions for solving waste management problems (UNESCO, 2008; Gautam,

2009). For instance, planning authorities have recently awarded a number of contracts to the private sector for setting up and operating integrated waste management facilities (which will be discussed in more detail below) and waste recycling units (Grant, et al., 2003). However, opportunities in the sector are still largely unexploited. Future efforts should be focused on addressing lack of proper practice and strength of waste collection, transportation, and handling infrastructure.

5. Integrated Solid Waste Management in GCC Countries

A vital component of future efforts will be integrated solid waste management (ISWM) schemes, which seek to manage municipal solid waste using all available means (e.g., disposal in a landfill; incineration; recycling; composting; mulching; and, where relevant, hazardous waste disposal). In these schemes, reduction, reuse, and recycling take priority over using landfills, with the ultimate goal of protecting both human health and the environment. ISWM plans incorporate several different approaches for handling the entire MSW stream. Therefore, they are easily adaptable and can be altered over time or to meet specific social, economic, environmental, or geographic requirements. In order for these plans to be holistic, they should include inputs from both the local government and relevant stakeholders (e.g., landfill operators). This will help accomplish the target of reducing MSW generation worldwide by 1% annually, as well as promoting environmental sustainability in general (Finnveden, & Moberg, 2005; Gamble, & Every, 2002; Hawken, 1999).

The following are the major techniques that can be utilized in ISWM plans:

5.1 Recycling

Recycling reduces energy-related CO_2 emissions in the manufacturing process (although not as dramatically as source reduction) and avoids emissions from waste management. Paper recycling increases the sequestration of forest carbon (Forbes, et al., 2001). However, recycling and composting are more than just separation and collection of post consumer materials. The materials must be processed and reused in order to have a beneficial effect on reducing the waste stream (Hansen, et al., 2005b; Smith, 2001). For instance, recovered products can be used in the production of metals and energy.

In the conventional management hierarchy, recovery of materials via recycling and composting means that waste materials are processed industrially and then reformed into new or similar products. This method can be used for preconsumer waste, such as factory cuttings or shavings, as well as post-consumer waste items, including cardboard, newspapers, plastic bottles, and aluminium cans. Although recycling is often viewed as a resource conservation activity, it may facilitate higher energy savings for many products.

5.2 Composting

Composting is a management option for food discards and yard trimmings. Because composting avoids CH_4 emissions, GHG emissions are lower when food discards are composted than when they are landfilled. However, emissions are higher for yard trimmings when they are composted, as landfilling permits only incomplete decomposition and therefore results in carbon storage. Composting and combustion of these materials result in a similar emission of GHG (Liamsanguan, & Gheewala, 2007).

In the conventional hierarchy, composting is used to reduce the quantity of MSW to be incinerated or landfilled by separately treating the organic fraction of MSW. However, there is no definite approach to calculate CO_2 emitted from composted items. Diverting organic materials from landfills also reduces CH_4 emissions (AlAnsari M., 2008; Kolln, & Prakash, 2002). Composting has become an increasingly utilised alternative for MSW treatment in GCC countries, despite the unfortunate failure of a large number of composting plants in the region since 1990's. These have been hindered by low performance, high operation and maintenance costs, and poor management—issues that will need to be addressed to make composting more viable in the future. Of the 3 million tonnes of MSW produced by all GCC states each year, an average of 47% (by weight) are compostable materials and potential feedstock for the GCC's several composting facilities. Approximately 1.4 million tonnes/year of such materials would be potentially available for composting plants (AlAnsari M., 2008; Zeng, et al., 2010; Khan, 1989), suggesting that it may be feasible to establish a regional facility.

5.3 Combustion

Combustion of waste allows energy recovery to displace fossil fuel-generated electricity from utilities, thus reducing GHG emissions from the utility sector and methane emissions from landfills. Relative global warming potential (GWP) is lower for combustion and incineration than for composting and landfilling. Despite this environmental benefit, it is also important to consider feasibility studies and economics when deciding whether to implement this method of waste management (Hassan, 1999). Complete combustion results in emission of CO_2 and N_2O. The emission of non-biogenic CO_2 but not biogenic CO_2 is considered to be beneficial during

GHG emission associated with combustion. Most waste combustors produce electricity that can be substituted for utility-generated electricity. It is important to note that combustion facilities must incorporate some form of heat recovery system in order for energy to be utilized economically; systems should be designed to maximise the efficiency of combustion facilities and incorporate modern air pollution control systems to reduce air pollution.

5.4 Disposal and Land Filling

In the conventional ISWM hierarchy, the last management option is disposal via landfill. Many disposed wastes cannot discharge GHGs, but instead store carbon. Current practices of solid waste landfilling are not sustainable, due to shortcomings in the design, construction, and operation stages of landfill development (Hiettiaratchi, et al., 2007). Gas extraction systems must be installed at landfills in order to control emissions of CH_4 and CO_2, which are produced in nearly equal concentrations due to biodegradation of organic waste. Despite such measures, a significant amount of non-controlled emissions is released into the atmosphere through landfill surfaces (Nolasco, et al., 2009). Some organic matter will not decompose at all and is eventually stored as carbon.

With combustion of CH_4 for energy recovery, credit is given for the electric utility since it avoids GHG emission. Regardless of the fate of CH_4, credit is given for the landfill carbon storage associated with landfilling of some organic materials. It is becoming increasingly easy to recover CH_4 from landfills, reducing GHG emissions by 65–72%. If CH_4 is used for electricity generation, CO_2 emissions can be reduced by 69-72% (Hansen, 2005a; USEPA, 2005a). Bioreactor landfill technology has the potential to further reduce the environmental impact of landfills and maximise CH_4 recovery from these systems, thus providing a positive use for what has historically been a non-valued disposal method.

5.5 Ecodesign

'Ecodesign' describes the concept of minimising a product's environmental impact over the course of its life cycle. Thus, attempts are made to use fewer hazardous chemicals, augment energy efficiency, and reduce ecological footprints. Especially important is the idea of 'resource-use efficiency,' or, in other words, doing more with less. This approach allows economic growth to continue without causing negative environmental impacts. The goal of resource-use efficiency has the potential to be well served by the hierarchy, especially if its emphasis is shifted upwards towards waste prevention and reduction. Unfortunately, solid waste managers in government and industry have little control over production decisions that influence waste generation, particularly in the absence of regulation. Thus, it is important for ecodesign to be advocated by individuals from other sectors.

5.6 Reduction/Avoidance

Waste reduction and/or avoidance, also referred to as "source reduction" or "waste minimisation", is the prevention of solid waste generation. In order to reduce the quantity and toxicity of materials entering the MSW system, waste reduction/avoidance techniques are considered at every stage of a product's life cycle, including design, manufacture, purchase, and use. Thus, this technique, located near the top of the management hierarchy, has the potential to conserve resources, save energy, and reduce pollutants and GHG emissions. It can also reduce solid waste collection system costs and reduce the need for new landfills and incinerators.

Avoidance plans and legislation also typically include the establishment of waste reduction/avoidance targets, economic incentives, and educational efforts, including promotion, technical assistance, planning, and reporting. Because of this broad focus, this method offers the opportunity to reduce GHG emissions in a significant way. For many materials, reduction in energy-related CO_2 emissions from the raw material acquisition and manufacturing process, and the absence of emissions from waste management, combine to reduce GHG emissions more than that using other options (Smith, 2001; Vollenbroek, 2002).

5.7 Resource Recovery

Resource recovery, which includes recycling, composting, and combustion, is the fourth step of the proposed waste management hierarchy because it is a 'waste reuse' technique. The benefits of resource recovery include conservation of natural resources, energy, and landfill space, and provision of useful products and economic benefits.

The need for consistency in quality and quantity, and the benefit of economies of scale, it is suggested that integrated waste management should be organised on a large-scale, regional basis. Further, any scheme or strategy incorporating recycling, composting, or waste-to-energy technologies must be market-oriented. When calculating the overall costs of ISWM plans, waste, energy, and other raw materials should be factored in as inputs, while reclaimed materials, compost, emissions to air and water, and residual landfill materials should be factored in as outputs. A parallel model calculates the overall costs of the ISWM system based on local cost data.

Once the waste management system has been described, the inputs and outputs of each chosen treatment process must be calculated, using fixed data for each process. The yield should be expressed as useful net energy consumption, air emissions, water emissions, landfill volume, recovered materials, and amount of compost produced.

6. Discussion

Current rates of resource consumption and pollution are unsustainable because they exceed the rates at which resources can be regenerated and wastes can be assimilated by Earth's natural systems. In order to increase sustainability, we will need to develop a more sophisticated understanding of the complex interactions between different environmental impacts, and develop radical new systems that lead to significant, and immediate, changes. In particular, it will be important to improve eco-efficiency, eliminate waste generation, and shift from products to services (Grant, et al., 2003).

New regional philosophies of waste management should be based on the proposed hierarchy shown in Figure 4. In this system, the following methods should be emphasized, in this order: (1) reduction (either at the source or later), (2) reuse, (3) recycling, (4) incineration, and (5) disposal. Successful implementation of this system at a regional level will facilitate successful implementation globally. An emphasis on ecodesign should also help to reduce waste production. Although economics and socioeconomics have not previously been an important consideration during the development of waste management plans, it is essential that they help shape future management schemes. Cumulatively, these techniques have beneficial social and political implications for the GCC region.

One method of maximising sustainability is to include plans for training and awareness as well as pursuing methods of re-engineering and optimisation in order to achieve waste reduction and recovery. Applying material management and economic recovery of residues for feedstock, or for energy production and utilisation, will also increase the success of ISWM.

Unfortunately, ISWM plans do not address performance or competency issues, which may often have negative impacts on waste safety and public opinion. Disposal plans must be reviewed periodically in order to consider changes in local conditions, processes, and technology

7. Conclusion

Waste hierarchies continue to be useful guides when developing waste management plans. However, it is increasingly important to use modified hierarchies that consider broader environmental, social, and economic impacts. For instance, modern hierarchies should emphasise ecodesign and reduction of GHGs. Given our current levels of consumption and production, it will be challenging to shift to more sustainable patterns in order to prevent and reduce waste. However, these are essential goals that should be considered in the future waste management plans of GCC countries, and, indeed, in countries around the world. Implementation of the new ISWM hierarchy worldwide will push both the private and public sector to rework the production process, eventually leading to decrease in CO_2 emissions from the energy used for solid waste transport as well as reduction in CH_4 and other non-CO_2 GHGs from anaerobic landfilling.

Throughout the GCC states, there has been a debate on how to facilitate a shift from waste management to resource efficiency. A significant issue is merging the concept of sustainability and its sub-components (e.g. the hierarchy) into programs that are effective across multiple sectors, disciplines, communities, and professions. In order to accomplish this, strategic thinking and creative action will be needed at all levels; furthermore, plans must be flexible so that they can evolve over time. There are currently many exciting and groundbreaking approaches to, and tools for, achieving resource efficiency, including Zero Waste targets, dematerialisation, life cycle thinking, ecological footprint analysis, sustainable consumption, and design for environment. However, they are generally applied in isolation. In order to develop their full potency, future efforts should attempt to integrate these techniques with each other and in the context of broader ISWM schemes.

References

ACT NO Waste. (2005). The Strategy: Progress Towards No Waste by 2010 (No Waste by 2010). [online] Available: http://www.nowaste.act.gov.au/strategy/statistics.html

Al.Ansari, M. (2008). Lecture notes on Solid Waste Management, *Series of Lectures on Scientific Research Week*, Bahrain Centre for Studies and Research, Manama; Kingdom of Bahrain.

Baumert, K. A., Perkaus, J. F., & Kete, N. (2003). Great expectations: can international emissions trading deliver an equitable climate regime?. World Resources Institute, Climate, Energy and Pollution Program, Washington

DC, USA; Climate Policy 3, 137–148. [Online] Available: http://ethree.com/downloads/Climate%20Change%20Readings/International%20Climate%20Policy/Baumert%20 0%20Great%20Expectations%20Emission%20Trading%20Equitable.pdf

Chen, C., & Lin, C. F. (2008). Greenhouse gases emissions from waste management practices using Life Cycle Inventory model. *J. Hazard. Mater*, 155, 23-31. http://dx.doi.org/10.1016/j.jhazmat.2007.11.050

European Commission: Sustainable Development Task Force. (2001). Consultation paper for the preparation of a European Union strategy for Sustainable Development.

Forbes, R., White, P. R., Franke, M., & Hindle, P. (2001). *Integrated Solid Waste Management: A Life Cycle Inventory*; Second edition published by Blackwell Science, 513.

Finnveden, G., & Moberg, A. (2005). Environmental systems analysis tools – an overview. *Journal of Cleaner Production*, 13(5), 1165–1173. http://dx.doi.org/10.1016/j.jclepro.2004.06.004

Gamble, D., Every, E., & Valentine, N. (2002). Integrated Waste Management at the Thyssen Krupp Steelworks in Duisburg, Germany. *Paper presented at Enviro 2002, Convention and Exhibition and IWA 3rd World Water Congress,* Melbourne Exhibition & Convention Centre, Australia 7-12 April.

Gautam, V. (2009). Solid Waste Management in GCC: Challenges & Opportunities. *South Asia & Middle East, Environmental & Building Technologies Practice*, 54, 22-28.

Gentil, E. C., Christensen, T. H., & Aoustin, E. (2009). Greenhouse gas accounting and waste management. *Waste Management & Research*, 27, 696-706. http://dx.doi.org/10.1177/0734242X09346702

Grant, T., James, K., & Partl, H. (2003). Life cycle assessment of waste and resource recovery options (including energy from waste). *EcoRecycle Victoria, Melbourne.*

Hansen, J., Nazarenko, L., Ruedy, R., Sato, M., Willis, J., Del Genio, A., Koch, D., et al. (2005b). Earth's Energy Imbalance: Confirmation and Implications. *J of Science*, 308 (5727), 1431-1435. http://dx.doi.org/10.1126/science.1110252

Hassan, M. N. (1999). The application of a life cycle inventory LCI model for so lid waste disposal systems in Malaysia. *Int. J .Life Cycle Assess*, 4, 188-190. http://dx.doi.org/10.1007/BF02979493

Hawken, P., Lovins, A. B., & Lovins, L. H. (1999). *Natural Capitalism: Creating the Next Industrial Revolution*. Little Brown, Boston, Massachusetts, 416.

Hiettiaratchi, J. P. A., Hurtado1, O. D., Hunte1, C., Hundal, J., Colbrynand C., & Smith, C. (2007). The Calgary biocell: A case study in sustainable solid waste management. *Paper presented in the proceeding of the International conference on sustainable solid waste management,* Chennai, India, 421-428.

Honkasalo, A. (1998). The EMAS scheme: a management tool and instrument of environmental policy. *Journal of Cleaner Production,* 6(2), 119–128. http://dx.doi.org/10.1016/S0959-6526(97)00068-1

Intergovernmental Panel on Climate Change. (2007). Report summary for policymakers. [Online] Available: http://www.ipcc.ch/pdf/assessment-report/ar4/syr/ar4_syr_spm.pdf

Khan, M. Z. A., & Burnet, F. A. (1989). Forecasting solid waste composition-an important consideration in resource recovery and recycling. *Resour Conserv Recycl*, 3–17.

Kolln, K., & Prakash, A. (2002). EMS-based environmental regimes as club goods: examining variations in firm-level adoption of ISO 14001 and EMAS in UK, US and Germany. *Journal Policy Sciences,* 35(1), 43– 67. http://dx.doi.org/10.1023/A:1016071810725

Lewis, H., Karli Verghese, K., & Fitzpatrick, L. (2010). Evaluating the sustainability impacts of packaging: the plastic carry bag dilemma. *Packaging Technology and Science,* 23, 145-160.

Liamsanguan, C., & Gheewala, S. H. (2007). Environmental assessment of energy production from municipal solid waste incineration. *Int. J. Life Cycle Assess*, 12(7), 529-536. http://dx.doi.org/10.1065/lca2006.10.278

McCarthy, J. J., Canziani, O. F., Leary, A. N., Dokken, D. J., & White, K. S. (2001). Climate Change 2001: Impacts, Adaptation and Vulnerability. *IPCC*, Cambridge University Press, pp. 9-13.

Moisio, T., Lähteenoja, S., & Lettenmeier, M. (2008). *Tavara MIPS - Kodin tavaroiden luonnonvarojen kulutuksen mittaaminen*. Measuring the natural resource consumption of household goods and appliances. [Online] Available: *http://www.sll.fi/luontojaymparisto/kestava/mips/kotimips/rucksackscore.*

Nolasco, D., Mora Fernández, N., de Paz Carmona, H., Padilla, G., Melian, G., Hernandez Perez, P. A., & Perez,

N. (2009). Non-controlled CO_2 and CH_4 emission from landfills: a useful parameter to evaluate landfill gas extraction efficiency. *American Geophysical Union, Fall Meeting. December 2009*. [Online] Available: http://adsabs.harvard.edu/abs/2009AGUFM.B11A0474N

Seadon, J. K. (2006). Integrated waste management - Looking beyond the solid waste horizon. *Waste Management*, 26(12), 1327-1336. [Online] Available: http://www.aseanenvironment.info/Abstract/41014379.pdf

Smith, A., Brown, K., Ogilvie, S., Rushton, K., & Bates, J. (2001). *Waste management options and climate change*. Final Report ED21158R4.1 to the European Commission, DG Environment, AEA Technology, Oxfordshire, 205.

Snow, W. (2003). Zero Waste. Does it mean an end to waste?. *In: Waste Management World*, 25-31.

UNESCO; Eleanor Bird; Richard Lutz and Christine Warwick. (2008). A Training and Resource Kit;United Nations Educational, Scientific and Cultural Organization at address 1, rue Miollis, 75732 Paris Cedex 15, France, UNESCO, Reference number CI/COM/2008/PI/2, [Online] Available: http://unesdoc.unesco.org/images/0015/001587/158787e.pdf

United States Environmental Protection Agency. (2005a). Air Trends (USEPA). [Online] Available: http://www.epa.gov/airtrends

United States Environmental Protection Agency. (2005b). Municipal Solid Waste (USEPA). [Online] Available: http://www.epa.gov/epawaste/index.htm

Vesilund, P. A., Worrell, W. A., Reinhart, D. R. (2002). *Solid Waste Engineering*. Brookes/Cole, California, United States of America.

Vollenbroek, F. (2002). Sustainable development and the challenge of innovation. *Journal of Cleaner Production*, 10, 215-223.

Zeng, X., Sun, Q., Huo, B., Wan, H., & Jing, C. (2010). Integrated Solid Waste Management Under Global Warming. *The Open Waste Management Journal*, 3, 13-17. http://dx.doi.org/10.2174/1876400201003010013

Table 1. Conventional hierarchy of integrated solid waste management

Goal	Attribute
Reduce	Preventative
Reuse	Predominantly ameliorative, partly preventative
Recycling and composting	Predominantly ameliorative, partly preventative
Treatment or incineration	Predominantly assimilative, partially ameliorative
Disposal and landfilling	Assimilative

Table 2. Rates of municipal solid waste generation in GCC countries

GCC country	Solid waste (Kg/capita/day)	Population (millions)	Total waste (tonne/year)	Land requirements for disposal (m^2)[a]	
				No recycling	Recycling
Bahrain	1.8	1.04	683,280	145,538.64	109,324.80
Kuwait	1.4	2.23	1,139,530	242,719.89	182,324.80
Oman	0.75	2.3	629,625	134,110.13	100,740
Qatar	1.5	0.46	251,850	53,644.05	40,296
UAE	1.4	2.3	1,175,300	250,338.90	188,048
Saudi Arabia	1.6	23	13,432,000	2,861,016	2,149,120

[a]Calculations are based on a density of 0.5 tonnes for MSW.

[b]Calculated based on an assumption of US\$ 661/m^2 as research over statistical land prices in GCC survey done by researcher over lands in the GCC(2011)
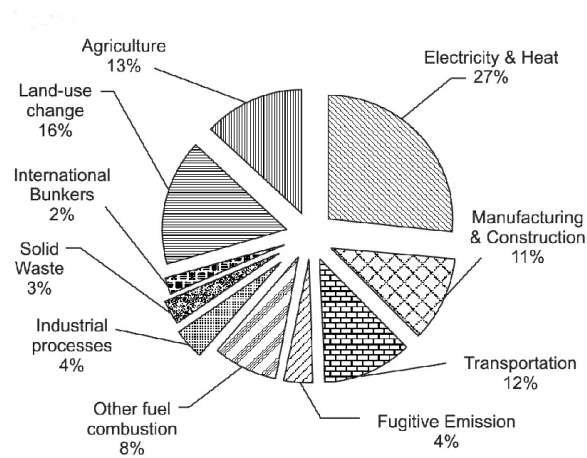
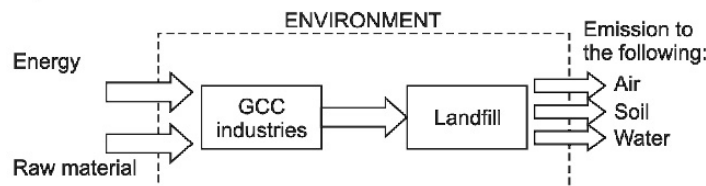Figure 1. Comparison of the sources of GHG emissions

Figure 2. The relationship between energy, raw materials, environment, and emissions
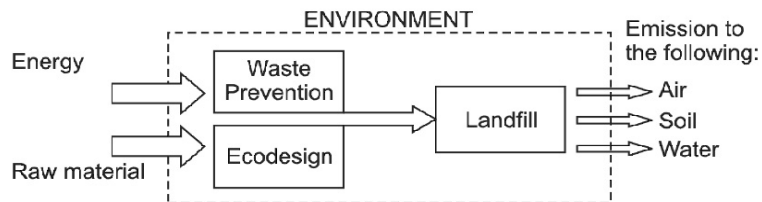

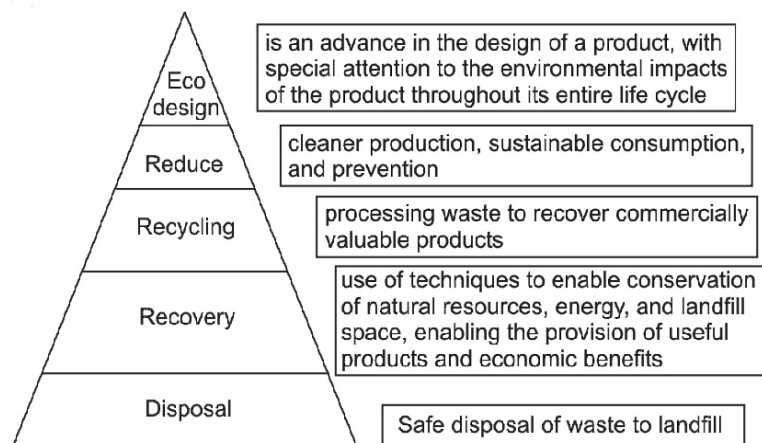Figure 3. Philosophy of waste prevention and minimisation.

Figure 4. Proposed hierarchy of integrated solid waste management. Figure reproduced courtesy of Zeng et al. (2010)

Optimization of Friction Surfacing Process Parameters for AA1100 Aluminum Alloy Coating with Mild Steel Substrate Using Response Surface Methodology (RSM) Technique

V. Sugandhi

Department of Manufacturing Engineering

Annamalai University, Annamalai Nagar 608002, Tamilnadu, India

Tel: 91-41-4423-9734　　　E-mail: sugiyogi2008@yahoo.com

V. Ravishankar

Department of Manufacturing Engineering

Annamalai University, Annamalai Nagar 608002, Tamilnadu, India

Tel: 91-41-4423-9734　　　E-mail: pravicdm@yahoo.co.in

Abstract

Friction surfacing was attempted with aluminum on a mild steel substrate. This paper focuses on the development of empirical relationship for the prediction of coating width, coating thickness of friction surfaced materials. Experimental part of the study is based on five level central composite designs of three process parameters. In order to investigate the effects of input parameters on coating width and coating thickness, an empirical relationship is constructed by multiple regression analysis. Optimization of the model is carried out to study the coating width and thickness using design-expert software. Deposit geometry measurements for all the specimens space carried out and compared with the relative impact of input parameters on coating width and thickness in order to verify the measurement errors on the values of the uncertainty in estimated parameters. The results obtained show that the developed empirical relationship can be applied to estimate the effectiveness of process parameters for a given coating width and thickness.

Keywords: Friction surfacing, Central composite design, Response surface methodology, Degree of freedom, Optimization, Deposit geometry

1. Introduction

Surfacing engineering has gained wide importance owing to the advantages realized of them. The friction surfacing process derivative of friction welding and retains all the benefits of solid state welding, such as forged microstructures and excellent metallurgical bond. The first patent on friction welding was issued in 1941 (Klopstock H., & Neelands A. R., 1994), and published reports on the development of friction surfacing from friction welding first appearing in 1959 (Tyager, Kh. A., 1959; Zakson, R. I., & Turukin F. G., 1965). In this process, the coating is extremely regular and flat, without the familiar meniscus section profile experienced with fusion welding methods. The thickness of the coated layer ranges from 0.5 to 3 mm depending on the material and diameter of coating rod. It is characterized by fine ripples and requires <0.1 mm to be removed to produce the finished surface. The friction surfacing processes have clean environment, no fumes, no spatter. It is also energy efficient because the heat is generated exactly where it is needed. During the coating cycle the applied layer of metal reaches a temperature just below its melting point whilst simultaneously undergoing severe plastic deformation. Thus, the coating is a product of a vigorous hot forging action as opposed to the casting mechanism of fusion welding and spraying processes. This important difference means that many of the defects commonly associated with fusion techniques are avoided, and dense, clean and fine microstructures with attendant excellent properties are generated. There is no dilution of the coating by the substrate and hence no need for multiple layering as is often the case with fusion processes. Further details about the process can be found elsewhere (Bedford G. M., 1990).

The friction surfacing process has become well established with a number of commercial applications. However, the existing models explaining the major relationships between process parameters are still generic. They are based on empirical rules and theoretical assumptions that account for a limited number of cases of current commercial interest. Many of these assumptions are implicit and have not been tested by using appropriate analysis and design of experiments. Consequently there is no method of determining the accuracy and sensitivity when changes in the process parameters are made (Bedford G. M., 1995; Nicholas E. D., & Thomas W. M., 1987).

In this paper, an empirical relationship between friction surfacing parameters and deposit geometry was constructed based upon the experimental dada obtained by three parameters –five levels central composite design. The empirical equation, simulating the friction surfacing, was carried out by multiple regression analysis (MRA) were derived from the basic equations. This analysis generally requires a definition of an objective function and design parameters. In this study, the objective function was chosen as deposit geometry, whereas process parameters (rotational speed, frictional force, traverse speed) were selected as the design variables. The present study mainly focuses on the determination of design parameters and the prediction of fine-tuning requirements of these parameters in friction surfacing process. The results revealed considerable information about the effect of process parameters and optimum surfacing conditions.

2. Plan of Investigation

In order to achieve the desired aim, the present investigation was planned in the following sequence as depicted in Figure 1.

2.1 Identifying the Important Process Parameters

Vitanov V. I. (2000) indicated that the predominant factors which are having greater influence on deposit geometry of friction surfaced coatings were identified. They are: (i) Rotational speed (N) in rpm, (ii) axial force (F) in N/mm^2 (frictional force), (iii) traverse speed (V) in mm/sec. These are primary process parameters contributing to the frictional heat and subsequently influencing the coating performance of friction surfaced materials.

2.2 Finding the Working Limits of the Parameters

A large number of trial runs were carried out using aluminum alloy (22 mm Ø) coated with mild steel substrate (150 mm x 100 mm x 6 mm) to find out the feasible working limits of Friction surfacing process parameters. Chemical composition of the base metal and consumable is presented in Table 1. Trial runs were carried out by varying one of the factors while keeping the rest of them at constant values. The working range of each process parameter was decided upon by inspecting the macrostructure (cross section of friction surfaced specimens) for any visible defects. From the above inspection, the few important observations were made and they are presented in Table 2. The chosen levels of the selected process parameters with their units and notations are presented in Table 3.

2.3 Developing the Experimental Design Matrix

The feasible limits of the parameters were chosen in such a way that aluminum alloy should be coated with mild steel substrate without any coating defects. Central composite rotatable design of second order was found to be the most efficient tool in response surface methodology (RSM) to establish the empirical relationship using the smallest possible number of experiments without losing its accuracy (Voutchkov I., 2001). Due to wide ranges of parameters, it was decided to use three factors, five levels, central composite design matrix to optimize the experimental conditions. Table 4 shows the 20 set of coded conditions used to form the design matrix. First experimental conditions are derived from full factorial experimental design matrix. All the variables at the intermediate (0) level constitute the center points while the combinations of each process variable either at lowest (-2) or it highest (+2) with the other three variables of the intermediate levels constitute the star points. The method of designing such matrix is dealt elsewhere (Gunaraj V., 2004; Gunaraj V., & Murugan N., 1999). For the convenience of recording and processing experimental data, upper and lower levels of the factors were coded as +2 and –2 respectively. The coded values of any intermediate value can be calculated, using the following relationship.

$$Xi = 2 \left[2X - (Xmax + Xmin) \right] / (Xmax - Xmin) \qquad (1)$$

Where,

Xi is the required coded value of a variable X;

X is any value of the variable from Xmin to Xmax;

Xmin is the lower level of the variable;

Xmax is the highest level of the variable.

2.4 Conducting the Experiments and Recording the Responses

The friction surfaced aluminum coating was performed on mild steel substrate (Figure 2) as per the conditions dictated by the design matrix (Table 4). Coating thickness, coating width was measured and they are presented in Table 4.

2.4.1 Coating Preparation

Friction surfacing was carried out by varying the parameters as prescribed by the design matrix and aluminium coating was produced over mild steel substrate. The friction surfaced specimens, coated rod (before and after), are shown in Figures 3.

2.4.2 Deposit Geometry Measurement

Deposit geometry measurements for all the specimens were carried out by optical profile projector (make: meterz, India) samples where cut in the required size. The friction surfaced specimens are shown in Figures 4.

3. Developing a Empirical Relationship

The coating characteristics of aluminum is represented by Y, then the response function can be expressed as

$$Y = f(F, N, V) \tag{2}$$

The model selected was a second degree response expressed as follows

$$Y = B0 + B(F) + B2(N) + B3(V) + B11(F2) + B22(N2) + B33(V2) + B12(F*N) + B13(F*V) + B23(N*V) \tag{3}$$

The values of the coefficient were calculated by regression with the help of the following equations. The final model was developed after determining the significant coefficient, which lead the following test.

Coating thickness:

$$Ct = 0.84 + 0.26*F + 0.04*N + 0.86*V - 0.01*F*N - 0.0625*F*V + 0.0375*N*V + 0.017*F2 + 0.08*N2 + 0.01*V2 \tag{4}$$

Coating width:

$$Cw = 24.01 + 0.79*F + 0.42*N + 1.05*V - 0.9*F*N - 1.96*F*V + 0*N*V - 1.82*F2 - 1.66*N2 - 0.93*V2 + 0.1*V2 \tag{5}$$

3.1 Checking the Adequacy of Model

The adequacy of the model was checked using the analysis of variance (ANOVA) technique. As per the technique, if the calculated value of the 'F' ratio for the desired level of confidence (say 99%). Then the model is conducted to the adequacy limit using the developed model for various mechanical and metallurgical properties. The predicted results of different combination are presented in the graphical form. ANOVA test result presented in the Table 5.

3.2 Effect of Process Parameters on Deposit Geometry

3.2.1 Effect of Rotational Speed on Deposit of Coating

The deposit tended to be greater in thickness with increasing rotational speed of consumable rod, regardless of the traverse speed and axial force. This might be due to an increase in torque during friction with demand rotational speed and due to an increase in the thickness of deposit because of an increased rate of deformation of consumable rod.

3.2.2 Effect of Axial Force on Deposit of Coating

The effect of axial force on the thickness of deposit decreased with increasing rotational speed of consumable rod, making the thickness of deposit almost uniform of the rotational speed.

3.2.3 Effect of Traverse Speed on Deposit of Coating

The width of the deposit tented to decrease with increased rotational speed and traverse speed on consumable rod. But it has almost uniform under the conditions of the rotation of consumable rod was slow, because effect of the traverse speed was limited. This might be because width of the deposit may be decreased by a decrease in the closure area of substrate and consumable rod. The effect of traverse speed on the thickness of deposit was demand with increasing rotational speed of consumable rod, making the thickness of deposit almost uniform at rotational speed.

4. Optimising the Parameters

Contour plots show distinctive circular shape indicative of possible independence of factor with response (Figure 5). A contour plot is produced to visually display the region of optimal factor settings. For second order response surface, such a plot can be more complex than the simple series of parallel lines that can occur with first order models. Once the stationary point is found, it is usually necessary to characterize the response surface in the immediate vicinity of the point. Characterization means, identifying whether the stationary point found is a maximum response or minimum response or a saddle point. To classify this, the most straightforward way is to examine through a contour plot. Contour plots play a very important role in the study of the response surface. By generating contour plots using software for response surface analysis, the optimum value is located with reasonable accuracy by characterizing the shape of the surface.

If a contour patterning of circular shaped contours occurs, it tends to suggest independence of factor effects while elliptical contours as may indicate factor interactions. Response surfaces have been developed for both the models, taking two parameters in the middle level and two parameters in the X and Y axis and response in Z axis. The response surfaces are clearly revealing the optimal response point. RSM is used to find the optimal set of process parameters that produce a maximum or minimum value of the response. In the present investigation the process parameters corresponding to the minimum coating thickness are considered as optimum (by analyzing the contour graphs and by solving the equation 4 and 5). Hence, when these optimized process parameters are used, then it will possible to attain the minimum coating thickness.

The presented three dimensional response surface plots for the response coating thickness obtained from the regression model. The optimum coating thickness is exhibited by the apex of the response surface exhibits almost a circular contour, which suggests independence of factor effect namely rotational speed. It is relatively easy by examining the contour plots that changes in the coating thickness are more sensitive to changes in rotational speed than to changes in axial force and traverse speed. Interaction effect between the combination of factors such as rotational speed and traverse speed, rotational speed and axial force and traverse speed and axial force on coating thickness and coating width also exists (Figure 6), which is evidenced from the contour plots. Increase in rotational speed resulted in increase of coating width and coating thickness is decreased.

Predicted optimum coating thickness obtained from the response surface and contour plots by using a combination of axial force 14 N/mm^2, rotational speed 2500 rpm and traverse speed 16mm/sec, which resulted in a coating thickness of 0.89 and coating width 20.22 mm. To demonstrate the validity of the model, actual experiments were conducted at the optimum values of process parameters to make a coating. The above values were also verified using statistical software Minitab.

5. Conclusions

Empirical relations were developed to predict coating thickness and coating width incorporating friction surfacing process parameters. The developed relationships can be effectively used to predict the coating at 95% confidence level and Friction surfacing process parameters were optimized using response surface methodology to attain minimum thickness and maximum width. The optimum conditions are: axial force 14 N/mm^2, rotational speed 2500 rpm and traverse speed 16 mm/sec.

References

Bedford, G. M. (1990). Friction surfacing for wear application. *Metals mater,* 6(11), 702-705.

Bedford, G. M., Ward, L. J., Tooley, P. J., Wilson, B. J., & Sharp, R. J. (1995). Large scale friction surfacing. In Proceeding of the EUROMAT'95 4th European Conference on Advanced Materials and processes, Italy, September, 441-444.

Douglas, C. M. (2007). Design and analysis of experimentas. *John Wiley & Sons,* New York.

Gunaraj, V., & Murugan, N. (1999). Application of response surface methodology for predicting weld bead quality in submerged arc welding of pipes. *Journals of materials processing technology,* 88, 266-275.

Klopstock, H., & Neelands, A. R. (1994). An improved method of joining and welding metals. Patent specifiction, No. 572789, U.K.

Nicholas, E. D., & Thomas, W. M. (1987). Metal deposition by friction welding. *Welding J.,* 7, 17-27.

Tokiwue, Hiroshi, Katoh, Kazuyoshi, Asahina, Toshikatsu, Ushiyama, & Toshio. (2004). Mechanical properties of 5052/2017 dissimilar aluminum alloys deposit by friction surfacing. *Journal of Japan institute of light metals,* 54(9), 373-379.

Tyager, Kh. A. (1959). Friction welding in the reconditiong of worn component. *Weldprod,* 10(1), 23-24.

Voutchkov, I., Jawaorsk, Bb., IVitanov, V., & Bedford, G. M. (2001). An integrated approach to friction surfacing process optimization. *Surface and coatings technology,* 141, 26-33. http://dx.doi.org/10.1016/S0257-8972(01)01127-6

Vitanov, V. I., Voutchkov, I. I., & Bedford, G. M. (2000). Decision support system to optimize the frictec (friction surfacing) process. *Journal of materials processing technology,* 107, 236-2. http://dx.doi.org/10.1016/S0924-0136(00)00710-X

William, G. C., & Gertrude, M. C. (1957). Experimental designs. *John Wiley & Sons,* Inc., London.

Zakson, R. I., & Turukin, F. G. (1965). Friction welding and hard facing of agricultural machine parts, *Avt svarka,* 3, 48-50.

Table 1. Chemical composition (wt %) of base metal

S.No	Material	Al	C	Mn	Mg	Zn	Fe	Si	P	Cr	Ni	Ti	Cu
1	Mild Steel	-	0.07	0.31	-	-	Bal	0.31	0.089		0.11	-	0.24
2	AA 1100	Bal	-	0.004	0.0015	0.0016	0.508	0.152	-	0.006	-	0.015	0.061

Table 2. Macrostructure observations of the friction surfaced specimens

Input parameters	Parameter range	Macrostructure	Probable reason
Rotational speed	<2000 rpm		In sufficient frictional heat and In sufficient metal deposition
Rotational speed	>3000 rpm		Further Increase less deposition
Axial force	<10 N/mm^2		In sufficient Axial force and in adequate heat generation
Axial force	>18 N/mm^2		Additional axial force lards to excess heat input and thinning of the metal deposited
Traverse speed	<10 mm/sec		Low frictional heat Generated
Traverse speed	>30 mm/sec		Increase in traverse speed resulted in Poor Plasticization on associated defect

Table 3. Important factors and their level

S.NO	Factors	Notation	Unit	Factor Levels				
				-2	-1	0	1	2
1	Axial force	F	N/mm^2	10	12	14	16	18
2	Rotational speed	N	rpm	2000	2250	2500	2750	3000
3	Traverse speed	V	Mm/sec	10	15	20	25	30

Table 4. Design Matrix and experimental result

Ex .no	Rotational speed (rpm)	Traverse speed (mm/sec)	Axial force (k N)	Coating thickness (mm)	Coating width (mm)
1	-1	-1	-1	1.37	25.46
2	+1	-1	-1	2.43	26.08
3	-1	+1	-1	1.60	20.47
4	+1	+1	-1	2.23	23.27
5	-1	-1	+1	2.37	26.84
6	+1	-1	+1	2.43	29.08
7	-1	+1	+1	1.30	25.82
8	+1	+1	+1	0.7	24.64
9	-2	0	0	2.23	28.22
10	+2	0	0	0.7	23.38
11	0	-2	0	1.8	24.64
12	0	+2	0	1.2	24.64
13	0	0	-2	2.4	20.26
14	0	0	+2	1.36	27.96
15	0	0	0	2.3	25.94
16	0	0	0	2.6	24.92
17	0	0	0	2.8	23.42
18	0	0	0	2.4	25.82
19	0	0	0	2.6	27.96
20	0	0	0	2.93	27.16

Table 5. ANOVA result for the deposit geometry

Source	Sum of Squares	df	Mean Square	F Value	p-value Prob >F	
Model	1.299866	9	0.14443	27.13377	<0.0001	Significant
A-A	0.911007	1	0.911007	171.1495	0.0001	
B-B	0.026761	1	0.026761	5.027479	0.0488	
C-C	0.100156	1	0.100156	18.81611	0.0015	
AB	0.0008	1	0.0008	0.150295	0.7064	
AC	0.03125	1	0.03125	5.87089	0.0359	
BC	0.01125	1	0.01125	2.11352	0.1767	
A2	0.004323	1	0.004323	0.81213	0.3887	
B2	0.094457	1	0.094457	17.74548	0.0018	
C2	0.145281	1	0.145281	27.29375	0.0004	
Residual	0.053229	10	0.005323			
Lack of Fit	0.042095	5	0.008419	3.781023	0.0854	Not significant
Pure Error	0.011133	5	0.002227			
Cor Total	1.353095	19				
Std. Dev.	0.072958		R-Squared	0.960661		
Mean	0.9805		Adj R-Squared	0.925257		
C.V.%	7.4409		Pred R-Squared	0.751144		
PRESS	0.336726		Adeq Precision	18.16749		
Model	148.8797	9	16.54218	43.40183	<0.0001	Significant
A-Axial force	8.530598	1	8.530598	22.38178	0.0008	
B-Rotational Speed	2.405248	1	2.405248	6.310663	0.0308	
C-traverse speed	15.14118	1	15.14118	39.726	< 0.0001	
AB	6.6248	1	6.6248	17.38153	0.0019	
AC	30.7328	1	30.7328	80.63383	< 0.0001	
BC	0	1	0	0	1.000	
A2	48.2217	1	48.2217	126.5196	< 0.0001	
B2	39.60479	1	39.60479	103.9113	< 0.0001	
C2	12.40209	1	12.40209	32.53943	0.0002	
Residual	3.811403	10	0.38114			
Lack of Fit	1.811403	5	0.362281	0.905701	0.5420	Not significant
Pure Error	2	5	0.4			
Cor Total	152.6911	19				
Source	Sum of squares	df	Mean Square	F Value	p-value Prob > F	
R-Squared	0.975038					
Adj R – Squared	0.952573					
Pred R-Squared	0.891152					
Adeq Precision	21.87096					
Std. Dev.			0.617366			
Mean			20.9965			
C.V.%			2.940326			
PRESS			16.62004			

WORK PLAN

Statement of the problem and its objectives

↓

Indentify the important input (Process) parameters   →   Form literature and experiment

↓

Identify the important output parameter   →   Based on application

↓

Find upper and lower limits for input parameters   →   Based on literature, prous. & knowledge (practical and theoretical understanding), trials, runs, macro structural studies.

↓

Developing the experimental designs matrix   →   Considering no. of replicates, randomize of order of experiments blocking or not etc. based on cast, time accuracy of information required and resources available

↓

Conducting the experiment as per design matrix and recording the response   →   Using FSW Machine

↓

Statistical analysis of data and development of a mathematical model by considering significant factors   →   Selecting suitable statistical software package using ANOVA graphical methods by conducting residual analysis and by checking the adequacy of the model.

↓

Validation of the developed model   →   By conducting further experiments and comparing actual and predicted values.

↓

No ◇ Are the results satisfactory.

↓

Yes

Optimize the process parameter sensitivity analysis   →   Using RSM

↓

Implementation of results   →   To identify the sensitiveness of process parameter

↓

Follow up

Figure 1. Work plan

Figure 2. Friction surfacing machine

(a) before coated rod   (b) after coated rod

Figure 3. The friction surfaced specimens

(a) friction surfaced materials   (b) friction surfaced specimens

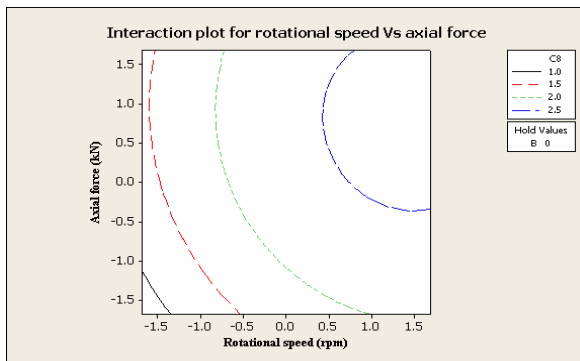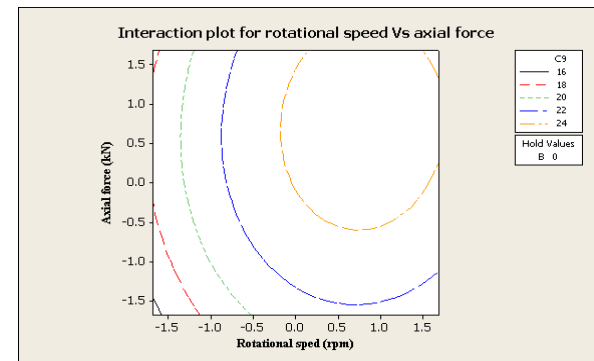Figure 4. The friction surfaced specimens by deposit geometry measurements
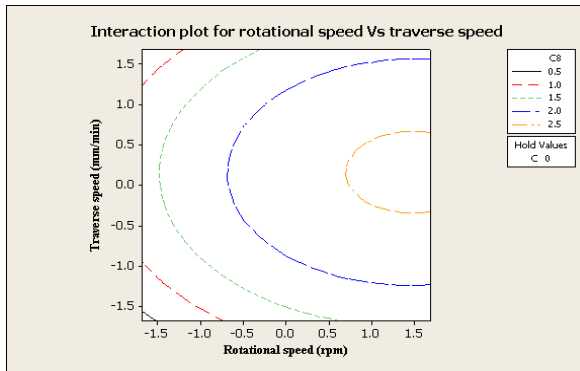
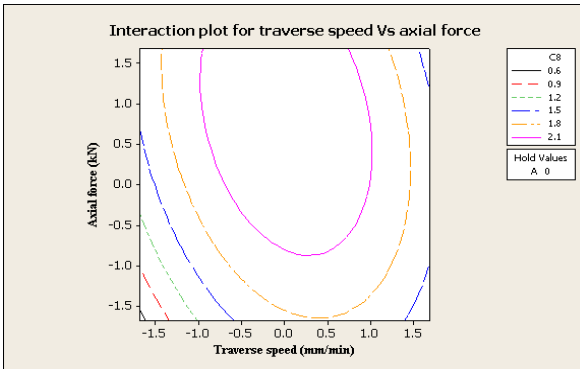(a) Coating thickness, traverse speed Vs. rotational speed
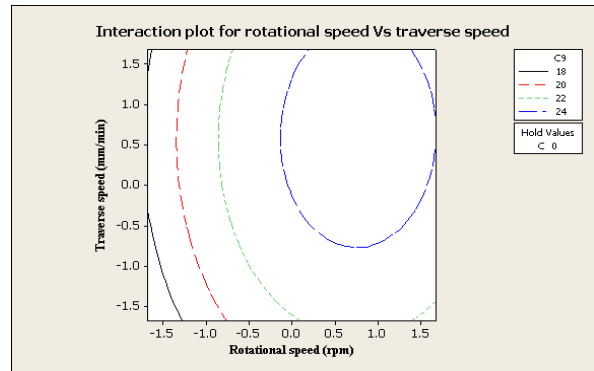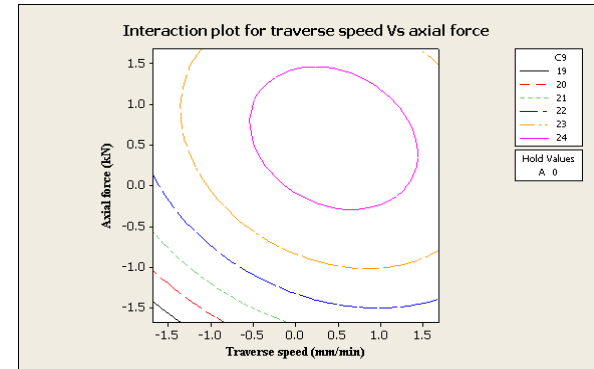
(b) Coating width, traverse speed Vs. rotational speed

(c) Coating thickness, axial force Vs. rotational speed

(d) Coating width, axial force Vs. rotational speed

(e) Coating thickness, axial force Vs. traverse speed
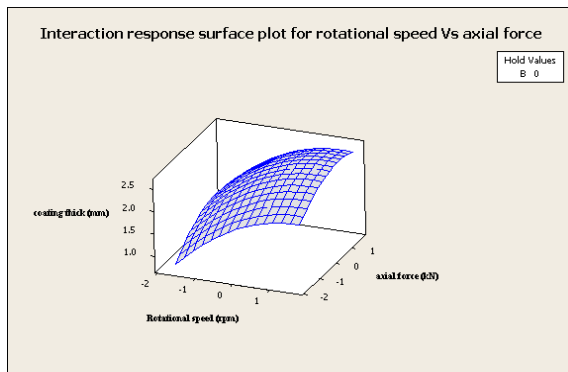
(f) Coating width, axial force Vs. traverse speed

Figure 5. Contour plot of possible independence of factor with response
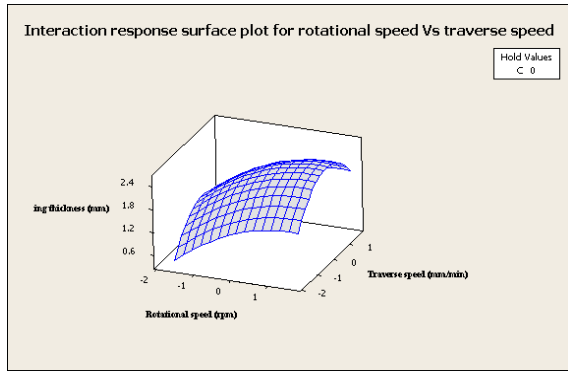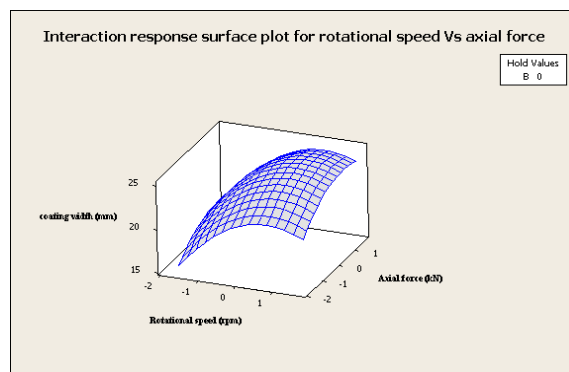
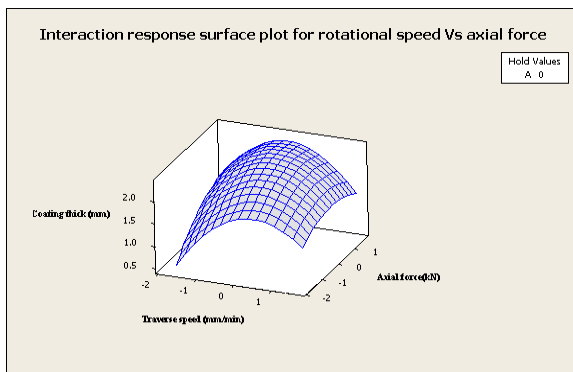(a) Coating thickness, V vs. N
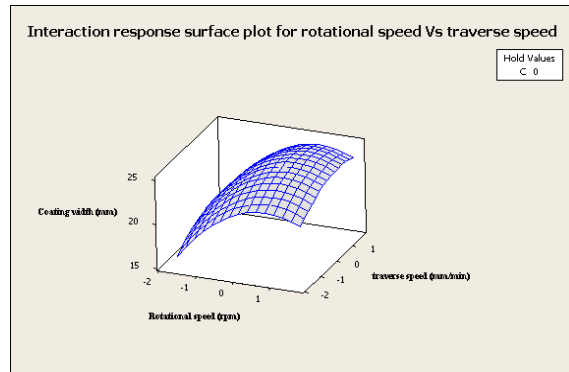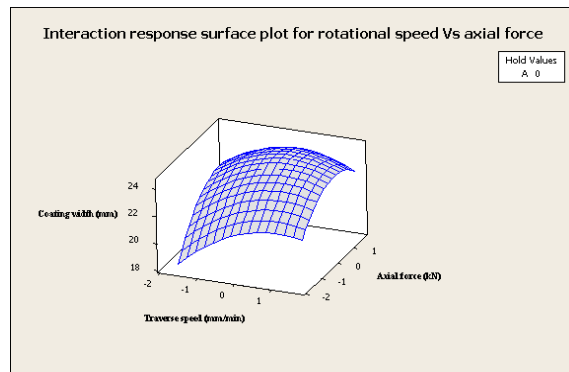

(b) Coating width, V vs. N

(c) Coating thickness, V vs. F

(d) Coating width, V vs. F

(e) Coating thickness, N vs. F

(f) Coating width, N vs. F

Figure 6. Interaction effect between the combination of factors

Rayleigh Instability of Plane-parallel Liquid Flows

B. M. Dakhel

General Required Courses Department, Jeddah Community College

King Abdulaziz University, Jeddah, Saudi Arabia

Abstract

Studying in this paper the stability of plane-parallel flows of an ordinary liquid can be naturally translated into the language of the theory of hydrodynamic resonances. Thus, resonant absorption of oscillations induces stability of the flows of an ideal liquid having a velocity profile without inflection points (Rayleigh theorem), while resonant emission leads to Rayleigh instability in the presence of an inflection point. The flow velocity profile has an inflection point. Thus, the presence of inflection points is a necessary condition for instability. If, however, the velocity profile has inflection points, the flow is stable (Rayleigh's theorem). Note that the sign of the jump depends on whether the neutral oscillations are regarded as the limiting cases of growing ($\text{Im}\,\omega > 0$) or damped ($\text{Im}\,\omega < 0$) oscillations.

Keywords: Rayleigh Instability, Plane-Parallel Liquid Flows

1. Introduction

Rayleigh has established in 1880 (Rayleigh, 1880), that plane-parallel liquid flows (Barston, 1991) of an ideal liquid, with velocity profiles that have no inflection points, are stable Rayleigh's theorem (Rayleigh, 1880).

Rayleigh instability (Khenner, et al., 1999; Wolf, 1970a, 1997b; Kumar, et al., 1994) occurs when a heavy fluid is supported by a lighter fluid. Any perturbation of the interface grows and leads to spikes of the heavier fluid penetrating into the lighter one.

It is known that vertical vibrations can lead both to the parametric excitation of waves at the interface and to the suppression of the Rayleigh–Taylor instability (Benjamin, et al., 1954; Miller, et al., 1983; Kumar, et al., 1994; Wolf, 1970), while the effects due to horizontal vibrations have been studied less. In experimental works by (Bezdeneznykh, et al., 1984; Piriz, et al., 2010) for a long horizontal reservoir filled with two immiscible viscous fluids, an interesting phenomenon was found at the interface: the horizontal vibrations lead to the formation of a steady relief. This formation mechanism has a threshold nature; it is noteworthy that such a wavy relief appears on the interface only if the densities of the two fluids are close enough, i.e. it does not appear for the liquid/gas interface.

Recently, (Dou, 2002; Kuznetsov, et al., 2011) proposed a new mechanism for flow instability and turbulent transition in parallel shear flows. In this paper, based on the previous work (Dou, 2002; Kuznetsov, et al., 2011), it is demonstrated that the stability of plane-parallel flows of an ordinary liquid can be naturally translated into the language of the theory of hydrodynamic resonances.

2. Basic Equations

Rayleigh's theorem deals with oscillations of an ideal liquid. The result of the theorem is valid for the flows of a real liquid as sufficiently large Reynolds numbers, when the influence of viscosity can be neglected. In this approximation, the equation of motion takes the following form

$$\frac{d\vec{V}}{dt} = -\frac{\nabla p}{\rho}$$
(1)

Where p is the pressure and ρ is the density of the medium.

If the liquid is incompressible, the velocity $\vec{V}$ must also satisfy the equation

$\nabla \cdot \vec{V} = 0$.

In the $xy-$plane the last equation will be satisfied if $\vec{V} = (\partial \psi / \partial y; \, -\partial \psi / \partial x)$, where ψ is the flow function.

Taking the z–component of the *curl* of (1) and expressing the velocity in terms of the flow current function, then

$$\frac{d}{dt}\Delta\psi = 0 \tag{2}$$

This equation is called the law of conservation of the velocity *curl* in an ideal incompressible liquid ($\nabla\times\vec{V}=z_0\Delta\psi$).

Linearizing (2) in terms of small perturbations, then becomes

$$\left(\frac{\partial}{\partial t}+V_0(x)\frac{\partial}{\partial y}\right)\Delta\psi_1 - \frac{d^2V_0}{dt^2}\frac{\partial\psi_1}{\partial y}=0 \tag{3}$$

It is assumed here that a small perturbation characterized by ψ_1 is applied to a stationary flow having a velocity directed along y–axis and varying along x–axis.

By using the following perturbation

$$\psi_1(\vec{r},t)=\psi_1(x)\,e^{-i(\omega t-ky)}$$

Then we get

$$\psi_1'' + \left(\frac{kV_0''}{\omega-kV_0}-k^2\right)\psi_1 = 0 \tag{4}$$

This equation is called Rayleigh equation.

We shall follow (Lin, 1955). We multiply (4) by ψ_1^* and subtract from the product of the complex conjugate

$$\frac{d}{dx}\left(\psi_1^*\frac{d\psi_1}{dx}-\psi_1\frac{d\psi_1^*}{dx}\right)=2i\frac{\mathrm{Im}\,\omega kV_0''}{|\omega-kV_0|^2}|\psi_1|^2 \tag{5}$$

Integrating (5) from one boundary of the flow to the other

$$W\Big|_{x_1}^{x_2}=k\,\mathrm{Im}\,\omega\int_{x_1}^{x_2}\frac{kV_0''}{|\omega-kV_0|^2}|\psi_1|^2\,dx \tag{6}$$

We have introduced in (6) the real quantity $W=(ik/2)[\psi_1(d\psi_1^*/dx)-\psi_1^*(d\psi_1/dx)]$. It defines the so-called Reynolds stress

$$\widetilde{W}_T=\rho W=-\rho\,\mathrm{Re}(V_{x_1}V_{y_1}^*) \tag{7}$$

in the oscillations.

Equation (5), which is the differential equivalent of (6), shows that at $\mathrm{Im}\,\omega=0$ the function W is constant in the intervals and undergoes a jump at the resonant point. Note that the sign of the jump depends on whether the neutral oscillations are regarded as the limiting cases of growing $(\mathrm{Im}\,\omega>0)$ or damped $(\mathrm{Im}\,\omega<0)$ oscillations.

The normal velocity component $V_{x_1}=ik\psi_1$ and with it the left-hand side of (6) vanish on the solid walls that bound the flow. For $\mathrm{Im}\,\omega\neq 0$, however, the right-hand side of this equation can vanish only if V_0'' reverses sign in the interval (x_1,x_2), i.e., the flow velocity profile has an inflection point. Thus, the presence of inflection points is a necessary condition for instability. If, however, the velocity profile has now inflection points, the flow is stable (Rayleigh's theorem).

3. Conclusions

In this paper we study the basic laws determining the stability of plane-parallel flows of an ordinary liquid can be naturally translated into the language of the theory of hydrodynamic resonances. Thus, resonant absorption of oscillations induces stability of the flows of an ideal liquid having a velocity profile without inflection points (Rayleigh theorem), while resonant emission leads to Rayleigh instability in the presence of an inflection point.

Note that at first glance Equation (6) applies equally well to growing $(\mathrm{Im}\,\omega>0)$ and attenuating $(\mathrm{Im}\,\omega<0)$ oscillations. One would therefore conclude from (6) that if some natural oscillations are in fact

analysis of damped oscillations $(\mathrm{Im}\,\omega < 0)$ calls for taking into account the viscosity, no matter how low, of the liquid.

Therefore all the conclusions concerning oscillations with $\mathrm{Im}\,\omega < 0$, based on an analysis of the equation of an ideal liquid, are, generally speaking, incorrect.

References

Barston, E. M. (1991). On the linear stability of inviscid incompressible plane parallel flow. *J. Fluid Mech.,* 233, 157-163. http://dx.doi.rog/10.1017/S0022112091000435

Benjamin, T. B., & Ursell, F. (1954). The Stability of the Plane Free Surface of a Liquid in Vertical Periodic Motion. *P. Roy. Soc. Lond. A.,* 225, 505-515. http://dx.doi.rog/10.1098/rspa.1954.0218

Bezdenezhnykh, N. A., Briskman, V. A., Lyubimov, D. V., Cherepanov, A. A., & Sharov, M. T. (1984). Control of the fluid interface stability by vibration, electric and magnetic fields, in: III All-Union Seminar on Hydromechanics and Heat/Mass Transfer in Microgravity, *Chernogolovka,* pp. 18–20 (in Russian).

Dou, H S. (2002). Energy gradient theory of hydrodynamic instability, Technical Report of National University of Singapore, also submitted, 2003.

Khenner, M. V., Lyubimov, D. V., Belozerova, T. S., & Roux, B. (1999). Stability of plane-parallel vibrational flow in a two-layer system. *Eur. J. Mech.B/ Fluids,* 18, 1085-1101. http://dx.doi.org/10.1016/S0997-7546(99)00143-0

Kumar, K., & Tuckerman, L. S. (1994). Parametric instability of the interface between two fluids. *J. Fluid Mech.,* 279, 49-68. http://dx.doi.rog/10.1017/S0022112094003812

Kuznetsov, S. V., & Nafasov, A. E. (2011). Horizontal Acoustic Barriers for Protection from Seismic Waves. *Advances in Acoustics and Vibration,* 2011, 150310-150318. http://dx.doi.rog/10.1155/2011/150310

Lin, C. C. (1955). Theory of hydrodynamic stability, *Cambridge Univ. Press.*

Miller, D. L., & Nyborg, W. L. (1983). Theoretical investigation of the response of gas-filled micropores and cavitation nuclei to ultrasound. J. Acoust. Soc. Am., 73, 1537-1544. http://dx.doi.org/10.1121/1.389415

Or, A. C. (1997). Finite-wavelength instability in a horizontal liquid layer on an oscillating plane. *J. Fluid Mech.,* 335, 213-232. http://dx.doi.rog/10.1017/S0022112062001366

Piriz, A. R., Prieto, G. R., Díaz, I. M., López Cela, J. J., & Tahir, N. A. (2010). Dynamic stabilization of Rayleigh-Taylor instability in Newtonian fluids. *Phys. Rev. E.,* 82, 026317-026328. http://dx.doi.org/10.1103/PhysRevE.82.026317

Rayleigh, L. (1880). On the stability or instability of certain fluid motions. *Proc. Lond. Maths. Soc.,* 11, 57-72. http://dx.doi.org/10.1112/plms/s1-11.1.57

Wolf, G. H. (1970). Dynamic Stabilization of the Interchange Instability of a Liquid-Gas Interface. *Phys. Rev. Lett.,* 24 (9), 444-446. http://dx.doi.rog/10.1103/PhysRevLett.24.444

Call for Manuscripts

Modern Applied Science is a peer-reviewed journal, published by Canadian Center of Science and Education. The journal publishes research papers in the fields of chemistry, environmental sciences, management and economics, physics, mathematics and statistics, geology, engineering, computer and information sciences, and biology. The journal is published in both printed and online versions. The online version is free access and download.

We are seeking submissions for forthcoming issues. The paper should be written in professional English. The length of 3000-8000 words is preferred. All manuscripts should be prepared in MS-Word format, and submitted online, or sent to: mas@ccsenet.org

Paper Selection and Publication Process

a). Upon receipt of paper submission, the Editor sends an E-mail of confirmation to the corresponding author within 1-3 working days. If you fail to receive this confirmation, your submission/e-mail may be missed. Please contact the Editor in time for that.

b). Peer review. We use double-blind system for peer-review; both reviewers and authors' identities remain anonymous. The paper will be peer-reviewed by three experts; one is an editorial staff and the other two are external reviewers. The review process may take 2-3 weeks.

c). Notification of the result of review by E-mail.

d). The authors revise paper and pay publication fee.

e). After publication, the corresponding author will receive two copies of printed journals, free of charge.

f). E-journal in PDF is available on the journal's webpage, free of charge for download.

Requirements and Copyrights

Submission of an article implies that the work described has not been published previously (except in the form of an abstract or as part of a published lecture or academic thesis), that it is not under consideration for publication elsewhere, that its publication is approved by all authors and tacitly or explicitly by the responsible authorities where the work was carried out, and that, if accepted, it will not be published elsewhere in the same form, in English or in any other languages, without the written consent of the Publisher. The Editors reserve the right to edit or otherwise alter all contributions, but authors will receive proofs for approval before publication.

Copyrights for articles published in CCSE journals are retained by the authors, with first publication rights granted to the journal. The journal/publisher is not responsible for subsequent uses of the work. It is the author's responsibility to bring an infringement action if so desired by the author.

More Information

E-mail: mas@ccsenet.org

Website: www.ccsenet.org/mas

Paper Submission Guide: www.ccsenet.org/submission

Recruitment for Reviewers: www.ccsenet.org/reviewer.html

The journal is peer-reviewed
The journal is open-access to the full text
The journal is included in:

AMICUS
CABI
CANADIANA
Chemical Abstracts database
DOAJ
EBSCOhost
Excellence in Research Australia (ERA)
Google Scholar
Library and Archives Canada

Open J-Gate
ProQuest
Scopus
Standard Periodical Directory
Ulrich's
Universe Digital Library
Wanfang Data
Zentralblatt MATH